UNIVERSITY OF BIRMINGHAM

Cycling Studies of Micro-tubular Solid Oxide Fuel Cells

By

Chinnan Maclean Dikwal

A thesis submitted to

The University of Birmingham

For the degree of

DOCTOR OF PHILOSOPHY

Chemical Engineering

School of Engineering

University of Birmingham

Edgbaston

Birmingham

B15 2TT

June, 2009

Abstract

A major problem of solid oxide fuel cells (SOFCs) is their long term durability under cyclic operation, for example during start-up and shutdown, where cracking can occur. The objective of this project is to understand these mechanisms of cyclic degradation for micro-tubular SOFC, then to set-up experiments to measure the degradation in terms of the drop in electrochemical performance and subsequently confirming the theories by dilatometry and scanning electron microscopy (SEM). In conclusion, the methods and conditions for minimizing degradation in SOFC have been put forward.

First, a theory of degradation based micro-crack propagation due to severe expansion and direct oxidation of the Ni anode were propounded. Several experiments were designed to illustrate the degradation phenomena.

The first was isothermal (steady state) ageing, which was performed to provide a benchmark of degradation for easy comparison with degradation under transient conditions (i.e. thermal, redox and load cycling). During this operation, sintering was found to dominate the degradation mechanism, causing irreversible deformation and decreasing the power output without obvious micro-cracking taking place.

With the bench mark for steady state degradation established, thermal cycling was performed by rapidly alternating between peak temperature and 200^{o}C. This was found to have a marginal effect on the electrochemical performance and no micro-

cracking was observed. However, thermal cycling with a temperature gradient imposed across the tubes was found to cause electro-chemical performance decrease and micro-cracking and de-laminations were observed.

Thirdly, redox cycling was performed by changing the fuel flow between 20mL/min and no-flow. This was essential to deprive the anode of fuel in order to allow for oxidation of the Ni anode to occur. Redox cycling was found to have an adverse effect on the electro-chemical performance of micro-tubes. Severe micro-cracking and de-laminations were observed.

Lastly, thermal and electrical shock test were performed. The critical fracture temperature (ΔT_C) was established by thermal shock at approximately 180^{o}C. Under electrical shock testing, the tubes were found to fail after 13 – 15 electrical shock cycles, depending on the shock temperature.

In conclusion, theories of micro-tubular SOFC cycling degradation have been proposed for thermal cycling, redox cycling and isothermal ageing and several experiments have provided confirmation.

Dedication

I dedicate this thesis to: My father, my mother, my brothers & sister; all of whom I cherish dearly.

Acknowledgements

Firstly, I would like to thank Prof. Kevin Kendall - my supervisor, for his guidance, insight and support throughout this project. His knowledge and input into this project has been truly in-valuable. Secondly, I would like to thank Dr. Waldemar Bujalski – my co-supervisor, who has been a great source of support and help. I am especially grateful to him for helping to sort-out most of the equipment necessary for this research and for providing me with guidance in performing the cycling of SOFCs. Also, I gratefully acknowledge the Petroleum Technology Development Fund (PTDF) and Univation, UK for generously funding this project.

I am also grateful to the members of the fuel cells group; Dr. Aman Dhir for computer support and for allowing me the use of his test rig, Mr. Gareth Thompson my colleague and housemate for 3 years for putting up with my mess and supporting me through-out. Mr. Raj Saini for assisting with electrical shock testing. Dr. Christian Mallon and Dr. Mathew Slinn for helping me settle into this research in the early days of commencing this project. I also acknowledge Mr. Babangida Jibrin for his in-valuable advise and insight.

Finally, I am greatly indebted to my Dad whom without, this project would not have been possible. His fervent prayers, selfless financial support and encouragement are gratefully acknowledged. I also gratefully thank my mum for her warmness, love and prayers all through. Bamnan for his moral support and advice. Also to my siblings, Walshak, Diretnan, Kwopnan and Emmanuel, I love you all.

Table of Figures

Chapter 1

Introduction

1 Project rationale

1.1 The Current Environmental and Energy Crisis

Climate change, environmental degradation and depleting fossil fuel reserves has prompted governments, research organization and the private sector to search for alternative energy sources to replace traditional fossil fuels. Carbon-rich fossil fuels like petrol, diesel and coal which account for over 50% of primary energy generation in the world are being replaced by relatively clean energy technologies like geothermal, solar, wind and bio-mass.

The European Union (EU) has over the last decade been at the forefront of advocating and negotiating a green and sustainable energy generation framework. It currently accounts for 22% of global greenhouse gas emissions yearly, In view of this, It enacted an integrated energy and environmental policy based on clear targets and time table for moving to a low-carbon economy This included cutting greenhouse emissions by at least 20% by 2020 and increasing by 20% the amount of renewable energy technology by 2020[1]. The EU's longer term plan is to achieve more than 50% of the energy for power generation, transport etc from carbon neutral sources. The commitment of the EU to reducing carbon emissions led to the creation of an emissions trading system in which a Company which emits less than the quota stipulated can sell its unused portion to a company which has exceeded its own. Quotas were introduced in major pollution sectors like energy, steel, glass etc, to promote efficient use of energy, cut pollution and will help the EU fulfil its promise to the international framework

convention on climate change (Kyoto Protocol) to cut carbon emission by 8% by 2012 based on 1990 emissions levels[2]. The Kyoto protocol was adopted in December 1997 and enforced in February 2005 by the countries which ratify it (181 parties as at May 2008). The EU has been the foremost advocate of the Kyoto protocol, negotiating with nations who have not ratified the protocol (like the United States of America, USA) to adopt it[3].

In the UK, a climate change framework was proposed to help cut carbon emissions by 60% (based on 1990 estimates) by 2050. Short term emissions targets between 16% - 32% have been set by 2020. As part of sustainable energy development, the UK government have considered several clean energy generation technologies; Wind power [4], Tidal wave, Solar power [5], Geothermal, Biomass/Bio fuels [6] and Fuel cells which will be discussed in greater detail in this study.

1.2 Fuel cells

1.2.1 Definition of a fuel cell

A fuel cell can be defined simply as an electrochemical device that converts the chemical energy of a fuel with an oxidant into electricity. In principle, the operation of fuel cells closely resembles batteries, but unlike batteries fuel cells consume reactants which must be replenished continuously, whereas batteries store electrical energy chemically in a closed system. So long as fuel and oxidant are present, a fuel cell

would produce electricity [7]. The basic components of an oxide based fuel cell are shown in Figure 1.1.

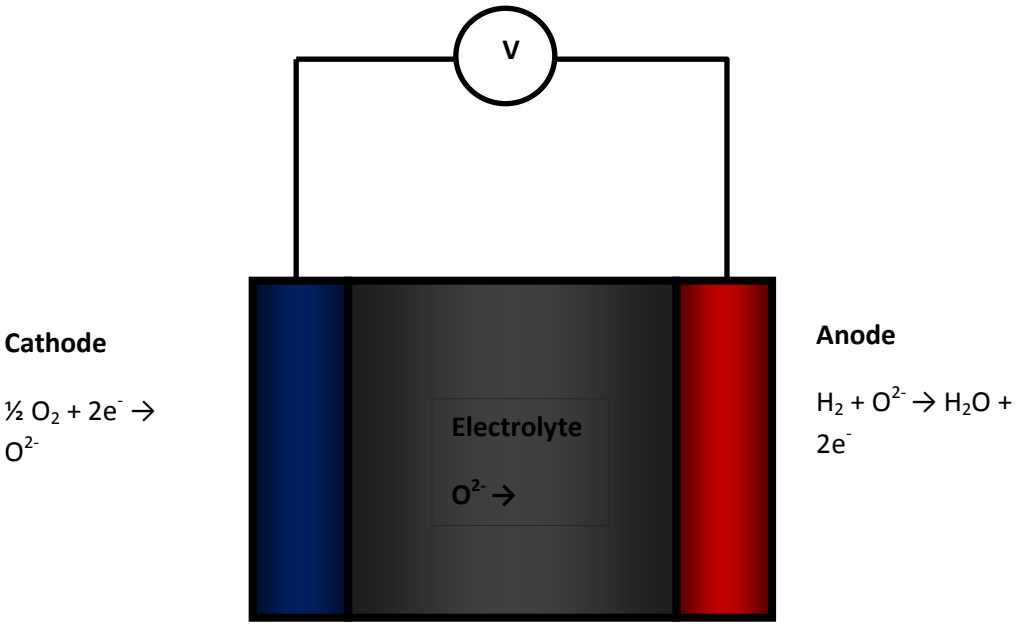

Figure 1.1: General operating principle of an oxide based fuel cell

The overall reactions in these electrodes are as follows.

Cathode half reaction:

$O_2 + 4e^- \rightarrow 2O^{2-}$ Eq. 1.2

Anode half reaction:

$4H_2\,(g) + 2O^{2-}\,(g) \leftrightarrow 4H_2O\,(g) + 4\,e^-$ Eq. 1.3

Since the fuel and oxidant combine directly to produce water and electricity, without an intermediate conversion step to mechanical energy as in heat engines, fuel cells can attain higher working efficiencies than heat engines. Other advantages over heat engines include; silent operation and zero green house emissions if hydrogen from renewable sources [8], hydrogen generated from renewable sources can be used to give it a more sustainable edge. The basic components of a fuel cell as depicted in fig 1.1 consist of an electrolyte sandwiched between a porous anode (Negative or fuel electrode) and cathode (Positive or air electrode). At the cathode, oxygen is broken down into its ions; these ions migrate through the conductive electrolyte to the anode side where they combine electrochemically with hydrogen to form water, with electrons released.[9]. A fuel cell will produce electricity as long as fuel and oxidant are fed to the anode and cathode respectively. Hydrogen and air are used as fuel and oxidant in many cases, although other hydrocarbon fuels have shown great potential in some fuel cell applications, where gases like methane and propane are available. The question is 'how long will the fuel cell run as the gases continue to be fed into it?' This is a durability problem.

1.2.2 Life Cycle and Durability; A major problem of fuel cells

It's difficult to estimate the lifetime of fuel cells, because their failure mechanisms are complex. Standard engineering failure test like mean-time-between-failures (MTBF) do apply because failure in fuel cells starts with gradual degradation in the

membrane-Electrode-Assembly (MEA) with time instead of abrupt failure. Durability of fuel cells is one of the issues that still remain largely misunderstood. Their complex degradation mechanisms, lengthy testing times (usually thousands of hours), and inability to perform *in-situ* non-destructive structural evaluation of the MEA are reasons why their degradation is misunderstood[10]. Degradation in fuel cells is usually estimated as percentage (%) per hour or mV/1000 hours in the case of a decrease in voltage. The recent commercial requirement of fuel cells is that they maintain a life span of 40, 00 0 – 50, 000 hrs so only low degradation rates are permissible. These marginal degradation rates are difficult to achieve especially when several starts-and-stops (thermal cycling) or redox cycle occur. Thus, the investigation of the effects of cycling on the electro-chemical performance of fuel cells is vital and is the subject of this thesis.

1.3 Outline of thesis

This thesis investigates the degradation pathways in SOFC with a view to understanding the mechanisms, then finding conditions/methods of minimizing their effect on the electro-chemical performance of micro-tubular SOFC. The work focuses on degradation modes i.e. micro-cracking, de-lamination, sintering and re-oxidation which occur in the electrode, electrolyte and interfaces.

Chapter 2 is a review of literature of previous work done on cycling degradation and the current status of the technology.

Chapter 3 focuses on the methods and materials used in this project; mainly describing the tube manufacturing techniques and preparation, the test rigs, testing methods and the equipments.

Chapter 4 is the first results chapter, describing new observations of the isothermal ageing of micro-tubes under steady state operation. This test was necessary in order to provide a bench mark for comparison with degradation due to transient operation (e.g. cycling).

Chapter 5 focuses on degradation due to thermal cycling. Thermal cycling was performed by rapidly changing the temperature or operation between peak temperature and 200^{o}C. Dilatometry was used to analyse the thermo-mechanical expansion of the tubes under thermal cycling.

Chapter 6 describes the results of electro-chemical degradation due to redox cycling. Results of the thermo-gravimetric analysis (TGA) of the micro-tubes during redox operation are also presented.

Chapter 7 focuses on the thermal and electric shock behaviour of the micro-tubes, describing the shock procedures, results and analysis techniques. The result of three-point-bend tests which were performed on the shocked tubes is also presented.

Finally, chapter 8 sums up the conclusion and future work.

Chapter 2

Solid Oxide Fuel Cells

2 SOFC literature review

2.1 Operating Principle

SOFCs operate at high temperature; in the 600°C – 1000°C regime. Their high temperature of operation makes it possible for non-precious metal (Ni, Co) catalysts to be used as the electro-catalyst in the electrodes.

SOFCs are operated in three different stages: Start-up, Steady state and shutdown[11-14]. During the start-up phase, the cell is heated from ambient temperature to operating temperature. Different methods are employed to achieve this; the use of preheated air (from the cathode side) helps to reduce degradation due to thermal shock[15]. Heating can also be achieved by the use of heating furnace[16]. The steady state phase is the constant temperature hold, when the cell is at its operating temperature. Degradation at this phase is due to temperature gradients which might develop due to the electrochemical reactions occurring – being an exothermic reaction. The operating temperature depends on the electrolyte thickness (thinner electrolytes allow lower operating temperatures), because the resistance to ion transfer is minimum.

The cooling down phase is thought to be the most delicate phase of operation as the difference in the coefficient of thermal expansion (CTE) of the components can cause differential shrinkage leading to internal weaknesses[17]. Cooling in most SOFC applications is by natural convection to the surroundings as such this uncontrolled

process can lead to hot and cold spots within the same material thereby promoting differential shrinkage.

In typical SOFC, commercially available fuels like natural gas, methane, propane, butane, biogas etc, can be used in SOFC conveniently[18-20]. The total electrical efficiency of the system can reach 60%, however when their exhaust gases are used in a gas or steam turbine total efficiency of the hybrid system is up to 85%[21, 22]. SOFC are favoured for large power generation applications (>500kW). SOFC are made into different geometries; integrated planar SOFCs like the Roll Royce® Fuel Cell Systems (RRFCS) design where the electrolyte is sandwiched between the electrolytes, these are easier to stack and fabricate. Tubular geometries like the Westinghouse® and Adelan® designs are also popular because of their robustness, rapid start-up, thermal cycling ability and due to the fact that gas sealings are not required.

2.2 Electrolyte

The electrolyte of typical SOFC is composed of ceramic oxides which posses ion-transfer capability at high temperature. The most common electrolyte is Yttria Stabilized Zirconia (YSZ), the amount of Yttrium doping ranging from 3mol% - 12mol%. The most widely used composition is 8 mol% Y_2O_3 – 92 mol% ZrO_2 for its high ionic conductivity (3 mol% YSZ gives good mechanical strength)[23, 24]. The electrolyte thickness depends on the temperature of operation of the fuel cells, because the conduction of ions through the electrolyte is temperature dependent[25-28]. For high operating temperatures e.g. 850°C – 1000°C, thick electrolytes (between 90µm -

150µm) can be used, the anode and cathode can be made thin (about 40µm) and the electrolyte acts as the support structure (these types of cells are called electrolyte supported cells)[26, 29-32]. For lower operating temperatures (700°C – 850°C) thinner electrolytes (10 - 20µm) are employed. Thinner electrolytes decrease the polarizations due to ohmic over-potential, thus faster ion transfer rates are achieved. For these thin electrolytes, thicker electrodes are required as supports (these cells are called electrode supported cells)[23, 33-38]. For temperature ranges between 500°C - 650°C, other electrolytes based on ceria are employed for good ion conductivity[26, 39, 40]. The fabrication of thin electrolytes is done carefully so as to maintain zero-porosity in the electrolyte to prevent gas cross over. It is important to fabricate electrolytes which can withstand assembly stresses, structural stress and remain stable during operation. The desired properties of electrolytes are; (1) High ionic conductivity and low electronic conductivity (2) Closely matched thermal expansion coefficient (CTE) to other cell components (3) Stability in both oxidizing and reducing atmospheres (4) High chemical stability with respect to the electrodes.

The high temperature of operation in SOFC is necessary in order to initiate the ion transfer; however this means that only specialised metal alloys and materials can be used as balance of plant and interconnects due to the high temperature. Cheap and available materials like steel are not suitable for high temperature applications and because of this, cost of SOFCs is still high. Several methods of reducing cost of SOFCs while maintaining high power density have been explored including reducing the

thickness of the electrolyte to a few micro-metres. Decreasing the electrolyte thickness also reduces costs by allowing a lower operation temperature[9, 41, 42].

2.3 Anode

Typical SOFC anodes are made of porous cermets (a mixture of coarse and fine metal and ceramic particles) of Nickel and Yttria Stabilized Zirconia (Ni/YSZ)[43-48]. Nickel is employed for its high catalytic activity, electronic conductivity and chemical stability in both reducing and oxidizing conditions and relative low cost. The YSZ component serves two functions; it serves to preserve the cermet microstructure by preventing Ni sintering and to extend the triple phase boundary layer necessary for ion conductivity[23, 49, 50].

However there are several problems associated with Ni in SOFC anodes; For instance the coefficient of thermal expansion (CTE) between a Ni and YSZ particles are significantly different. Thermal stresses will be induced in the structure due to this difference[51]. Also, sintering of Ni is a major concern in high temperature applications because Ni agglomeration will lead to decreased porosity and reduced TPB layer which is necessary for fuel oxidation. Ni agglomeration can be minimized by forming a YSZ matrix around the Ni particles to prevent the particles from moving. The YSZ in the anode also serves to provide a thermal expansion similar to the YSZ electrolyte thus; reducing the difference in the CTE.

When hydrocarbon fuels are used in Ni based anodes, carbon deposition is a likely occurrence because Ni is a good hydrocarbon cracking catalyst. Carbon deposition

causes clogging of electrode pores, de-activation of the catalyst surfaces and decreased performance. In cases where hydrocarbon fuels are used, anodes based on other metals are employed or the cell operating conditions are altered to minimize carbon deposition[52-56].

2.3.1 Alternative Anode Materials

The drawbacks associated with conventional anode materials (Ni/YSZ) prompted researches into alternative anode material which are not susceptible to the afore mentioned limitations. Mixed conducting ceramics like ceria (CeO_2), doped with gadolinium (GDC) can be used to replace traditional SOFC anodes because of their ability to conduct both ions and electrons effectively[57-61]. However, the redox behaviour of ceria is not completely stable because Ce^{4+} can be reduced to Ce^{3+} thereby changing the microstructure and causing bulk volume changes, but doping with 10 mol% gadolinium can considerably diminish this redox effect[62].

In recent SOFC studies, alternative anode materials Ni/GDC[63, 64] and Cu/GDC[65-68] have been shown to perform brilliantly with hydrocarbon fuels. Ni was found to cause coking with high chain hydrocarbon because of its high catalytic activity[69-71], it was found to be most suitable for low chain hydrocarbon fuels e.g. methane because of their low carbon content and kinetics, also temperatures below 550°C was found to diminish coking[52, 72]. On the other hand, Cu is not plagued by coking but its electro-catalytic ability is low compared to Ni and it has a low melting point (1084.62°C) therefore not suitable for high temperature applications[66, 67, 73].

A recent study by Zhao et al[74], reported a novel anode material $La_{0.3}Sr_{0.7}Sc_xTi_{1-x}O_{3-\delta}$, which is a mixed conductor; capable of conducting both electrons and ions. The Sc was the B-site dopant with the primary objective of increasing the ion conductivity of the structure. Increasing the amount of Sc in the structure was found to significantly increase the ion conductivity between 500 - 1000°C; this was made possible by increasing the oxygen vacancy spots in the structure.

Novel material for simultaneous use as anode/cathode based $La_{0.75}Sr_{0.25}Cr_{0.5}Mn_{0.5}O_{3-\delta}$ were also reported by Ruiz-Morales et al[75]. This symmetrical configuration was found to have enhanced electrochemical properties in both reducing and oxidizing conditions with improved porosity and stability.

The desired properties of SOFC anodes are: 1. High catalytic activity, 2. High porosity and sufficient area for fuel oxidation, 3. Good thermal expansion match to other cell components, 4. Stability in both reduction and oxidation conditions, 5. Tolerance to impurities.

2.4 Cathode

The cathode of most SOFC is made from semi - conducting ceramics such as Lanthanum Strontium Manganate (LSM)[76-78] or other cheap and available materials like Lanthanum Strontium Cobalt ferrite (LSCF)[79-81]. Their desired properties are similar to that of anodes including high catalytic activity for oxygen reduction, good porosity to enhance surface area for oxygen reduction and closely match CTE with other cell components. At the beginning of SOFC development, platinum was used as

the cathode for most SOFC applications because it demonstrated the best catalytic activity and alternative materials were yet undiscovered but this was soon found impractical because of its cost - being a precious group metal. Since then, other alternatives have been considered including lanthanum Manganite ($LaMnO_3$)[82-84], which can be doped with rare earth metals like strontium and ceria to enhance its electrical conductivity.[85-87]. Perovskite oxides of LSCu have also been reported by Yu et al[88] to be ideal cathode materials for intermediate temperature applications due to their high oxygen vacancy concentration and electrical conductivity. In the study, the valence state of Cu ions, the thermal expansion, cathode over-potential, reactivity with YSZ and the LSCu/YSZ polarization resistance were evaluated at 800°C and found to be satisfactory. Several other material including $Pr_{0.7}Sr_{0.3}Co_{1-y}Cu_yO_{3-\delta}$[89] and $Ba_{1.2}Sr_{0.8}CoO_{4+\delta}$–GDC[90] have been reported as alternative cathode materials.

2.5 Interconnect Materials

Interconnects are metal components which are used to separate stack layers, and provide electrical contact to electrodes. They are also used to separate fuel and oxidant streams from adjacent cells[91-93]. The desired characteristics of SOFC interconnect materials include; Compatible CTE with other cell components, High electrical conductivity, stability in redox atmospheres, ease of manufacture and low cost of manufacture. Several alloys meet the afore mentioned characteristics, including lanthanum chromite and stainless steel which have shown a great deal of promise for intermediate temperature (650°C – 800°C) applications [94, 95]. Ferritic

steels with Cr content greater than 16% have demonstrated the best suitability so far[96]. However, the formation of a ferric oxide at high temperature is a major concern because of the increase in electrical resistance associated with this. To undermine this oxidation phenomenon several alloys including Crofer 22 APU[97-99] and ZMG232 have been developed as replacements for typical SOFC interconnects. The minute amount of Mn which is contained in them results in the formation of a conductive oxide $(Mn,Cr)_3O_4$ which helps to reduce their overall polarization resistance[100]. Other Ferritic steel alloys like F18TNb, IT-11, E-brites have been used as SOFC interconnects.

2.6 Overview of SOFC Manufacturing Processes

SOFCs are formed into variety of geometries; because of this several manufacturing techniques are used to fabricate them. Tape casting, screen printing, electrochemical vapour deposition (EVD) and extrusion are the most widely used techniques to produce SOFCs at present. However, other techniques like laser deposition, spray pyrolysis, electrophorectic deposition are gaining wide application[101].

The choice of a method for SOFC fabrication is governed by the cost effectiveness of the process, quality or specification of cells required and production capacity. Screen printing has gained wide application for most planar SOFC manufacturing processes principally because of its cost effectiveness and large production capacity compared to other methods. The control of process variables like material thickness, in-film defect levels and porosity become critical to ensure good cell performance[102].

Extrusion is the main technique employed for the manufacture of tubular and micro-tubular SOFC. Typical extrusion techniques required the use of die-presses and hydraulics to press the slurries and form them into tubes. Extrusion processes are relatively cost effective but their process variability between cells is a problem especially in un-automated processes.

Co-extrusion is used to extrude more than one cell component at a time, this makes it possible for thin electrolytes to be deposited[103].

2.7 SOFC Geometry

Design and fabrication of SOFCs is contingent upon satisfying the electrochemical, mechanical and durability requirements. The main factors to be satisfied before fabrication include:

- Electrochemical/Electrical performance: - Activation, Ohmic and mass transport irreversibilities which occur during SOFC operation must be minimized. The practical ways of diminishing these effects include reducing the electrolyte thickness and increasing the water management in the cell by enhancing the porosity of the anode[9].

- Mechanical Integrity: - The structural integrity of SOFC is very important during assembly, handling and operation, as such attention has to be given to their mechanical strength. Fabrication process usually involves slurry precipitation and screen printing or extrusion. During these processes, significant volume

change is involved which is capable of causing failure under inappropriate conditions.

- Durability: - Typically SOFC are operated over long periods of time (40,000 – 50, 000hrs) under different conditions. In view of this, materials which have the capacity to withstand rapid and continuous operation are required. Thermal stresses are known to accumulate in SOFC during operation due to cycling, thermal shock or thermal gradients as these are inevitable during operation. This accumulation can lead to performance degradation and eventual failure in some cases, thus durable materials are required[104].

Two distinct SOFC geometries exist; Planar and tubular. Both have their different applications and suitability. Their principle of fabrication are however similar; One of the cell components is formed as the support structure for the others. For instance, In most planar SOFC the electrolyte is usually formed as the support structure i.e. the other electrodes are screen printed onto the electrolyte sheets[105]. In this case the electrolyte is usually about(120 – 250µm) thick, while the thickness of the electrodes could range between 20 - 50µm[106, 107]. This type of fabrication technique offers several benefits including high mechanical strength and lower susceptibility to redox effects because of its thin electrodes; however certain factors like high ohmic over-potential due to the thick electrolyte and high temperature of operation may affect their performance. In electrode supported cells, either the anode or the cathode are used as the mechanical support. Cathode supported cells are not very popular

compared to anode supported ones, very few research groups have been investigating their potential in the recent past[35, 108, 109].

Anode supported cells have received a lot of attention because of their thick anodes structures which provide sufficient area for fuel oxidation. The tubular anode supported designs have anode thicknesses in the range of 400µm and 3000µm. They benefit from increased conductivity (thinner electrolytes) and lower operating temperatures. Their disadvantages include decreased mechanical strength and increased mass transport losses due to the thick anode.

Micro-tubular anode supported SOFC (*Adelan®* micro-tubes) are a miniature version of typical tubular SOFC geometry (*Westinghouse®* design) though fuel is delivered in the middle of the tube as against the outside as in the Westinghouse design. Their anode thickness range between 100µm - 300µm with thin electrolytes 10µm - 20µ.They have several advantages including rapid start-up, good thermal cycling resilience, thermal shock resilience, and fast ionic conductivity. On the other hand, they suffer from low mechanical strength and could also be plagued by mass transport polarisations.

2.7.1 Planar SOFC

Planar SOFCs offer the potential of high power density and cost effective manufacturing. Their planar geometry allows for simple and cheap manufacturing techniques to be employed, further reduction in capital cost of manufacturing can be achieved if cheap and available ferritic stainless steels are used as interconnects and

gas manifolds. However, thermal ageing due to high temperature of operation makes it impractical for these alloys to be employed except for intermediate temperature SOFCs.

A common way of reducing operating temperature in SOFC is the use of anode supported cells. Anode supported cells allow for thinner electrolytes to be fabricated, thereby reducing their ohmic over-potential. Work at Forschungszentrum Julich have shown that the operating temperature of SOFC can be reduced significantly to750°C when anode supported cells are used as compared to 900°C when electrolyte supported cells are used[110, 111]. A reduction in temperature will allow for a reduction in operating cost and a reduction in the balance-of-plant equipment cost, by allowing cheap components like heat exchangers, compressors and fans etc to be used. Other companies which produce planar SOFC include Versa power, Forschungszentrum Julich, Topsoe fuel cells and CFCL. Figure 2.1 is a CFCL planar SOFC.

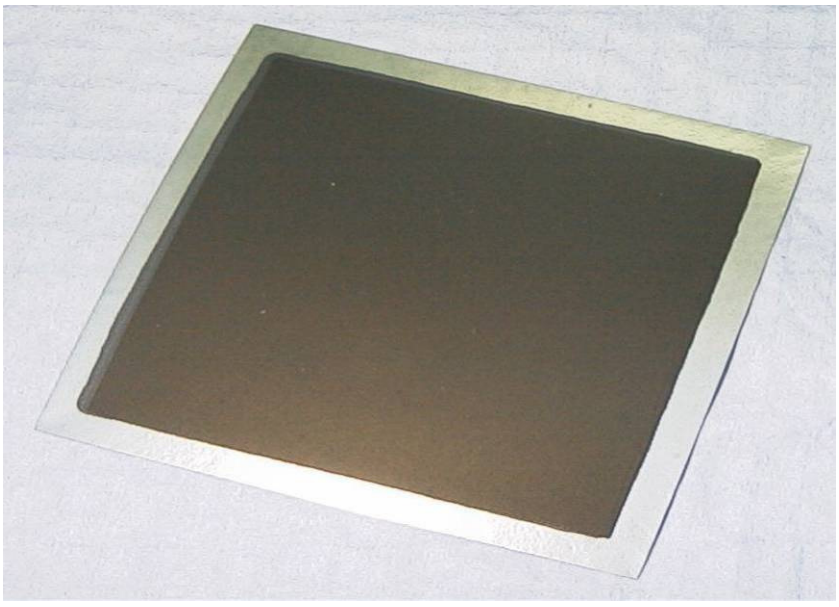

Figure 2.1 A planar SOFC [112]

2.7.2 Tubular SOFC

Tubular SOFC have a number of advantages including rapid start-up and thermal cycling and shock resilience. Their tubular geometry allows fast radial-to-axial heat transfer which severely limits the un-equal expansion and contraction during thermal cycling. Also, their tubular geometry helps to eliminate the need for excessive gas sealings which have the tendency to cause differential expansion and contraction due to the difference in CTE of the sealing materials compared to the SOFC.

The tubular geometry was first developed by *Westinghouse Electric Corporation* (now Siemens-Westinghouse). These cells are > 15mm in diameter and up to 600mm in length. Another geometry which has gained significant attention over the years is the micro-tubular SOFC, developed by K. Kendall in the early 1990's[113, 114]. These cells were less than 4mm in diameter and about 50 – 100mm long. Figure 2.2 is an image of a micro-tubular SOFC.

Figure 2.2 Image of a micro-tubular SOFC

2.8 Applications

At present, SOFCs find their widest applications in sensor for automobile catalyst because of their ability to oxidize flue gases but over the last few years, many other applications of SOFC have emerged, including stationary power generation, back-up systems etc. Residential micro-CHP systems are an ideal application for SOFC because of their unique advantage of high electrical efficiency, ability to utilize conventional fuels, compactness and silent operation. CFCL Australia, has developed a CHP unit based on natural gas from the grid with an electrical efficiency of >50% and an overall efficiency >80%[112], Figure 2.3 It formed commercialization partnerships with heating system manufacturers in Japan, Netherlands, Germany, France and the United Kingdom for market integration. The companies involved in this partnership include; *E-on®*, Gledhill® – **UK**, *Gaz de France®*, De Dietrich® – **France**, Nuon® – **Netherlands**, EWE®, Bruns® - **Germany**.

Figure 2.3 CFCL semi Integrated Alpha-Unit (a partnership with *EWE*)[112]

Adaptive materials® Inc, USA (AMI) develops portable back-up power systems which have the capacity to utilize propane and butane gases as fuel. These back-up devices have the capability to produce between 25 – 250W. The cells which make up these appliances compose of stacked micro-tubular SOFC each capable of producing 1 -2W. AMI® focuses its attention on developing portable power appliances, unmanned vehicles and remote sensing application for military purposes[115]. Figure 2.4 below is the Amie 150, a portable system capable of producing 150W continuous power at 25V

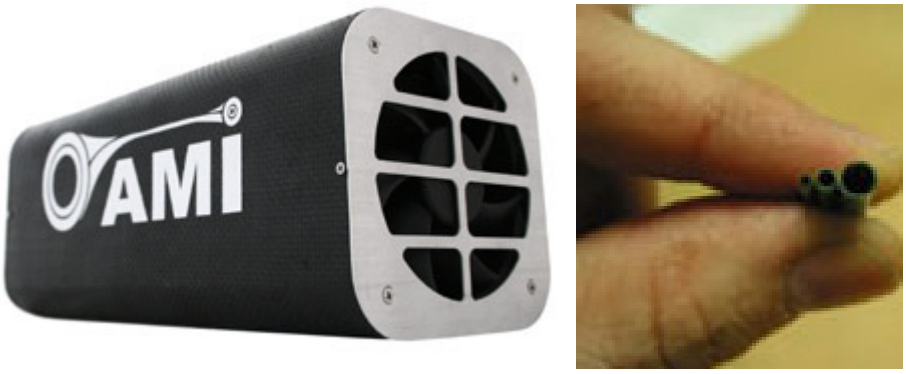

Figure 2.4 The Adaptive Materials portable power module - Amie 150[115]

Hexis® LTD has also developed a residential CHP unit (*Galileo 1000N*) for households. The system delivers electrical output of 1kW and 2kW of heat energy. Additional heating of up to 20kW can be obtained from an integral gas burner in the system if required. The system attains an electrical efficiency of > 30% and an overall efficiency of > 95%. The integrated stacks compose of circular electrolyte supported planar cells and metal interconnects, Fig. 2.6. The stacks were reported to have shown improved degradation resistance over the last few years, from a high degradation rate of

15%/1000hrs in 2005 to 2%/1000hrs in 2008. Their thermal and redox cycling resilience were also improved from 2 – 3 during a stack life time to about 10 at present. Figure 2.5 shows a picture of the Galileo 1000N[116].

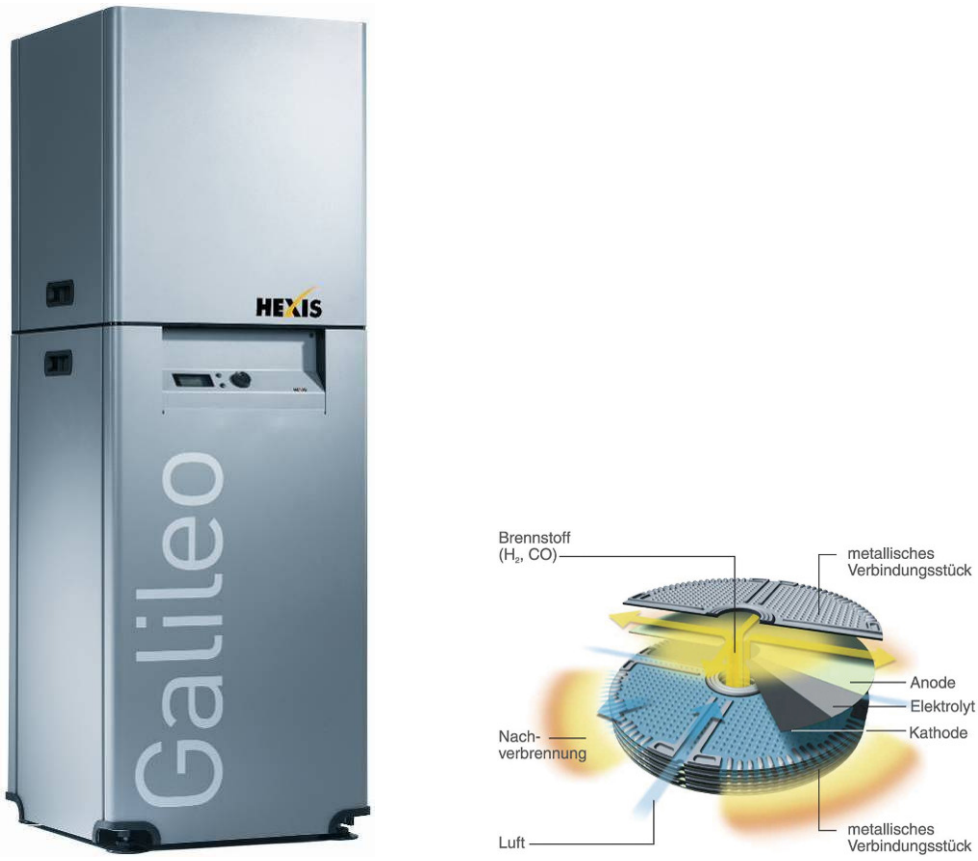

Figure 2.5 The Galileo 1000N from Hexis Ltd with the circular electrolyte supported SOFC stack[116]

Other companies involved in R & D and Commercialization initiatives include; *Topsoe Fuel Cells* – **Denmark**[117], *Siemens* – **USA**[118], *Versa power systems* – **Canada**[119], *Delphi Corporation* – **USA**[120], and *Rolls Royce* – **UK**[121].

2.9 Thermal Stress Induction in SOFC

SOFCs are composite materials; as such they are prone to thermal stress induction due to differences in CTE between the metal and ceramic components. Stress starts to build up from the fabrication stage when the slurry condenses into a dense structure. After fabrication, the composite structure is sintered at high temperature in order to densify and adhere the components. At this temperature the components are at equilibrium with each other and the stress induction is at a minimum, however the Cooling down from sintering temperature to room temperature is very critical as stress induction is very likely because of uncontrolled cooling which is usually based on natural convection to the surroundings. During this phase, the metal component which naturally has a higher CTE compared to the ceramic shrinks by a greater index. This difference in CTE will enhance thermo-mechanical stress induction [122].

The start-up phase is also known to be responsible for significant thermal stress induction depending on the heating method adopted. The use of pre-heated air to heat up SOFC stacks might produce better results than the use of radiative heating from the coils of high resistance wires. This is because of the uneven heat distribution associated with this technique, the radiated may also have a degrading effect on SOFC materials.

2.9.1 Stresses Occurring During Fabrication

The fabrication of SOFC is usually carried out in four distinct stages; blending of powders, compacting of slurry, structure formation and firing. The blending of powder

is essential to improve the packing ratio by mixing powders of different size distributions to achieve the desired composition required and to add sufficient binder to hold the structure. The Slurry compacting is carried out so as to increase the density of the structure and increase mechanical strength. Compacting can be achieved by the use of die presses or high shear hydraulic compacters. The formation step gives the desired shape (tubular, planar etc) to the structure. The most common process used for structure formation for tubular SOFC is extrusion or co-extrusion for cases where more than one cell components are extruded together[103, 123, 124]. Firing is the final operation in SOFC fabrication which helps to adhere the components.

Stresses start to develop during the transformation from powder-binder slurry into a dense ceramic because of the large volume change associated with it. Inappropriate drying and handling procedures could result to severe cracking and delamination during this step. Additionally, materials of similar CTE are usually matched closely so as to minimize stress accumulation due to differential expansion and contraction.

The firing step is also a stress inducing stage during SOFC fabrication. At the first stage of firing, when the structure is ramped-up to sintering temperature, significant amount of volume change occurs due to binder burn-out and solvent evaporation; residual stresses will develop due to this change in volume. Once at the sintering temperature, the components are at equilibrium with each other and the structure is stable. The elastic mismatch stress at this stage due to difference in CTE might be diminished due to the viscous behaviour of the structure at the sintering

temperature[125]. The cooling from sintering temperature to room temperature is very delicate as this is the stage in which the difference in CTE will be pronounced. Metal components generally shrink more than ceramics, thus creating tension at the interface. Figure 2.6 below shows the effect of CTE mis-match during cooling from sintering temperature.

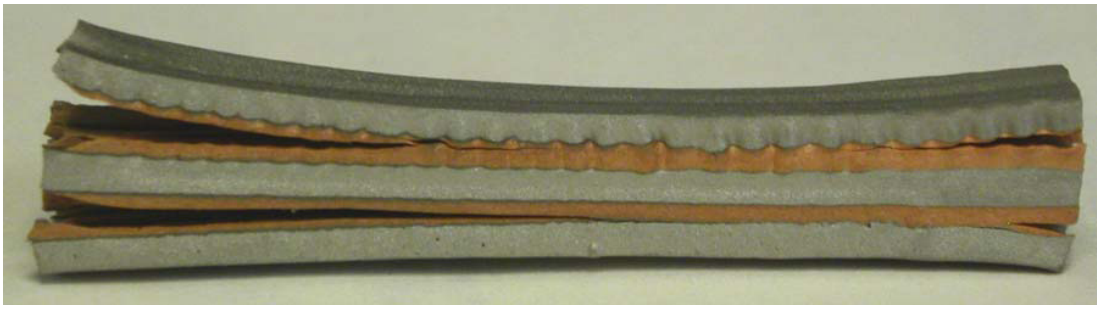

Figure 2.6 Showing de-lamination due to differences in CTE during cooling from sintering temperature[126].

Previous studies[14, 127, 128] modelled the stress-strain behaviours of SOFC using the thermo-plastic and thermo-elastic properties of components during start up, steady state and cooling. The objective was to compare material composition and geometry with the behaviour of components at high temperature. They found that residual stresses in planar SOFC were low, principally because most planar cells were electrolyte supported and were only constrained by thin anodes and cathodes when they expanded during start-up. Also, Eiselel et al[126] found that the intimate contact between metal and ceramic components at high temperature can result to plastic deformation in the metal phase, causing degradation in performance.

2.9.2 Stresses Occurring during Operation

SOFC undergo several transient conditions during their operation, these conditions include varying electrical loads and temperature. These transient conditions have the capacity to affect the performance of SOFC during operation. The factors which affect SOFC during operation include: Thermal Shock (due to rapid start-up), fatigue (due to cycling or long operating periods), mechanically applied stress (due to constraints from other cell components), thermally induced stress (due to thermal gradients from electrochemical reactions), residual stresses and CTE mis-match. Thermal stress induction due to CTE mis-match cannot be eliminated completely in SOFC because of the composite nature. Such stresses can cause delamination and micro-cracking in electrode interfaces leading to performance degradation and eventual failure. Thus, a comprehensive thermal stress analysis might be required to evaluate this phenomenon.

Montross et al[129] studied the thermal stresses due to CTE mis-match in ceramic components with the view of evaluating their effect on the strength of the components. They put forward an approach to predict the allowable CTE mis-match for a reliable and durable SOFC. Their study was based on the zirconia electrolyte which they identified as the major structural component; they found that the difference in CTE between other components and Zirconia must be less than 1%.

Also, Zhang et al[128]developed an analytical model to predict the residual stresses in YSZ based SOFCs. They found that the major principal stresses in the anode are tensile

while they are compressive in the electrolyte and cathode. It was also reported that the anode failure probability decreases with an increase in anode thickness and a decrease in electrolyte thickness. It was concluded that to keep the anode failure probability below 1 X 10^{-6}, the anode thickness should be greater than 700µm with and electrolyte thickness of 10µm and cathode of 20µm.

Selimovic et al[17] also developed a tool for the assessment thermal stresses and electrochemical performance of planar SOFC during start-up, steady state and shutdown. The steady state and transient profiles generated were entered into a finite element code to predict the thermal stresses in the cells. The failure criterion adopted was based on the strength of the components and the principal stresses developed by the thermal loading.

The thermal stress models[17, 128, 129] discussed above, provide only an oversimplified view of the problem. In [17] for instance, attention was paid to the evaluation of thermal stresses in the individual layers of the PEN structure without considering the structural interaction between the three components and changes due to sintering at high temperature, temperature gradients etc. Also, [128, 129] failed to consider the interaction of PEN with interconnects and sealants. In practical SOFC operations, the interactions are complex, thus more factors need to be considered during analysis.

A more comprehensive thermal stress model which took into consideration most of the important parameters was developed by Chih Kuang-Lin et al[130]. Finite element

analysis was used to characterize the thermal stresses at various stages. The parameters used to develop the model included the PEN assembly, interconnects, nickel mesh and gas tight glass-ceramic seals. The effects of temperature gradients, CTE and viscous behaviour in the glass-ceramic sealants were also characterized. It was found that the thermal expansion of the metal interconnect/frame had a greater influence on the thermal stress distribution of the cells than the glass-ceramic sealings.

Another study which investigates the thermal stresses in anodes supported SOFC is [131] in which numerical as well experimental techniques were used. The residual stress of the anode supported electrolyte was found to be 650MPa (compressive) at room temperature, and 240MPa (compressive) at 800°C. The stress in the anode was found to be tensile with a value of 4MPa at room temperature and 2MPa at 800°C.

2.10 Degradation Phenomena in SOFC

The degradation of electrodes, electrolyte and interconnecting materials in SOFC has remained a major problem to their commercialization. Cell degradation becomes accelerated after long periods of operation especially when cycling is performed. This has led several researchers to look for alternative materials which can diminish degradation. However, what remains clear is that a good understanding of the degradation pathways in SOFC is critical in the search for degradation resilient materials.

The most common cause of degradation in SOFC is the mis-match of the coefficients of thermal expansion (CTE) between the different layers of the cell. This difference in CTE becomes a major issue during start-up and shutdown (thermal cycling); this can lead to de-lamination or micro-cracking in extreme cases.

Another factor of degradation is the generation of thermal gradients due to the un-even thermo-dynamic reactions that occur in the TPB of the cells. The release of large amounts of thermal energy in different sections of the cell is likely to accumulate thermal stresses which are capable of weakening the bonds of the material.

Additionally, the formation of a less electrically conductive chromium oxide layer on the electrode (cathode) and interconnect surfaces is also known to increase the cells ohmic resistance.

Further more, the ageing of the electrodes due to long operational times at elevated temperature is also a factor in causing electro-chemical performance degradation. Since the electro-chemical combination of the fuel and oxidant occurs in the porous electrodes i.e. the TPB layer- which can extend a few microns into the anode, any degradation mechanisms that affect the electrode micro-structure can cause catastrophic effects to the electro-chemical performance of the tubes. The common instances of micro-structural degradation include;

- Sintering of the Ni/YSZ phase – this occurs due to the extreme mobility of Ni particles at high temperature, thereby decreasing the electro-active area and porosity of the tubes[132-136].

- Carbon deposition – Ni being a coking catalyst promote this reaction. Solid deposits of carbon become deposited on the anode, thereby compromising the porosity, electro-active area and structural integrity[137-139].

- Sulphur poisoning of the anode – this occurs when there are traces of sulphur in the fuel stream. Sulphur present in the form of H_2S can become absorbed on the Ni surface as a monolayer thereby blocking electro-active site. However, the sulphur desorbs upon re-introduction of a sulphur free stream, making it reversible at low concentrations[140-143].

- Poisoning of the cathode with chromium oxide/compounds – this occurs mainly when steel interconnects are used. Chromium products become deposited on the cathode from the interconnect, leading to loss of electro-active area. This has been reported extensively in literature[144-147].

Summarily, the study of SOFC degradation and durability is key to their commercialization. Previous researches done are shown in the table 2.1 below.

Research Group	Researchers	Field of Study	Reference
Tokyo Gas	K. Fujita et al	Interconnect oxidation	[148]
EPFL	D. Larrain, J. van Herle, D. Favrat	Interconnect oxidation	[149]
Illinois institute of Technology	Y. Hsiao, R. Selman	Electrode de-lamination	[42]
Fuji Electric	T. Iwata	Nickel Sintering	[150]
University of Calgary	S. Paulson, V. Birss	Chromium Poisoning	[151]
FZ Jülich	E. Konysheva et al	Chromium Poisoning	[152]
Risø Nat. Lab.	A. Hagen, R. Barfod, P. Hendriksen, Y.	Delamination & Anode poisoning	[153]
Korea Inst. Of Energy Reserch	Jong-Hee Kim, Rak-Hyun Song	Interconnect degradation	[154]
Colorado School of Mines	W.G. Coors, J.R. O'Brien	Electrolyte degradation	[155]
University of Calgary	Natasha Galea, Tom Ziegler	Sulphur Poisoning	[141]

Table 2.1. Previous researches done on the degradation of SOFC

2.11 Cycling of SOFC

Cycling is inevitable during typical SOFC operation, because of the transient conditions that exist during start-up, steady state and shutdown. Degradation can increase progressively with an increase in the number of cycles[156, 157]. Three types of cycles exist during SOFC operation: Thermal cycling, electrical load cycling and redox cycling. Redox cycling is known to have the greatest deleterious effect, with one cycle capable of causing severe cracking and de-lamination in PEN[158]. It is a rule of thumb during SOFC fabrication to find the optimum composition which will minimize degradation due to cycling. Cycling is also known to be dependent on the membrane architecture and design[157], tubular SOFC show more cycling resilience compared to planar SOFC because of their architecture which allows for uniform heat transfer axially as well as radially[159]. The effects of cycling have been reported previously in [160-162], but require further elucidation.

2.11.1 Electrical Load Cycling

During load cycling the cell is loaded electrically in a cyclic manner. The cyclic loading of SOFC is a natural phenomenon in most SOFC application, e.g. CHP and stationary power generation units etc. In these applications, the power consumption at anytime depends on the consumers. In the UK, morning periods between 06:30 – 08:30hrs and evening periods between 18:00 – 20:00 are the period for the highest energy demand and consumption in households because of the lifestyle of customers. During this period, the power demand (load) is at its highest, compared to other periods in the

day when the energy demand per household is relatively low. Such cycles between peak power demands and low demands can have adverse effects on fuel cell durability. The main degradation caused by load cycling in SOFC is electrode ageing; a phenomenon which significantly increases the resistance of the electrodes.

Bujalski et al[157] studied the transient behaviour of the integrated planar (IP) Rolls Royce Fuel Cells Systems (RRFCS) tube under load cycling. The project was part of the REAL-SOFC project, an EU project aimed at solving the generic problem of ageing with planar SOFC. 93 electrical load cycles were performed with marginal degradation in performance; however a slight increase in electrode resistance was observed which was attributed to electrode ageing, see Figure 2.7. Other studies on electrical load cycling of SOFC [42, 163] used standard experimental techniques (AC impedance spectroscopy) to analyse the electrode ageing mechanisms. The effect of electrical load cycling on SOFC is minimal compared to other forms of cycling; whether thermal or redox.

Figure 2.7. The Advanced Measurements Instruments rig, used for the electrical load cycling of RRFCS integrated planar SOFC.

2.11.2 Thermal Cycling

This is the most common form of cycling that most SOFC undergo on a frequent basis during their operational period. It involves a cyclic change in temperature, usually between room temperature and operating temperature. This is typified by start-up, steady state and shutdown operations. The effect of thermal cycling can be devastating or marginal[158], depending on the SOFC geometry and design architecture. Tubular and micro-tubular SOFC have been reported to have greater thermal cycling resilience than planar or integrated planar tubes, reason being that their tubular geometry makes it possible for uniform radial and axial heat distribution. Figure 2.8 shows the *Adelan®* micro-tubular SOFC demonstrator which has performed over 500 thermal cycles. The typical start-up times of micro-tubular SOFC from

ambient temperature to operating temperature (800°C) is < 1 minute as against > 2 hours for typical planar architecture. Ramping rates of 200C/min and 80°C/sec have been reported for micro-tubular SOFC while that of the RRFCS IP SOFC is 15hrs [158].

Figure 2.8. The *Adelan®* SOFC demonstrator which has performed over 500 thermal cycles.

Thermal cycling damages SOFC by causing differential expansion and contraction in the PEN. The different materials which compose the PEN each expands by the index of its CTE during ramp up and contracts by the same during cooling down. Expansion and contraction have damaging effects on SOFC especially at the material interfaces leading to stress accumulation and eventual failure. During thermal cycling, the whole sample expands or contracts relieving some internal stresses as against an expansion by only one component (anode) as in the case of redox cycling. The effect of thermal cycling can be minimized by closely matching the CTE of the components.

Previous studies on thermal cycling[164-166] performed only a few thermal cycles and failed to consider the contribution of other factor like sintering and temperature gradients to degradation during thermal cycling.

2.11.3 Redox Cycling

Redox cycling is the most damaging of the three cycling types discussed, it has the capability of utterly damaging SOFC anodes by causing gross cracking and de-lamination. Anodes based on Ni/YSZ are most susceptible to re-oxidation because of the high catalytic activity of Ni with oxygen[167]. Unlike thermal cycling where there is bulk volume displacement in the whole SOFC due to change in temperature, redox cycling affects SOFC anodes only. Since the expansion occurs in the anode only, the anode-electrolyte interface is under severe stress due to the constraint of the electrolyte.

Typical SOFC anodes are cermets of Ni/YSZ; with the onset of oxidation, the Ni/YSZ cermet is converted to NiO/YSZ causing expansion in the anode. Similarly, reduction causes the NiO/YSZ cermet to be converted to Ni/YSZ causing shrinkage and inducing stress. This cyclic expansion and contraction in the anode will lead to micro-cracking and delamination[104]. Non Ni based anodes of semi-conducting ceramics e.g. ceria are not plagued by redox effects, but they lack the high catalytic activity that Ni-based anodes posses[168, 169].

In [104], the result of 52 redox cycles performed on micro-tubular SOFC is reported. A slight decrease in performance is reported after each cycle; a degradation rate of 0.3%

per cycle was observed. The degradation per cycle during thermal cycling and electrical load cycling is lower than compared to redox cycling. One redox cycle was reported to cause catastrophic cracking in the *Forschungszentrum Julich* cells reported in [158]. The redox tolerance of Ni/YSZ anodes is one of the parameters considered during SOFC design and fabrication. Compositions which can tolerate redox cycling, as well as provide optimum electro-catalytic performance is sought after.

David Waldbillig et al[170] studied the redox kinetics of Ni/YSZ anodes by thermo-gravimetry (TGA) and thermo-mechanical analysis (TMA) between 450°C and 800°C. They found that there was no bulk volume change in coarse Ni/YSZ sample after re-oxidation or reduction because the expansions and contractions were accommodated in the pores of the structure. Fine samples however, did not change in volume after reduction but expanded between 0.9% -2.5% after re-oxidation, with some cracks propagating in the structure. The cracking was reduced considerably by lowering the Ni content in the anode. They also found that reduction of NiO/YSZ followed first order kinetics with activation energy of 78kJ/mol, while re-oxidation of Ni/YSZ followed parabolic kinetics at temperatures lower than 700°C; activation energy of 87kJ/mol was calculated. From this, it can be inferred that redox effects are dependent on the grain size of the anode particles. Coarse particles are less susceptible to redox deformation because they posses large pores which can accommodate such expansions. Fine particles on the other hand are more prone to redox effects because of their tiny pores which cannot accommodate expansion and thus translates to bulk volume displacement.

Redox degradation studies where the anode was re-oxidized under controlled conditions of gas atmosphere and time are reported in [167, 171]. It was reported that degradation progressed steadily with an increase in redox cycling. This is in line with reports where it was reported that each redox cycle causes micro-crack formation which increases the overall anode over-potential due to longer electron paths. Furthermore, delaminations were shown to cause masking zones at interfaces, thus inhibiting ion transfer from the electrolyte to the TPB layer.

Redox cycling is a likely occurrence in SOFC because of emergency system shutdown, leakages in fuel pipes etc, this will lead to physico-chemical changes in SOFC microstructure compromising their integrity and leading to failure.

Chapter 3

Methods and Materials

3 Micro-tube Manufacture and Preparation

Anode supported micro-tubular SOFC 55mm long and 2.3mm in diameter were co-extruded and supplied by Adaptive Materials Inc USA (see Figure 3.1). The tubes were provided already sintered, comprising NiO/YSZ as the anode and YSZ as the electrolyte.

Figure 3.1 Image of the NiO/YSZ tube supplied by Adaptive Materials Inc

The anode was 200µm thick while the electrolyte measured between 15 - 20µm, see Figure 3.2. Cathode formulations were applied and sintered on the tubes in order to convert the raw tubes into functional fuel cells. Subsequently, silver paint and silver wires were used as interconnects to help with electron transfer. The cathode preparation technique is discussed in greater detail in the following section below.

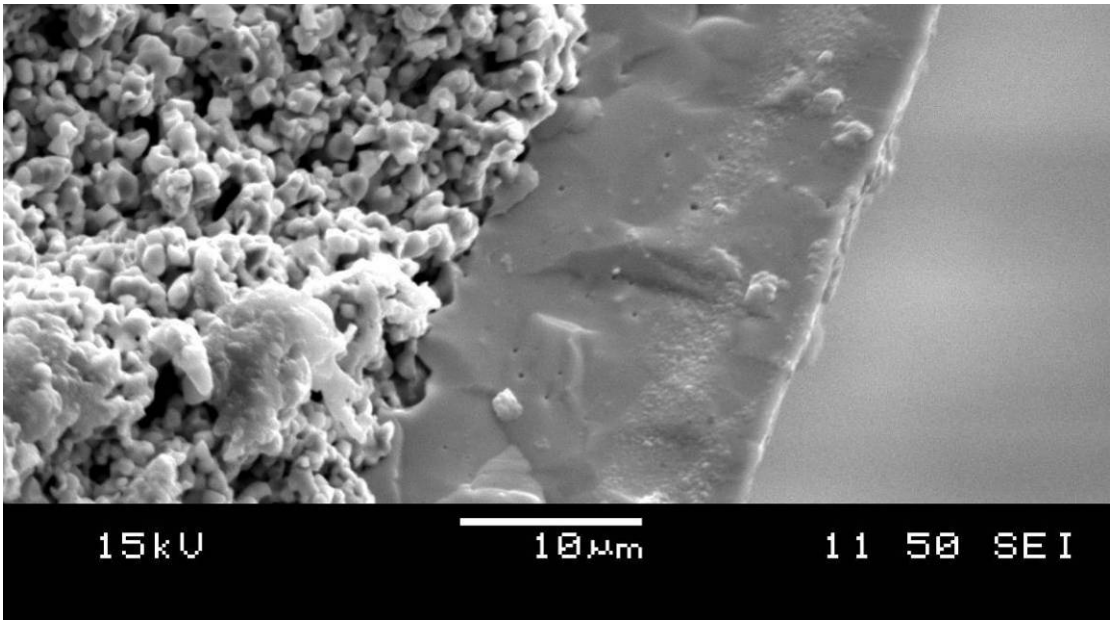

Figure 3.2. The micro-structure of the tube

3.1 Cathode

The cathode was necessary to provide adequate reaction sites for the electrochemical reduction of oxygen to its ions. The porosity, tortuosity and pore sizes were taken into consideration in order to produce an optimized cathode layer. To do this, two distinct cathode layers were synthesized; (a) a 50%/50% – LSM/YSZ layer and (b) 100% – LSM layer. The powders of the two mixtures were weighed out and mixed in separate bottles according to the compositions specified in table 3.1 and acetone was used as the mixing solvent. The two compositions were then milled in a vibro-miller for 24 hours after which 2 grams of Terpinol was added into the 100% LSM mixture followed by additional vibro-milling for 10 minutes.

Ingredient	50%/50% – LSM/YSZ layer	100% – LSM layer
LSM (Merck 0.82/0.18)		20g
LSM (SSC 0.5/0.5)	6.5g	
TOSCH (TZ8Y)	6.5g	
KD2	0.25g	0.4g
Acetone	16ml	14ml
Glycerol Triolate Triolein	0.2g	
Mill beads	13 beads	16 beads
Terpinol (24hrs later)		2g

Table 3.1 The compositions for cathode formulation

The cathode formulation is followed by painting on the raw tubes. About 30mm of the 50%/50% – LSM/YSZ cathode ink is painted on the raw tubes and allowed to dry under atmospheric conditions for 24 hours. This is followed by painting the 100% – LSM cathode ink on the previously painted 50%/50% – LSM/YSZ ink with 12hrs drying time. The painting of the cathode layers was centred (see Figure 3.3) so as to provide allowance for the fuel injector on which the fuel cells are suspended.

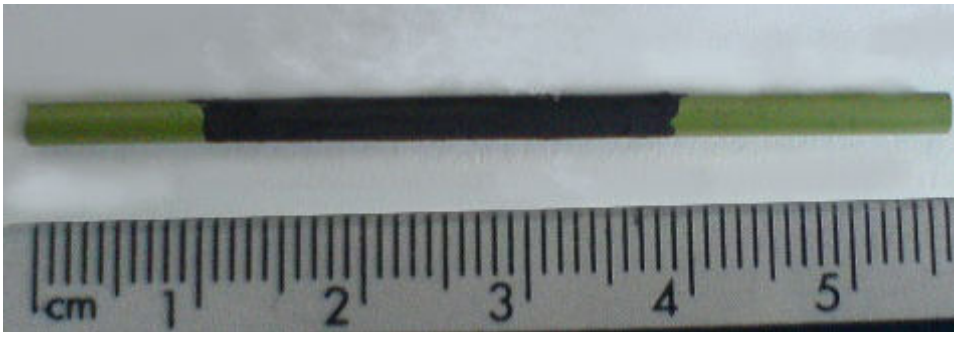

Figure 3.3. Showing a micro-tube with cathode applied.

The painted cells were sintered in a Carbiolite™ furnace under a programmed temperature profile as shown in Figure 3.4. Four distinct stages were undertaken during the sintering process as seen by the dotted red line (temperature profile), the first stage consisted of a slow ramp up at 1.5°C/min to 500°C during which the binder and solvent were burnt out. The second is the rapid ramp up at 12.5°C/min to the sintering temperature. The third phase was the sintering at 1150°C for 2 hours in order to adhere the two cathode layers. The final phase was the cooling at 20°C/min to room temperature, it should be noted that the micro-tubes are very robust which is why they can be cooled at this high rate, other fuel cell geometries are not able to withstand such rapid cooling[158].

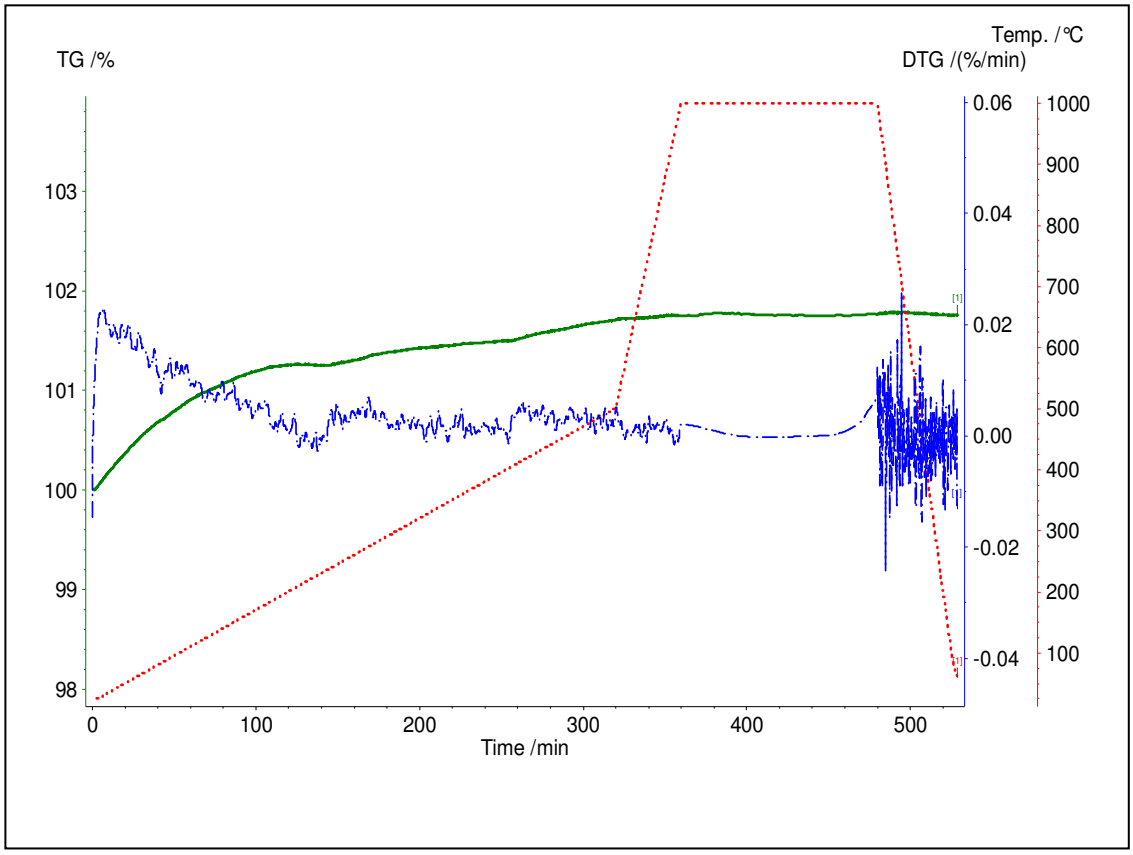

Figure 3.4. Sintering profile for the micro-tubes

SEM characterization of the sintered layer showed a cathode thickness of approximately 50µm, see Figure 3.5. The hand painting of the cathode does not give a uniform microstructure due to natural imperfections; this makes the cathode thicker in certain areas and thinner in other. However, the difference in performance between cells prepared in this manner was not significant.

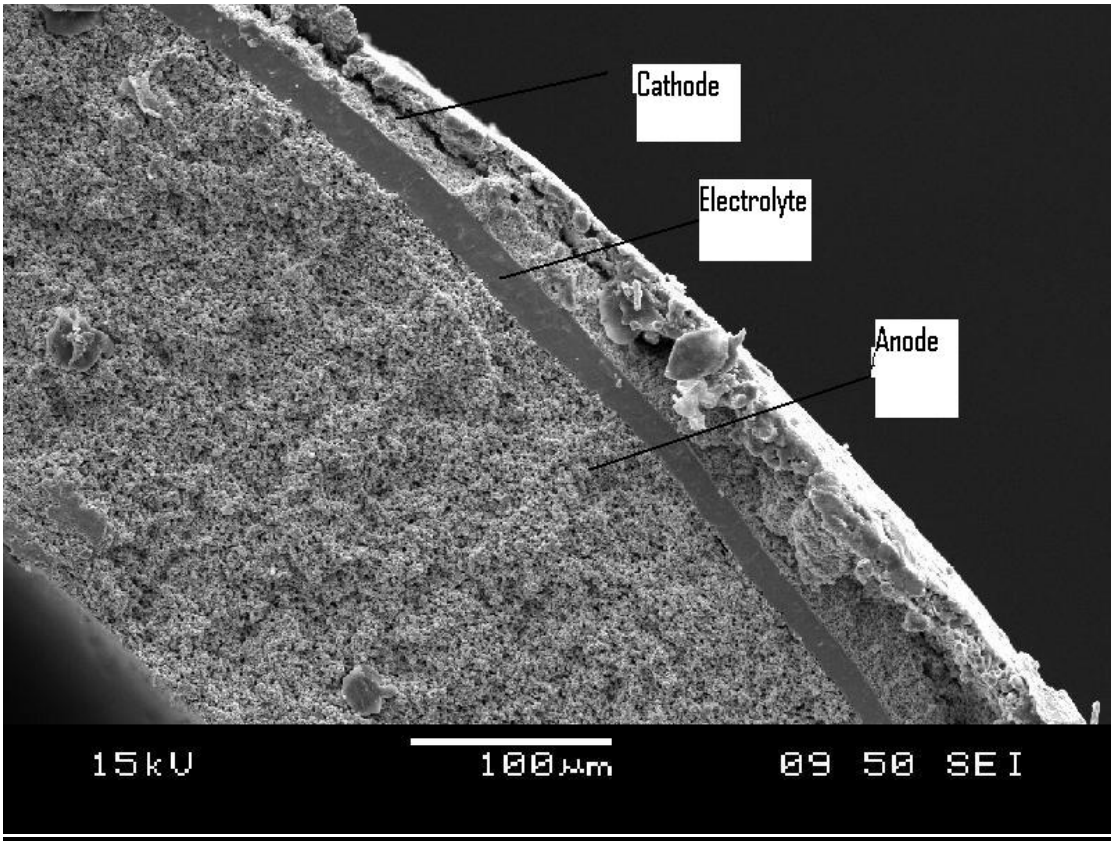

Figure 3.5. SEM of a micro-tube microstructure

3.1.1 Cathode Interconnection

Silver ink (Alfa Aesar) was used to improve the electrical conductivity of the cathode; it was painted in four rings along the circumference of the micro-tube with one long stripe connecting the four bands, see fig.3.6. The silver rings were made as thin as possible so as to minimize masking the cathode area with silver paint. Approximately 40% of the cathode area was covered by the silver paint. Subsequently, silver wire (Good fellow 99.9% pure, 0.25mm diameter) was wound firmly around the silver bands for current collection. The length of the silver wire used was 50 cm.

The silver wires were wound four times on each silver ring and then carefully twinned along the stripe line to the next ring. Passing the wire along the stripe line helped to maximize the cathode area for effective oxygen reduction reaction. About 10 cm of silver wire was left un-twined for attachment to the potentiostat.

3.2 Anode

Initially, Nickel mesh (Dexmet microgrid) was inserted into the micro-tube and held in place by Ni pin. This proved to be ineffective as the Ni mesh became loose at high temperature, leading to increased contact resistance. For the bulk of this study however, the anode current collection was achieved by carefully polishing off the thin electrolyte, with the aid of a fine abrasive files to expose the Ni surface. Approximately 7mm was polished off one of the ends of the micro-tube and care was taken not to exert too much force as the cells were quite brittle. Subsequently the Ni surface was wiped off with clean cloth to remove the abrasive sediments and silver ink was painted so as to enhance conductivity between the silver wire and the Ni anode, see Figure 3.6. The painted silver was allowed to dry for 6 hours and then silver wire was wound around it. The silver wire was wound around the whole painted section for maximum contact and approximately 10 cm of wire was left unwound for connection to the potentiostat.

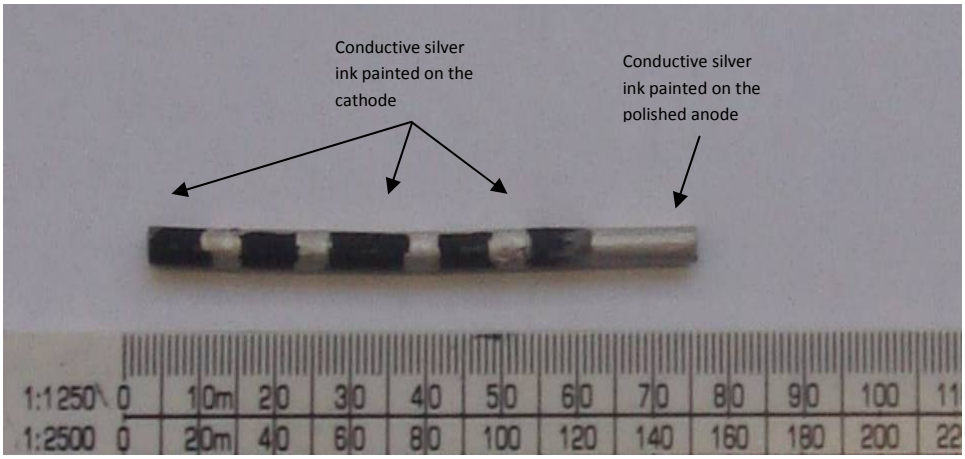

Figure 3.6. A micro-tube with silver ink painted on the anode and cathode for interconnection.

3.2.1 Anode Reduction

Reduction of the cells proceeded after the sintering of the cathode layers. This was performed by passing 20ml of nitrogen through the cells and ramping up the furnace at 200°C/min to 750°C. Once at the reduction temperature (750°C), hydrogen was passed and the cell was held for 45 minutes until complete reduction was achieved. After reduction was achieved, the cell was cooled back to ambient temperature with the hydrogen still flowing at the rate of 120°C/min.

3.2.2 Anode Current Collection Technique

Two methods of collecting current from the anode were explored; the first ('Ni mesh-and-pin' technique) was based on a Ni mesh structure which is inserted into the anode side to be in intimate contact and provide interconnection. The second was a direct current collection technique from the anode where a portion of the anode was polished to provide a contact point. The two methods are discussed below.

3.2.2.1 Internal Nickel 'Mesh-and-Pin' Interconnection Technique

A standard Ni 'mesh-and-pin' structure was used as the anode side interconnect. The Ni mesh (DexMet Micro-grid) was cut to 1.2 times the length of the micro-tube and rolled to the tube's diameter (2.3mm). The length of the Ni mesh allowed for a small percentage of the mesh to extend on the exterior of one of the tube ends for interconnection. While the commensurate diameters between the mesh and the micro-tube allowed for sufficient contact between the anode and the mesh. After the insertion of the Mesh, a 2.3mm wide Ni pin (Micro-metallic) was inserted into the Ni mesh structure to hold it in place. Previous researchers who have employed this technique include, [113, 172-182]. **Figure 3.7** shows the Mesh rolled up and ready for insertion, while **Figure 3.8** shows the micro-tube with the mesh in place.

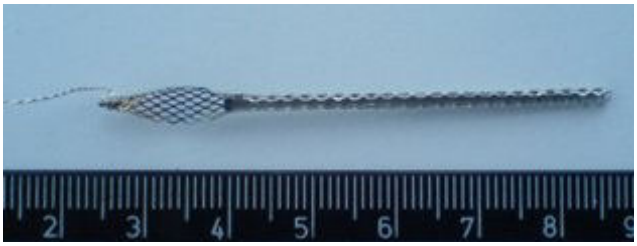

Figure 3.7 Showing the Ni mesh structure

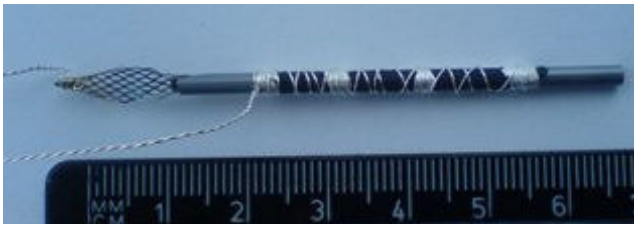

Figure 3.8**.** Showing a micro-tube with the Ni mesh inserted

Figure 3.9 shows the electro-chemical performance of a micro-tube with this current collection technique. An initial high power density is observed at 0.65W, this high polarization curve is likely to be due to the several advantages of the Ni mesh in providing (a) extra surface area for fuel oxidation (b) adequate mixing by serving as a fuel baffle (c) acting as a heat sink. However, this high value was only sustained for short periods as degradation due to loose contact between the mesh and the anode set-in, thus increasing the contact resistance and causing performance drop. Also, the total cost of tube manufacture was significantly increased by using the Ni mesh.

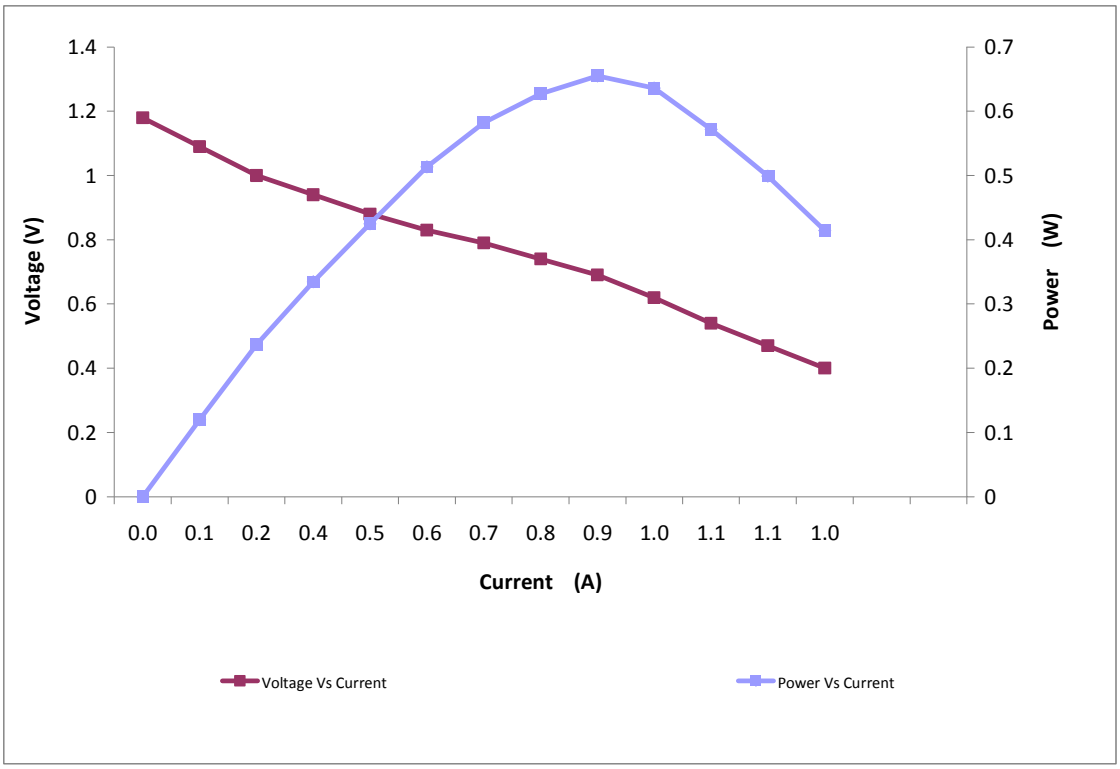

Figure 3.9. The power curve after 3 minutes of a micro-tube operated with mesh-and-pin interconnection.

The loose contact between the anode and the Ni mesh made it impractical for long-term operation because the cells failed constantly. The modes of failure were unpredictable and erratic; sometimes the micro-tubes failed abruptly and at other times they degraded gradually over a few hours. Repeated testing of the micro-tubes showed inconsistent behaviours as shown in **Figure 3.10** and **Figure 3.11** below.

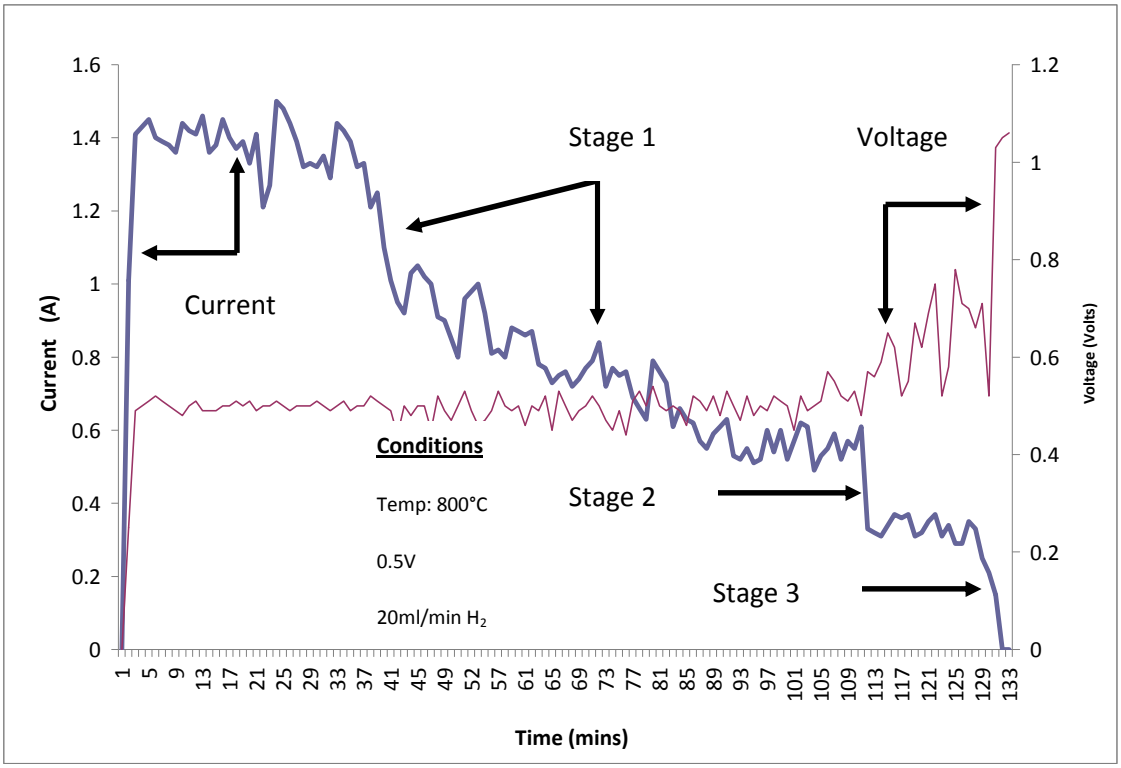

Figure 3.10. Showing a graduate decrease in performance when a mesh and pin structure was used.

From **Figure 3.10**, degradation is seen to occur in three stages. In stage 1, the electrochemical performance is seen to decrease gradually from its initial peak value of 1.42A to 0.6A in 60 minutes; a degradation rate of 57.7% is calculated for this stage.

In stage 2, an abrupt decrease in performance is observed from 0.6A to 0.25A; a degradation rate of 58.3% is calculated for this stage. The final stage is the cell failure point where the cell performance decreased from 0.25A to 0.

The high current (1.42A) observed at the commencement of the experiment might have been because of the numerous advantages of the Ni mesh as stated above (i.e. extra surface area for fuel oxidation and fuel baffle). At the commencement of heating, the Ni mesh-and-pin structure would expand steadily by virtue of the increase in thermal energy and it would be in adequate contact with the Ni anode, thus minimizing contact resistances. From Figure 3.10, it is seen that this high current was sustained for about 35 minutes until a drop in performance was observed, this decrease might be related to the severe sintering in the structure. The mesh-and-pin structure being almost wholly Nickel would sinter at a higher rate than the anode which was a cermet of Ni/YSZ. Thus, the first stage of degradation might be due to this phenomenon. With sintering in progress, a steeper degradation curve is seen which gradually levels off when the mesh-and-pin structure and the anode found a temporary optimum contact position. This equilibrium was maintained for 20 minutes until the next stage of degradation kicked in. The second stage of degradation was characterized by an abrupt decrease in performance which is attributed to a shift in the equilibrium contact position between the mesh-and-pin structure and the anode. This sudden drop in performance can be a consequence of several degradation mechanisms including, further mesh-and-pin sintering, anode sintering or mesh dislodgement. Isolating a single degradation mechanism from a set of mechanisms is

difficult, because in reality these mechanisms occur concurrently. The final stage of degradation was characterized by further drop in performance which might be due progressive sintering, in which case the contact resistance would increase significantly due to the loose contact. This loose-contact problem made long term testing difficult and the actual degradation of the tube components due to electrode ageing and electrode sintering could not be characterized. SOFCs are usually made for applications where long term operation is required like CHP units which should have a life normal lifespan of between 40,000 and 50,000 hours as such durable testing is imperative.

Figure 3.11 shows further erratic behaviour as another micro-tube is tested with the mesh-and-pin technique. The electrochemical performance degradation is seen to proceed in two stages; stage 1 sees a sharp drop in performance from a current of 1.39A to 0.34A; giving a degradation rate of 78.5%. In stage 2, the tube degrades rapidly from 0.3A to 0 after maintaining at 0.3A for 65 minutes.

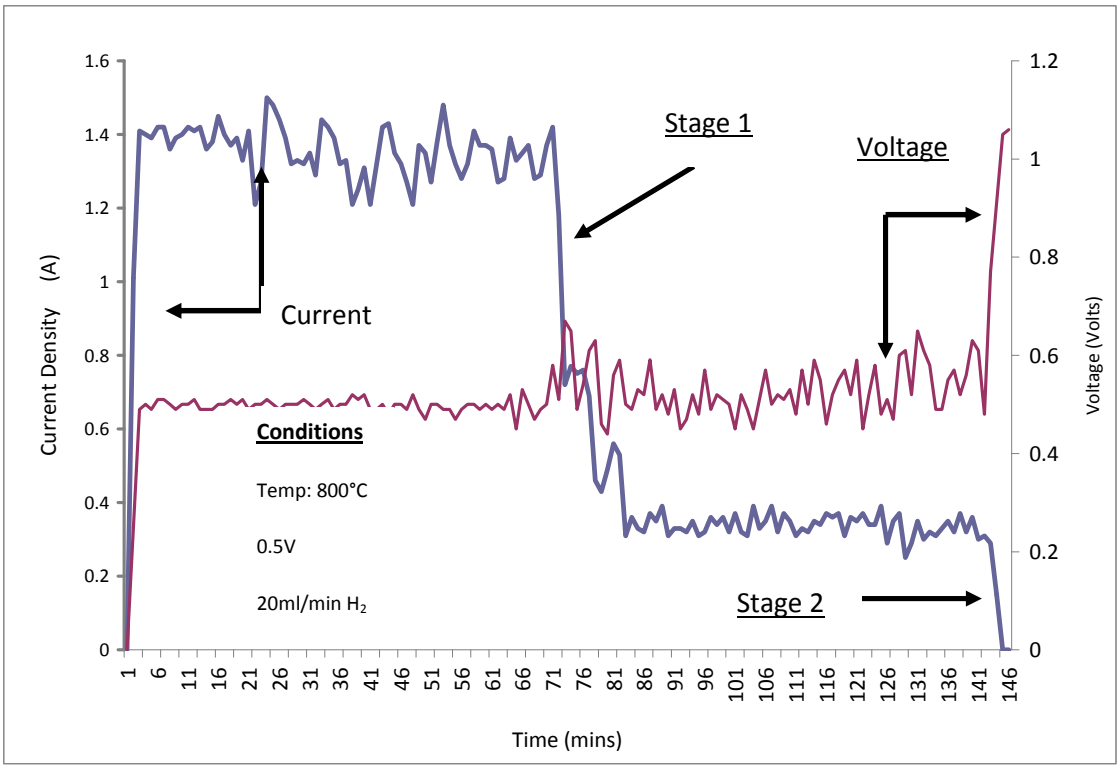

Figure 3.11. Showing abrupt decrease in electrochemical performance when mesh and pin structure was used.

At the commencement of the experiment a peak current of 1.39 A was observed for 70 minutes, during this period of sustained peak performance, the Ni mesh structure and the Ni anode were in intimate contact, offering low contact resistance and high electrochemical performance. This is in contrast to the previous case reported in **Figure 3.10**, where degradation was seen to set-in after 35 minutes and carry on progressively. This shows the un-predictable and erratic nature of the mesh-and-pin technique.

The degradation as seen in stage 1 might be due to an increase in the contact resistance due to sintering. As stated earlier, both the Ni mesh and the anode

sintering proceed concurrently giving a complex degradation mechanism. In stage 2 of the degradation, a stable current of 0.3A is observed, this might be due to an equilibrium contact between the mesh structure and the anode. During isothermal operation, the electrodes, electrolytes and the interconnects degrade altogether, but using this interconnection technique it is difficult to analyse the degradation in the PEN. Thus a more stable method where there is steady contact is required.

3.2.2.2 External (Direct) Anode Interconnection Technique

This was a huge improvement over the mesh-and-pin technique. The current was collected directly from the anode; as such the loose contact problem was completely eliminated and no additional costs were incurred as the mesh-and-pin was not required. As reported by Dhir et al [172], the direct current collection technique was achieved by carefully polishing-off the thin electrolyte in-order to expose the anode. The electrolyte polishing was achieved by the use of a fine abrasives file. Silver ink (Alfa Aesar) was applied on the polished anode to provide adequate contact between the Ni anode and the silver wires (Good fellow 99.9% pure, 0.25mm diameter) which collected the current. Each cell was reduced at 750°C in 20ml min^{-1} of hydrogen for 45 minutes and operated at 800°C. Current was drawn at 0.5 V and sustained throughout the experiment. Figure 3.12 is an image of a cell prepared by this technique.

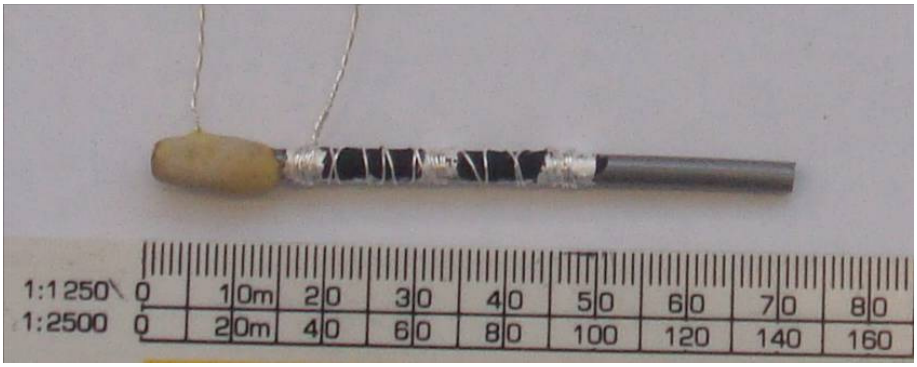

Figure 3.12**.** Showing a cell prepared by external current collection technique

The collection of current directly from the anode enhanced the durability and reliability of the cells, making long term testing and operation possible. The investigation of the degradation of PEN of the micro-tubes was also achievable because any degradation observed in the cell under this circumstance was that of the cell materials and not that of an interconnecting material.

However a few disadvantages plagued this technique including; an increase in the overall ohmic polarization of the anode due to longer electron paths. The current is collected at one end of the micro-tube and because of this the electrons produced have to travel longer paths to the current collection point. Thus, the current was slightly lower than reported for the mesh-and-pin technique. Also, the manual polishing of the electrolyte to expose the anode had a tendency to propagate micro-cracks in the PEN bulk, increasing the failure probability. Because of the reliability of this technique, it was adopted for all subsequent electrochemical testing in this project.

3.3 SOFC Testing and Analysis

3.3.1 The testing rig

Cycling was performed in a setup that comprised a brick furnace with Nichrome ribbons (Advent Ni80/Cr20 1.5mm x 0.13mm) as the heating element. The Nichrome ribbons were wound around ceramic rods which were embedded in the fire brick (see Figure 3.13). Power was supplied to the furnace by *Eurotherm*™ 2404 controller, the controller was fully programmable for thermal cycling or other temperature profiles.

Hydrogen gas was supplied to the tube via a steel manifold. The steel manifold was necessary in order to help in pre-heating the gas before it entered the tube.

A potentiostat was attached to the terminals of the fuel cell for voltage-current measurements. The cell loading was performed via a *labview*™ software which interfaced with the potentiostat, a schematic and picture of the cycling rig is shown in Figure 3.14 and Figure 3.15. Also, a K-type thermocouple was situated close to the cell in order to control and monitor the cell temperature.

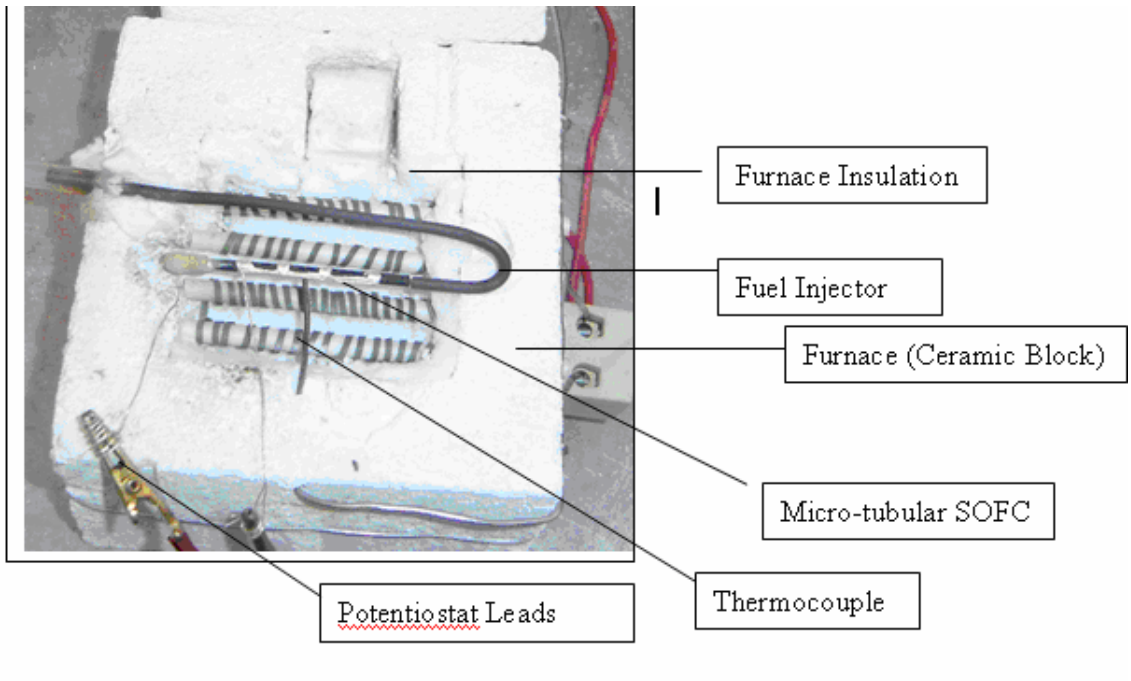

Figure 3.13. Brick furnace used for SOFC testing

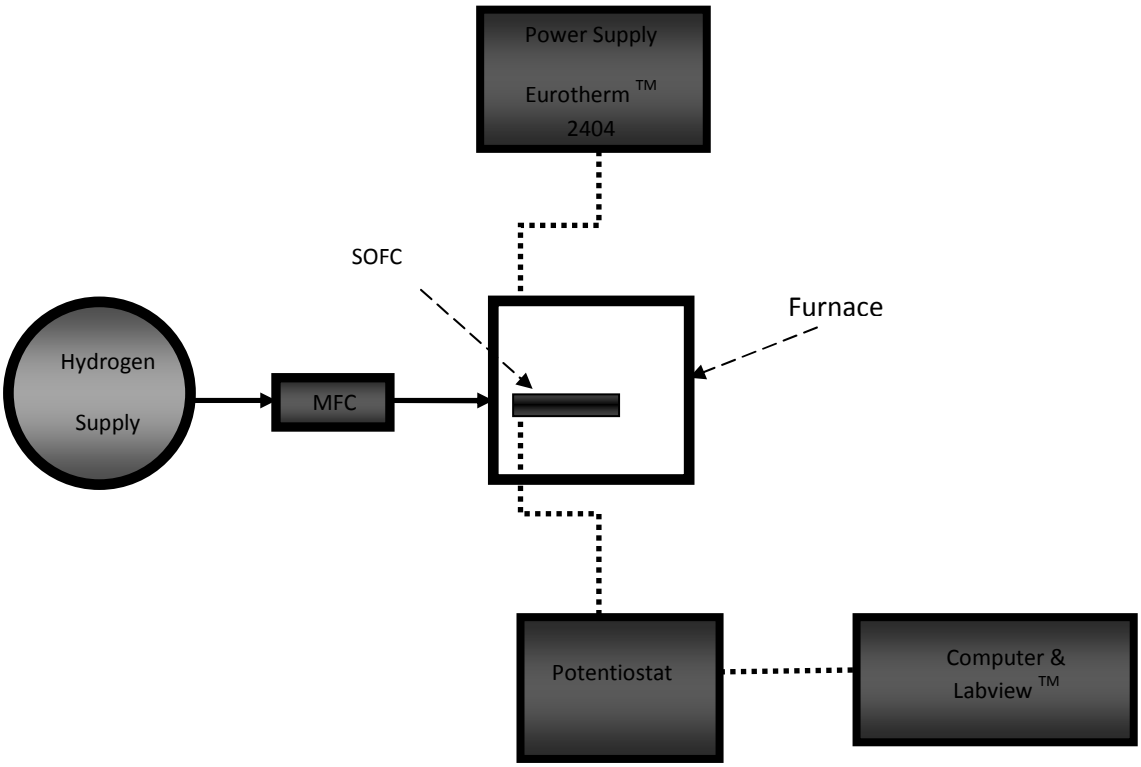

Figure 3.14. Schematic of the test rig

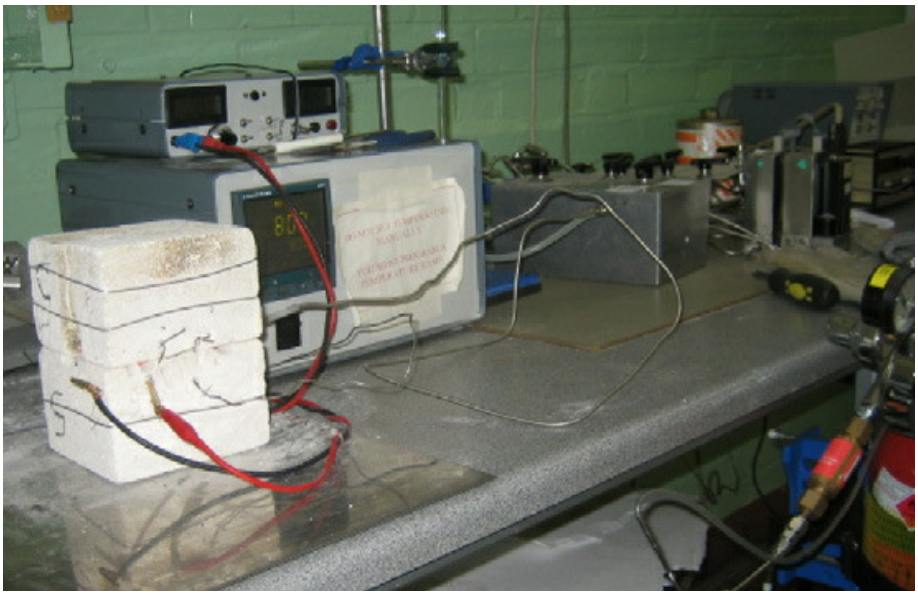

Figure 3.15. The cycling set-up

3.3.2 Isothermal operation Test

Iso-thermal ageing of the tubes was performed by raising the tubes to the desired temperature (this was varied) in 20ml/min of hydrogen. Once at the desired temperature, the tube was held at constant temperature while current was drawn at 0.5V for the duration of the experiment. The degradation was characterized in terms of decrease of electro-chemical performance with time.

3.3.3 Electrical load Cycling

Electrical load cycling was performed by heating the cell to 800^{o}C in hydrogen at a constant ramp rate. Once at this temperature, current was drawn at 0.5V for 10

minutes and then it was subsequently dropped to 0 (i.e. OCV) and allowed to dwell at this state for 10 minutes before the sequence was repeated 30 times.

It can be seen from Figure 3.16, that the current fluctuated between 0 and 1.2A at OCV and 0.5V respectively. At the end of cycling (30 cycles), a slight degradation of 0.082%/cycle (0.2%/hr) was observed. This degradation index is similar to that observed when only iso-thermal ageing is performed (i.e. when sintering dominates the degradation as seen in **Figure 3.17**). It can be seen clearly that degradation trends are similar. In view of this, the effect of electrical load cycling on the performance of these micro-tubes was adjudged to be minimal. The sintering effect is explained in greater detail in chapters 4 and 5 where iso-thermal ageing of the micro-tubes is performed. The marginal degradation rate observed is in agreement with past findings by Bujalski et al[157], who reported marginal degradation rates over 100 electrical load cycles. Also, a slight increase in temperature (~2°C) was observed at the instance of loading the tube. This was due to the increase in resistance to electron flow when current is drawn. In a large system, such a temperature increase can be significant and can lead to thermal shock, however in this system its effect is ignored due to its small magnitude.

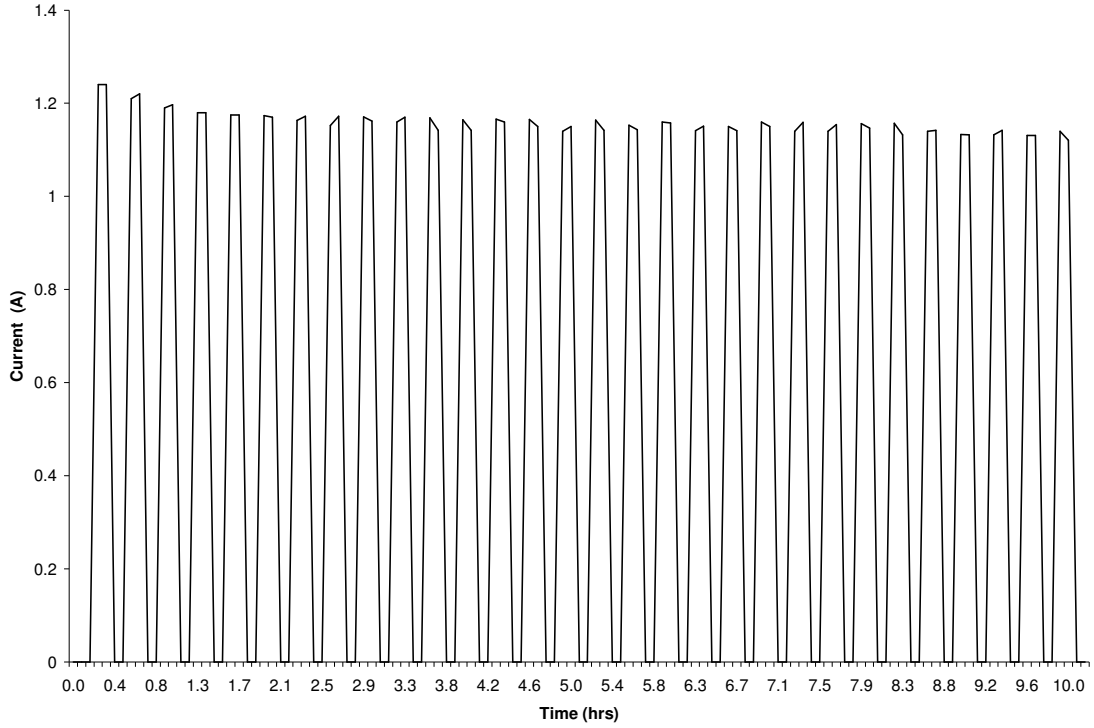

Figure 3.16. The result of electrical load cycling of a micro-tube between 0 and 5V at 800°C

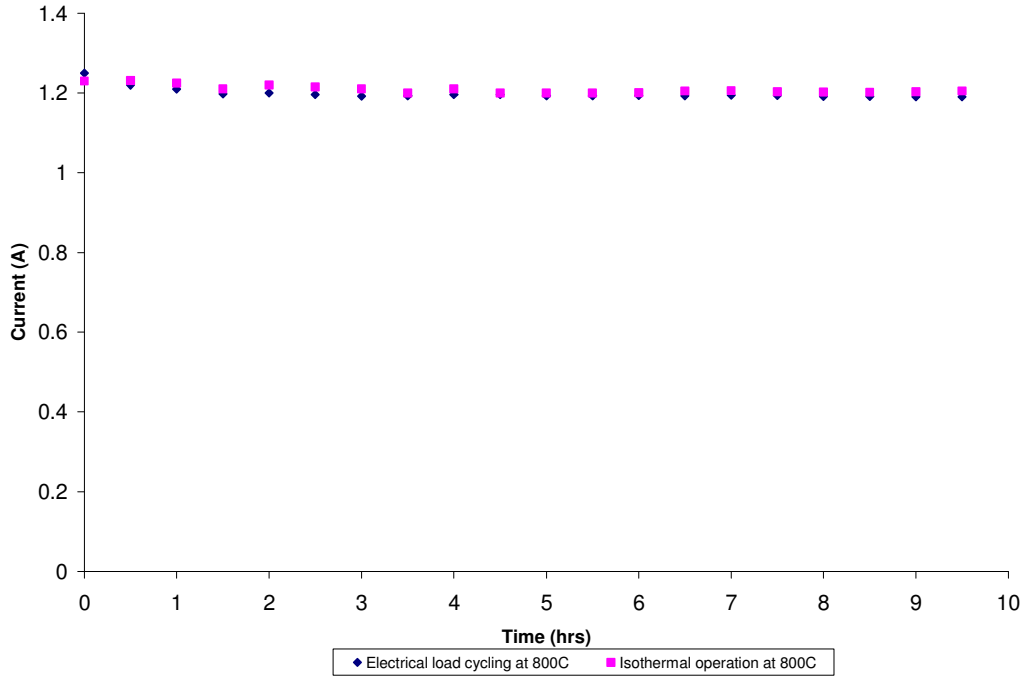

Figure 3.17 Comparison of isothermal operation with electrical load cycling at 800°C

3.3.4 Thermal Cycling Experiments

Thermal cycling was performed in four distinct segments. In the first segment, the micro-tube was raised to the desired temperature (this was varied) at a constant rate in 20ml/min of hydrogen gas. Secondly, the tube was held at this temperature for a specified length of time before being cooled at a constant rate to 200^{o}C. Lastly, it was held at 200^{o}C for a specified length of time before the sequence was repeated again. Current was drawn at 0.5V throughout the experiment.

Also, thermal cycling was performed with a gradient imposed across the tube. This was done by flowing 25% excess (25 ml/min) hydrogen through the tube for combustion to occur at the fuel outlet.

3.3.5 Redox Cycling Experiments

Two different redox cycling test were performed; partial redox cycling and complete redox cycling. During partial redox cycling, the hydrogen supply was shut-off for 3 minutes while the cell was at the target temperature; this was to enable the oxidation of the Ni anode to occur. Only 7% of the anode was oxidized during this period. The hydrogen supply was subsequently turned-on and for 5 minutes for reduction to occur. Current was drawn at 0.5V throughout the experiment. This procedure was repeated several times and the decrease in electro-chemical performance was characterized. Partial redox cycling was performed at 600^{o}C, 700^{o}C and 800^{o}C.

Complete redox cycling was performed by turning off the hydrogen supply for as long as it takes for complete anode oxidation to occur. Reduction was also performed by turning on the hydrogen supply until complete reduction occurred. Complete oxidation and reduction was performed at 600^{o}C, 700^{o}C and 800^{o}C. Degradation was characterized in terms of the decrease in electro-chemical performance. Current was drawn at 0.5V all through the experiment.

3.3.6 Thermal & Electrical Shock Tests

3.3.6.1 Thermal Shock test

Thermal shock analysis was performed on two different types of micro-tubes; anode-supported and electrolyte supported micro-tubes. The anode supported tubes were 2.3mm in diameter, with an electrolyte thickness of approximately 20µm and an anode thickness of 200µm while the electrolyte supported tubes were 2.8mm in diameter, with an electrolyte thickness of 220µm. Both SOFC types were approximately 55mm in length.

Thermal shock was performed by heating the tubes to the shock temperature and holding for ten minutes, before shocking in bowl of water at ambient temperature. The tubes were then dried up and prepared for strength analysis using a three point bend machine. Thermal shock was performed between temperature ranges 100^{o}C - 300^{o}C.

3.3.6.2 Electrical Shock Test

Electrical shock tests were performed only on the anode supported micro-tubes. The tubes were prepared by polishing off the electrolyte on both ends of the tube to expose the anode. Silver ink was then applied on the polished anode surface and allowed to dry after which silver wire was wound around these areas for current collection. Finally, a cement-binder formulation was applied on these ends so as to prevent oxidation of the anode to occur. Figure 3.18 shows a tube prepared in this manner

Electrical shock was performed by pass current through the anode of a micro-tube while using the inherent resistance of the tube to heat it up to the desired temperature. Once at this temperature, the cell was held for a specified time (varied) before the sequence was repeated again.

Also, a constant-temperature-hold-electrical-shock-test was performed where current was passed and the cell was held at high temperature (800^{o}C) until it failed.

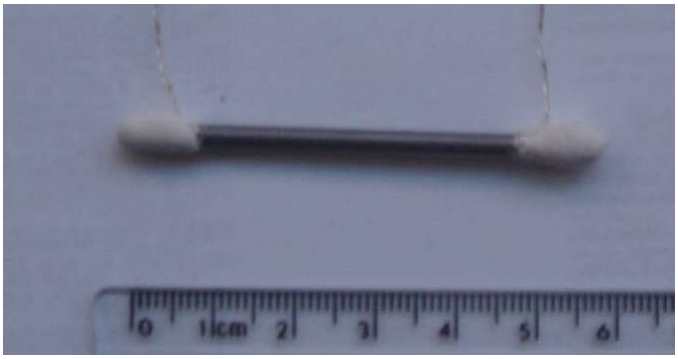

Figure 3.18. Cell prepared for electrical shock testing

3.3.6.3 Strength Test

Three-point-bend-test was performed on the tubes that we previously shocked (both thermally and electrically) in order to determine their strength. The tubes were suspended on a two point contact frame while a third point which was attached to a force sensitive force transducer was lowered on to the middle of the tube by a motor. Force was exerted on the middle section of the tube by the third point until the sample failed; this minimum failure force was measured by the transducer. The force at failure is proportional to the strength of the sample.

3.3.7 Thermal Analysis

3.3.7.1 Dilatometry

Dilatometry was employed in order to measure the thermo-mechanical expansion of the micro-tubes at high temperature; a *Netzsch*™ 402C pushrod dilatometer was used. It comprised a silicon carbide furnace, alumina protective tubes and sample holder. Temperature measurements were achieved using an S-type thermocouple, and the system was calibrated using alumina standards prior to measurement. *Proteus® software* was used to control the temperature programme during which the change in length of the sample is transduced via a pushrod to a linear variable differential transducer system (LVDT). The position of the push rod and therefore the change in length of the sample is registered and converted into electronic signal which is measured as ΔL/L (%).

The system was evacuated and back-filled with nitrogen prior to commencing the experiments. A schematic and a shot of the system are shown in Figure 3.19 and Figure 3.20.

Oxidation experiments were performed by raising the micro-tubes to the desired temperature in 50 ml/min inert atmosphere (Nitrogen) at a specified ramp rate. Once at this temperature, the gas flow was switched to air and oxidation was allowed to occur for certain time duration after which it was cooled down to ambient temperature in air.

Reduction measurements were performed in a similar manner to that of oxidation as reported above; however hydrogen was used in place of air.

Thermal cycling experiments was performed by heating the sample to high temperature and cooling down repeatedly while the expansion and shrinkage were measured with respect to temperature.

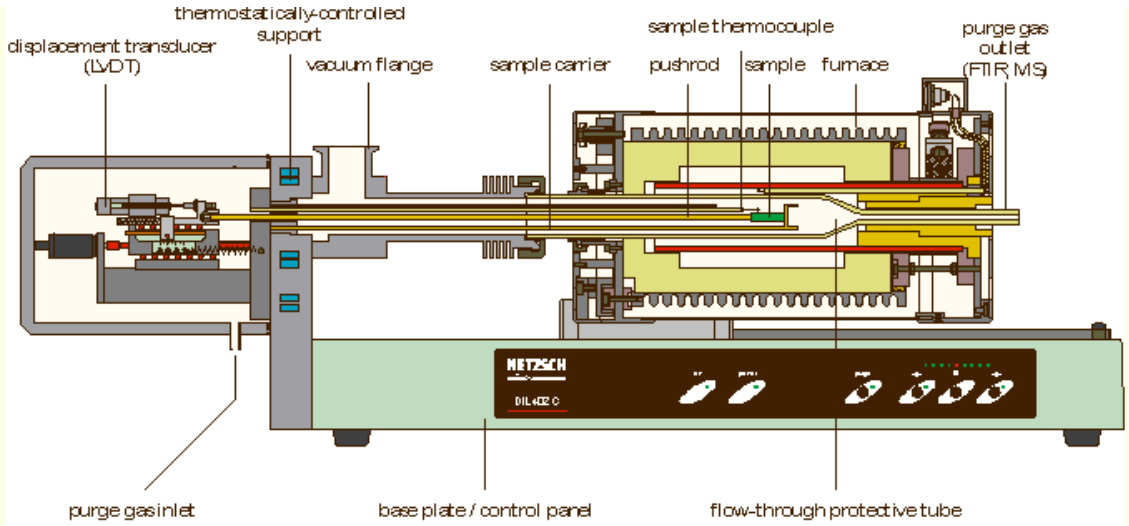

Figure 3.19. Showing the components of the dilatometer

Figure 3.20. The image dilatometer.

3.3.7.2 Thermo-Gravimetric Analysis (TGA)

Thermo-gravimetric analysis was used to measure the weight change of the tubes during oxidation and reduction. It was used to clearly establish the onset and end of these activities. A *Netzsch*® 209 F1 thermo-gravimetric analyser was used, it had a vacuum tight and gas tight design, capable of conducting measurements in controlled sample atmospheres. Alumina standards were used to calibrate the sample prior to measurements. The mass change was made possible by the micro-balance on which the sample holder and sample were suspended. The micro-balance works based on

the principle of electro-magnetic power compensation and is enclosed by a vacuum tight housing. The vacuum housing is thermostatically controlled to avoid temperature influences. The sample holder is located above the micro-balance and is connected to the balance by a sample holder support. A schematic and picture of the system are shown in Figure 3.21 and Figure 3.22

Oxidation was performed by heating the micro-tube to the desire temperature in inert atmosphere (nitrogen) and subsequently using air for oxidation at this temperature. This was followed by cooling to ambient temperature in air.

A similar procedure was adopted for reduction, but hydrogen was used instead of air.

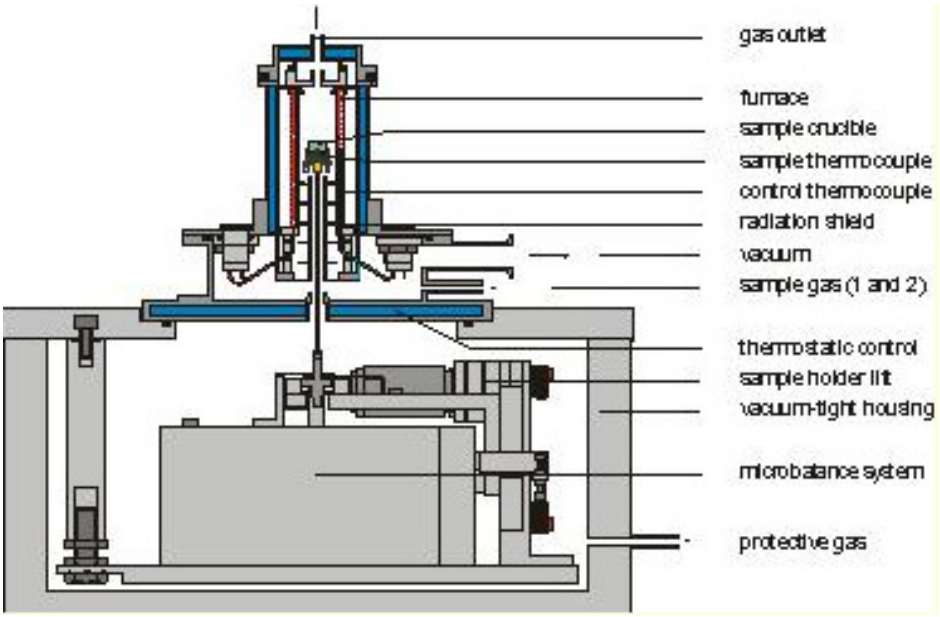

Figure 3.21**.** A schematic of the TGA system

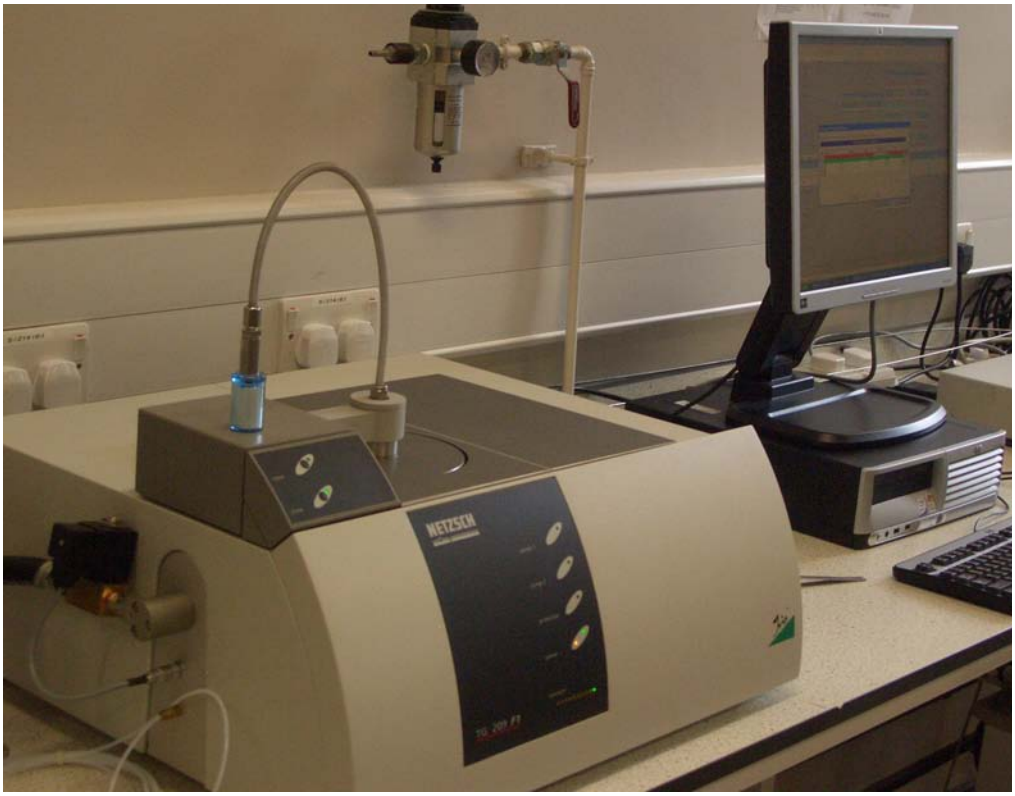

Figure 3.22. A picture of the TGA system

3.4 Conclusion

In this chapter, cell preparation/fabrication has been introduced, methods involved have been discussed and equipments/testing procedures outlined. Having performed all these, the testing and cycling of micro-tubes will be discussed in subsequent chapters. Additionally, the electrical cycling behaviour of micro-tubes was investigated and presented briefly in this chapter. No micro-structural damage or measureable decrease in performance was recorded and its effect was adjudged to be marginal.

Chapter 4

Iso-thermal Operation

4 Objective

The objective of this chapter is to understand the isothermal operation of SOFCs, by investigating the factors that cause degradation at steady state. The theory is that high temperature of operation causes extreme mobility in the Ni structure, leading to Ni agglomeration. Electrochemical measurements have been set up to characterize the decrease in performance during this operation and dilatometery is used to confirm the theory proposed.

4.1 Introduction to Cell Degradation at steady state

The recent commercial requirement of SOFCs is that they maintain a life time of between 40, 000 – 50, 000hrs[183], therefore very small degradation rates are acceptable (less than 1% per 1000hrs based on solid state energy conversion alliance - SECA targets). Durability has been one of the major factors that have plagued and delayed SOFC commercialization. Cell degradation is usually manifested as an increase in the overall resistance of the electrodes and electrolyte, leading to lower operating voltages at constant current. The degradation occurs mainly in the PEN of the cells especially at the electrodes and the interfaces between the components [184]. Degradation at the material interfaces arises due to coefficient of thermal expansion mis-match. This is not uncommon when composite materials like Ni/YSZ are used. Also degradation due to Ni agglomeration is a common problem in SOFC anodes based on Ni because of its tendency to sinter and form a dense structure at high temperature.

Ni agglomeration can be diminished by operating at lower temperatures e.g. 600°C. Mallon et al[122] have shown that Ni sintering can be diminished by optimally depositing carbon particles between Ni particles. This helps to minimize sintering by retarding Ni particle mobility at high temperature.

4.2 Experimental

4.3 Isothermal Ageing of Micro-tubular SOFC

Isothermal ageing was performed in-order to investigate degradation pathways of micro-tubular SOFC at steady state. The cells were ramped-up at constant rate and held up a high temperature (800°C) and the modes of degradation were characterized. Micro-tubular SOFCs are favoured for micro-CHP units, which will be required to operate steadily for long periods of time as such; their isothermal degradation mechanism is of prime importance.

.

4.4 Results and Discussion

4.4.1 Isothermal degradation; The Sintering Theory

The theory of Ni agglomeration has been investigated briefly by a few researchers including[41]. However, the mechanism of sintering especially as it relates to performance decrease has not been fully understood. The theory of sintering

postulated in this study is based on Ni agglomeration between YSZ phases, leading to decreased TPB layer and irreversible change in micro-structure. Dilatometry is used to confirm these irreversible changes at high temperature. The sintering theory is presented below in Figure 4.1. The cathode and electrolyte are represented by the dense brown and grey structures while the anode is represented by a mixture of black and grey particles. The black particles represent the Ni particles while the grey ones represent the YSZ particles. In the first part of this figure, a postulated schematic of the micro-structure before sintering is presented, a uniform distribution between the Ni particles and YSZ phases is presented while in the second part, the extreme mobility of the Ni particles due to their low melting point caused them to agglomerate into a coarse and dense structure, thus reducing the TPB and changing the anode micro-structure.

Micrographs showing changes in micro-structure and distribution of the Ni particles in the YSZ phase before and after Ni agglomeration have been discussed and presented in [41].

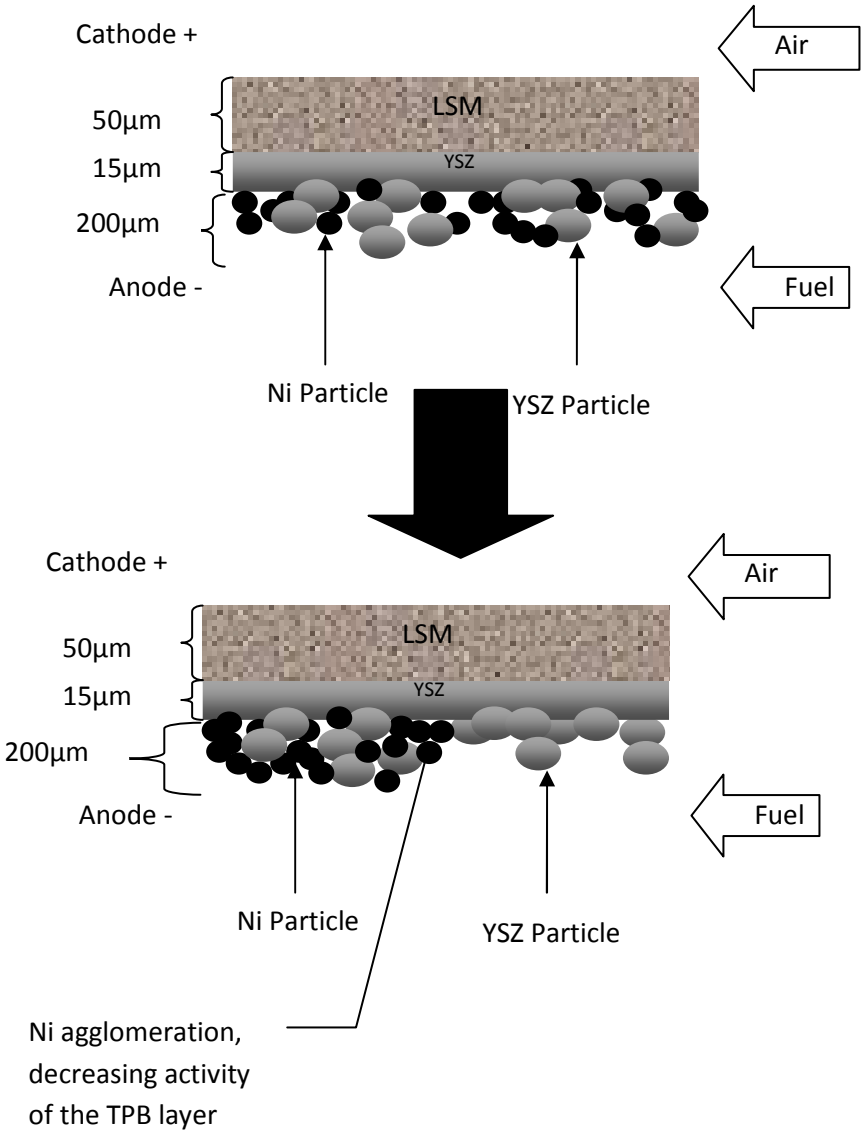

Figure 4.1. The postulated sintering effect in the anode

4.4.2 Ni Sintering Investigation

Dilatometry was employed to confirm the theory of sintering postulated. In doing this, the micro-tube was heated-up to 800°C in inert atmosphere and held for 5 hours, before being cooled down to ambient temperature at a slow rate. The temperature, bulk displacement and time data were recorded, as shown in Figure 4.2. The red

dotted line represents the temperature profile while the bold purple line is the expansion of the sample. It is seen that as the sample was cooled down from 800°C to room temperature, there was irreversible deformation because the sample failed to return to its original length. This irreversible change is usually accompanied by changes in distribution of the Ni and YSZ phases, as reported by [41].

The degree of sintering and distribution of Ni particles in the YSZ phase post-sintering can further be investigated by other surface techniques. These techniques will help to shed more light on the decrease in electro-active surface area necessary for fuel oxidation. Ni agglomeration is further discussed in chapter 5, where sintering during thermal cycling is shown in Figure 5.12

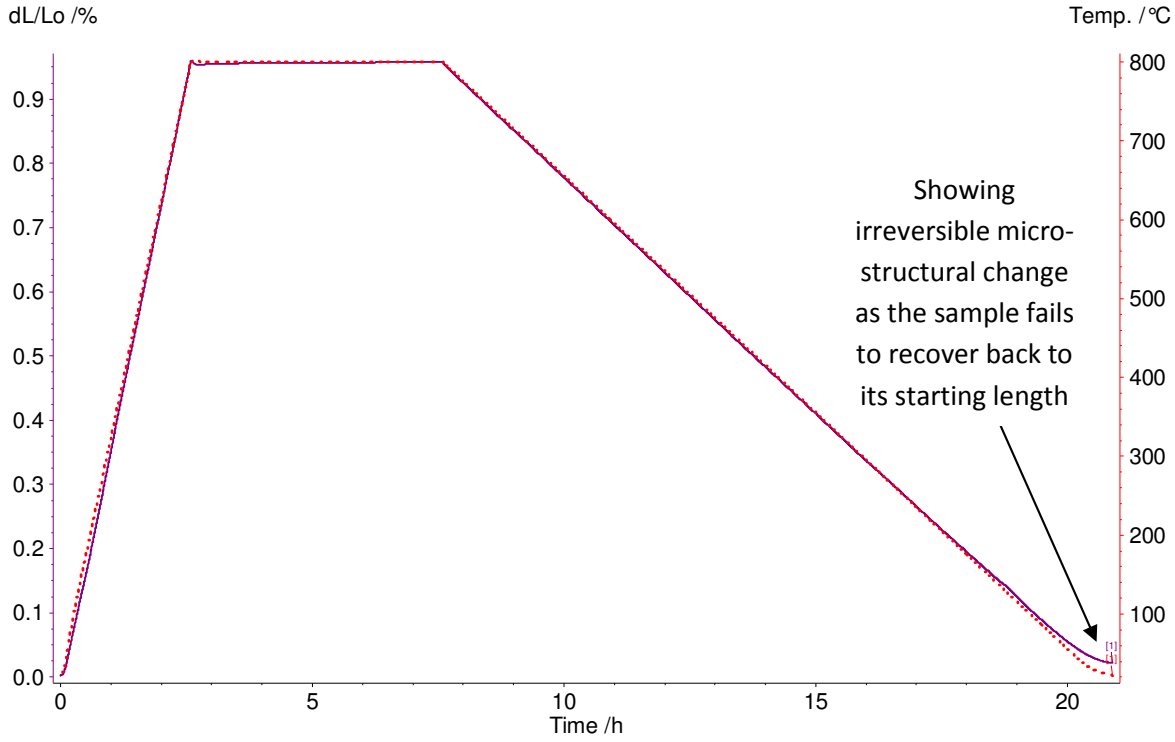

Figure 4.2. Showing irreversible deformation due to Ni sintering

4.5 Iso-thermal Operation of Micro-tubular SOFC

To characterize the electro-chemical degradation of a micro-tube at steady state, iso-thermal ageing was performed, Figure 4.3 shows the results. The micro-tube was held at a voltage of 0.5V and temperature of 800°C for the duration of the experiment. Initially, a current of 1.2A is observed, then it was sustained for a short period, before degradation set-in. The mechanism of this degradation is explained below.

4.5.1 Electro-chemical Degradation: A case of Ni sintering

From Figure 4.2 it was shown that when a micro-tube is heated to high temperature and cooled back to room temperature, irreversible deformation in the micro-structure

occurs. To characterize the effect of this deformation on the electrochemical performance, a sample was heated from ambient temperature to 800^{o}C in hydrogen so that the effect of irreversible change can be analysed.

The initial current observed at the commencement of the experiment was 1.2 A, this was sustained at this value for a few hours before slight decrease in the current is observed. The decrease in performance in this early stage corresponds to the irreversible change observed when the sample was heated up and cooled down by dilatometry. This micro-structural change can lead to decrease porosity and a decrease in the Ni electro-active sites, leading to lower fuel utilization and lower power output[51].

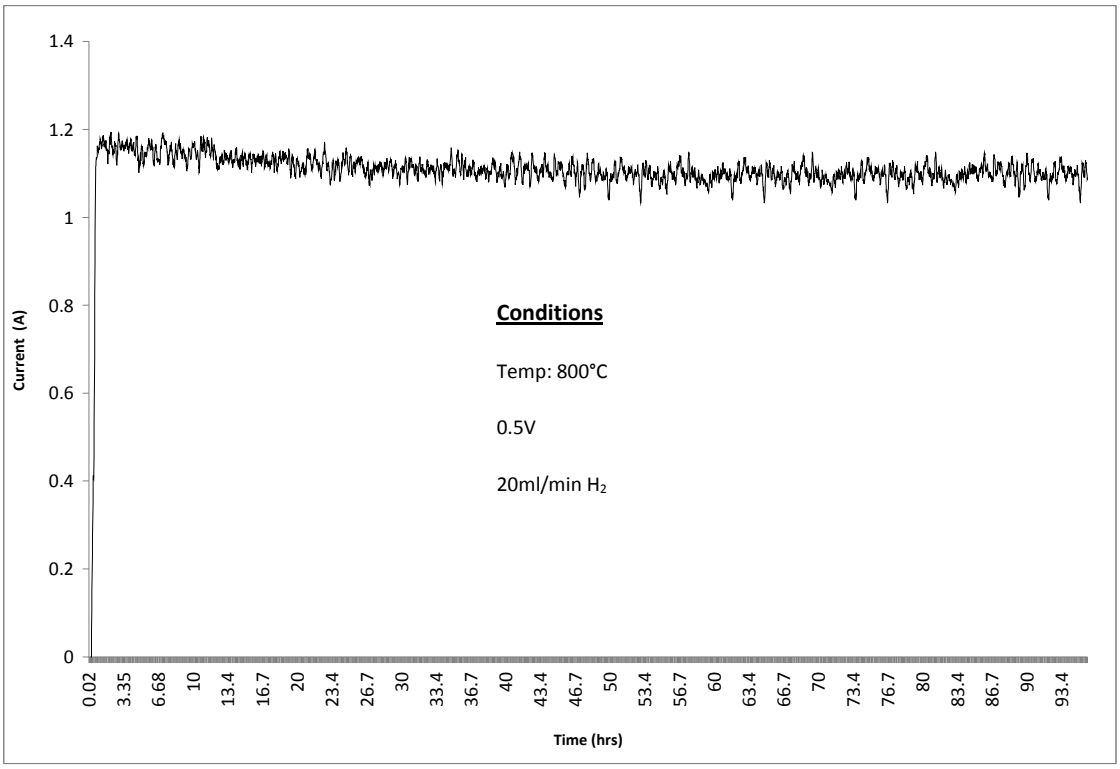

Figure 4.3. Showing the electrochemical performance of a micro-tubular SOFC during iso-thermal operation

Following this drop in performance, the current assumed a near-steady value as quasi-equilibrium is reached between the agglomerated Ni particles and the YSZ phase in the anode. This equilibrium was evidenced by steady electrochemical performance at 1.12A for 84 hrs. It is believed, that at this stage, most of the change in microstructure was complete and the cell achieved a stable microstructure. Similar Ni sintering behaviours, where sintering proceeds rapidly in the opening hours and gradually diminishes has been reported in studies by Dhir et al[172].

4.5.2 The Effect of temperature gradients on the isothermal ageing of micro-tubular SOFC

To investigate the effect of temperature gradients on micro-tubes during isothermal operation, two types of micro-tubes were characterized; 55mm long tubes (hereinafter referred to as long cells) and 25mm long micro-tubes (hereinafter referred to as short cells). The objective was to investigate the effect of temperature gradients on the micro-tubes with respect to their sizes. The cells were both operated in 25% excess hydrogen flow at 800°C. The excess fuel flow was necessary so as to cause combustion at the fuel outlet and raise the temperature of this end, thus creating a temperature gradient along the tube.

As shown in Figure 4.4 the short tubes presented higher current than the long tubes. This is primarily because of the high ohmic resistance across the long tubes due to

longer electron paths in which the electrons produced had to travel to arrive at the current point. The current of the short cells started at 1.30 A and gradually decreased with time. The final current after 14 hours was 1.20A, which is slightly lower than the onset, giving a degradation rate of 0.832% hr^{-1}. The long cell on the other hand showed a slightly lower current, starting at 0.90A and gradually decreasing to 0.79A, giving degradation rate of 0.87% hr^{-1}. For both samples the trend of degradation is similar. The first several hours show a decrease in performance which is attributed to Ni particle agglomeration. The trend of degradation for both the short and long micro-tubes is similar to those reported in earlier studies by Dhir et al[172] where the cells were operated in isothermal conditions. In that study, it was reported that sintering of the Ni anode dominated the first few hours of operation, accounting for most of the initial degradation before degradation due to ageing of the electrodes set in.

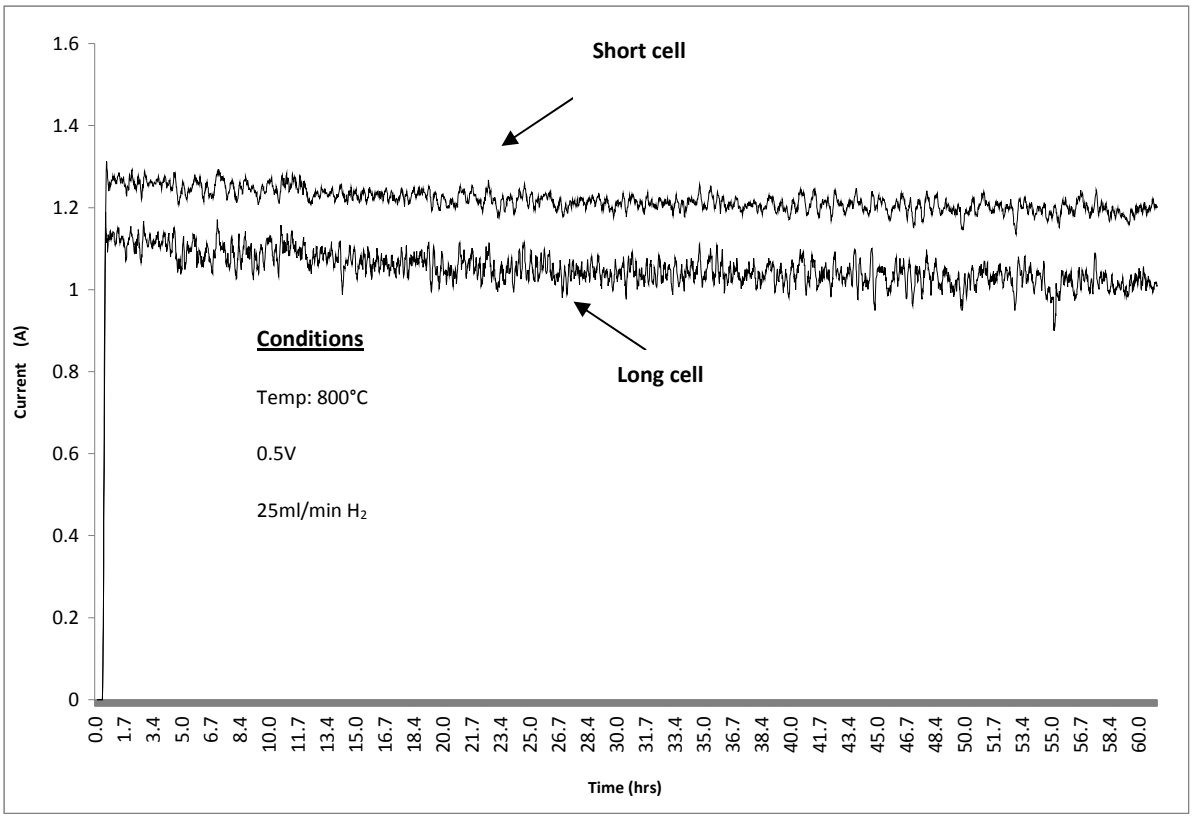

Figure 4.4 Showing electrochemical performance of a short and long micro-tube

The effect of the thermal gradients across the tubes was not prominent and can be concluded to be marginal since no micro-cracks were observed in the cells by SEM, as shown in Figure 4.5 (a) and (b). The temperature gradient imposed gave rise to an expansion differential along the tube, but no micro-cracking or de-laminations were observed. This therefore confirms the resilience of the tubes to thermo-mechanical degradation however, the possibility of stress induction due to the differential expansion cannot be ruled out. An preliminary investigation of thermal shock resilience of these tubes has been reported by Bujalski et al, where rapid heating of up to 300°Cmin^{-1} were reported [158]

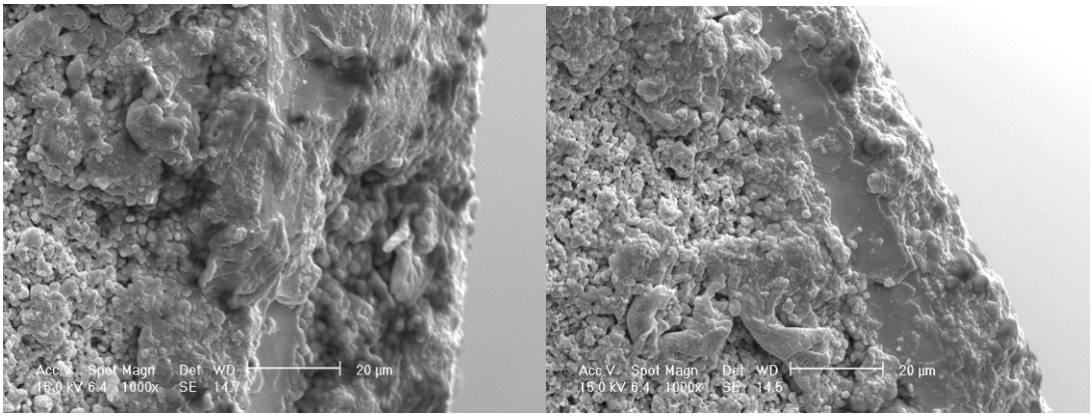

(a) (b)

Figure 4.5**.** Showing the micro-structure of the 25mm and 55mm long tubes after thermal cycling with a gradient imposed**.**

Subsequent studies will be looking at the critical gradient necessary to cause fracture and micro-cracking, this is very important because in real life conditions an excess or incomplete utilization of fuel can impose a gradient along the tube causing fracture damage. Also, thermal shock is a likely occurrence in micro-tubular SOFCs due to their rapid start-up[158]. Figure 4.6 (a) and (b) illustrate the temperature gradient along the short and long tubes respectively.

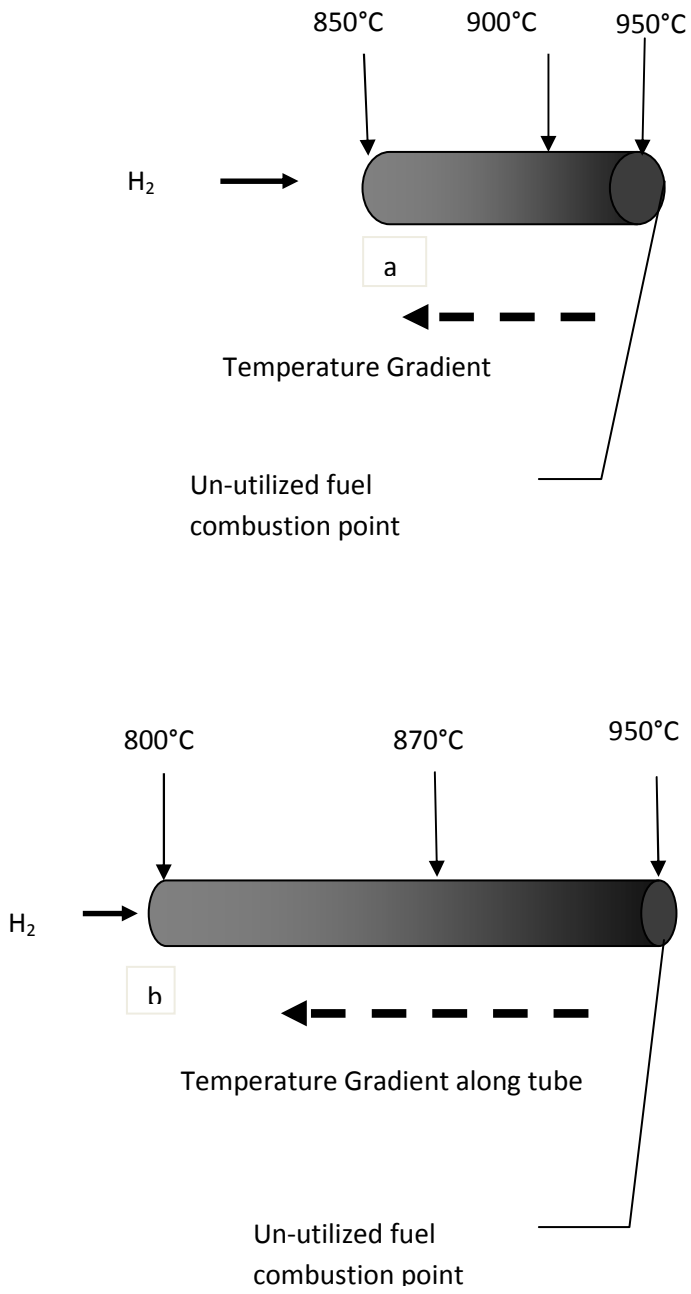

Figure 4.6 (a) and (b). Showing the temperature gradients along the micro-tubes

At the combustion point, the temperature of the cell is 950^{o}C; this temperature decreases as you move along the tube. A K-type thermo-couples was used to measure the temperature gradients.

For the short cell, the difference between the inlet and outlet temperatures is smaller compared to the long cell. The thermal gradient across the long tube was roughly 150°C. (i.e. gradient of 27.3^{o}C/cm). Naturally, this would cause the cell outlet (the combustion end) to expand by a larger index than the other end, causing stress induction. The shorter cell on the other hand had a gradient of roughly 100°C (i.e.40^{o}C/cm). In both cases however, no micro-cracking was observed in the microstructure, thus it can be inferred that the temperature gradient imposed only had a contributive effect to stress accumulation in the bulk of the cells, but did not cause gross micro-cracking.

4.5.3 Expansion and Contraction during Isothermal Operation

To show the extent of bulk volume displacement occurring in the micro-tubes at high temperature, dilatometry was performed. The micro-tube was heated up to 800°C in inert atmosphere and the expansion of the sample was analysed.

From Figure 4.7, an expansion of 0.97% is observed at 800°C, this is represented by the bold purple line. The thermal expansion coefficient (CTE) was calculated at 12.5 X 10^{-6}/°C for the bulk sample. This CTE is the result of the cumulative effect of the individual CTE of the components. Ni is known to have a CTE of approx. 13.0 X 10^{-6}/°C, while that of zirconia is approx. 9 X 10^{-6}/°C. Since each of the components that

comprise the micro-tube are different, they will each expand by different indexes at 800°C. The end result will be an increase in the residual stresses of the tubes as the interfaces of these materials come under severe stress due to different expansions. The dotted purple line shows the rate of change of the expansion Δ(dL/L)dt with respect to time, this line shows the response of the samples at different periods of heating and cooling.

The behaviour of these composite materials will be tested further in the following chapter (i.e. chapter 5), where thermal cycling is used to test the adherence and CTE mis-match of the different components.

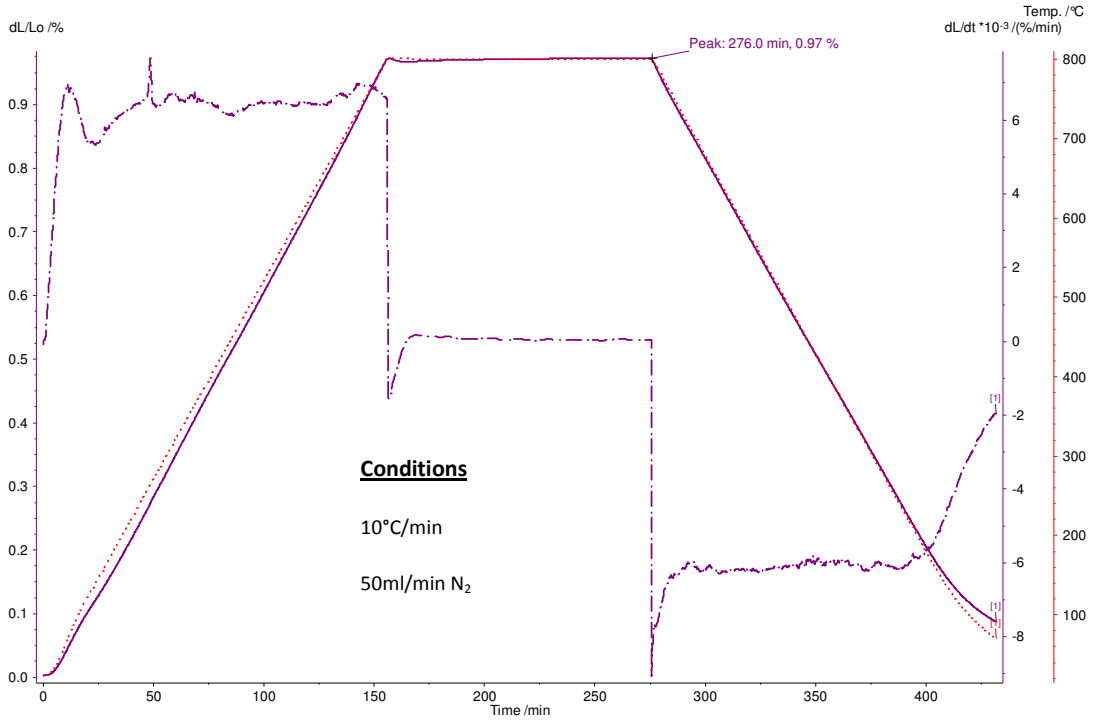

Figure 4.7. Showing the expansion of a micro-tube at 800°C

4.6 Conclusion

In this chapter, the isothermal ageing of micro-tubular SOFCs were investigated. Sintering of the Ni anode was identified as the main factor of degradation during the isothermal operation of the micro-tubular SOFC. It was found to proceed rapidly for the first 10 hours and diminish afterwards. To diminish this sintering effect, lower temperatures of operation are proposed. However, implementing this, will lead to a higher ohmic resistance across the electrolyte. Thus, a critical trade-off between accelerated degradation and low power output due to high ohmic resistance has to be struck, in order to operate at optimum conditions.

Thermal gradients imposed across the micro-tubes by flowing excess fuel through the tubes did not cause micro-cracking in the bulk of the tubes. However, they were adjudged to have contributed to stress induction in the tubes.

In conclusion, the theory of sintering and micro-structural change at constant temperature postulated has been confirmed by experiments.

Chapter 5

Thermal Cycling

5 Thermal Cycling

5.1 Objective

The objective of this chapter is to investigate and understand the degradation of micro-tubular SOFCs when subjected to transient (cyclic) conditions of temperature. The theory is that temperature gradients which arise during start-up/shutdown and during transient conditions like thermal cycling will cause stress accumulation and de-lamination at the interfaces. Several thermo-mehcanical (dilatometry) and electrochemical measurements were set up to characterize this decrease in performance and SEM was used to investigate micro-cracking and de-lamination in the micro-structure.

This investigation is important because SOFCs will undergo several thermal cycles during their life span due to routine and unplanned shutdowns and start-ups when they are used for applications like CHP and stationary power generation systems.

5.2 Experimental

Thermal cycling was performed in four segments; first the tubes were rapidly heated to 800°C at 200°C/min, they were then held at 800°C for a specified length of time before being cooled down to 200°C at 160°C/min, the final segment was the constant temperature hold at this base temperature (200°C) for a specified time before repeating the sequence again. The cooling from the peak temperature to the base temperature was however largely dependent on natural convection to the

surroundings. The degradation was characterized in terms of the decrease in electrochemical performance with progress in cycling, and post-mortem analysis was performed by SEM. Post mortem analysis was important in order to investigate micro-cracking and de-laminations which can compromise the integrity of the tubes.

To investigate the effect of temperature gradients on micro-tubular SOFC, two cell types were characterized; 25mm long tubes (hereinafter referred to as short cells) and 55mm long tubes (hereinafter referred to as long cells). The cells were both subjected to thermal cycling and their electrochemical performance is presented.

Dilatometry was subsequently used to understand the expansion behaviours of the micro-tubes at high temperature, different heating rates and holding (dwell) times were used to characterize the sample behaviours. Also, thermal cycling was performed under dilatometry by raising the sample to high temperature and cooling down repeatedly in inert atmosphere in order to understand their thermo-mechanical behaviour.

5.3 Results and Discussion

5.3.1 Theory of degradation due to thermal Cycling

The theory under investigation is based on the idea that the ceramic materials in the cells contain defects , which can be extended by stress, restricting current paths and increasing resistance, while ultimately causing brittle fracture. This process is driven by thermal expansion of the cells, which was measured by dilatometry to give a

thermal expansion coefficient (CTE) of $\alpha = 12.5x10^{-6}/^{o}C$ over the temperature range 20 to $800^{o}C$. Based on previous studies by [158], it is presumed that the fuel cells comprise materials which are all well-matched in thermal expansion coefficient such that only marginal differential stresses are built up when temperature is raised uniformly across the cell. Therefore, according to this theory, no damage should be observed under steady temperature conditions. However, if the sample is heated rapidly or if itis restrained from expanding by interconnects or rigid supports, then considerable amounts of thermal stresses can be generated. During the heating-up phase of thermal cycling, the stresses that result are compressive since the body tends to expand against the restraining body. On cooling however, the stresses become tensile due to the severe contraction.

Temperature differentials which arise due to rapid heating during thermal cycling generate stresses which can propagate cracks according to the Griffith equation to cause damage and consequent loss of electrochemical performance. The classic thermal shock parameter is given by

$$\theta_c = (1-\nu)\,\sigma/E\alpha \qquad (5.1)$$

where θ_c is the critical temperature change causing fracture, ν is the Poisson's ratio, σ is cracking stress, E is Young's modulus and α is the CTE. Crack propagation is described by the Griffith equation

$$\sigma = (ER/\pi c)^{1/2} \qquad (5.2)$$

Where R is the fracture energy and c the crack length. Typically a thermal stress experiment to measure the critical fracture temperature for the micro-tubes gave a critical temperature of approximately 180^{o}C. Thus, any thermal cycling below this temperature range should not cause degradation. If we presume that increasing the cycling range above 180^{o}C causes a linear increase in degradation rate, then the following equation is proposed

$$C_R = 180 + m\ R_D \qquad (5.3)$$

Where C_R is the cycling range, R_D the degradation per cycle and m the gradient.

To validate this theory, electro-chemical and dilatometry measurements were performed andSEM was employed to confirm micro-cracking and de-lamination in the micro-structure. The results of the electro-chemical characterization are presented in the section below**.**

5.3.2 Thermal Cycling Investigation

Figure 5.1, Figure 5.2 and Figure 5.3. show the thermal cycling results of micro-tubes cycled between 200°C - 600°C, 200°C - 700°C and 200°C - 800°C respectively in 20ml/min of hydrogen.

In Figure 5.1, a peak current of 0.85A is observed at the commencement of cycling, this value was sustained for a few hours until slight degradation set-in, giving a final current of 0.82A, a degradation rate of 0.05%/cycle was evaluated.

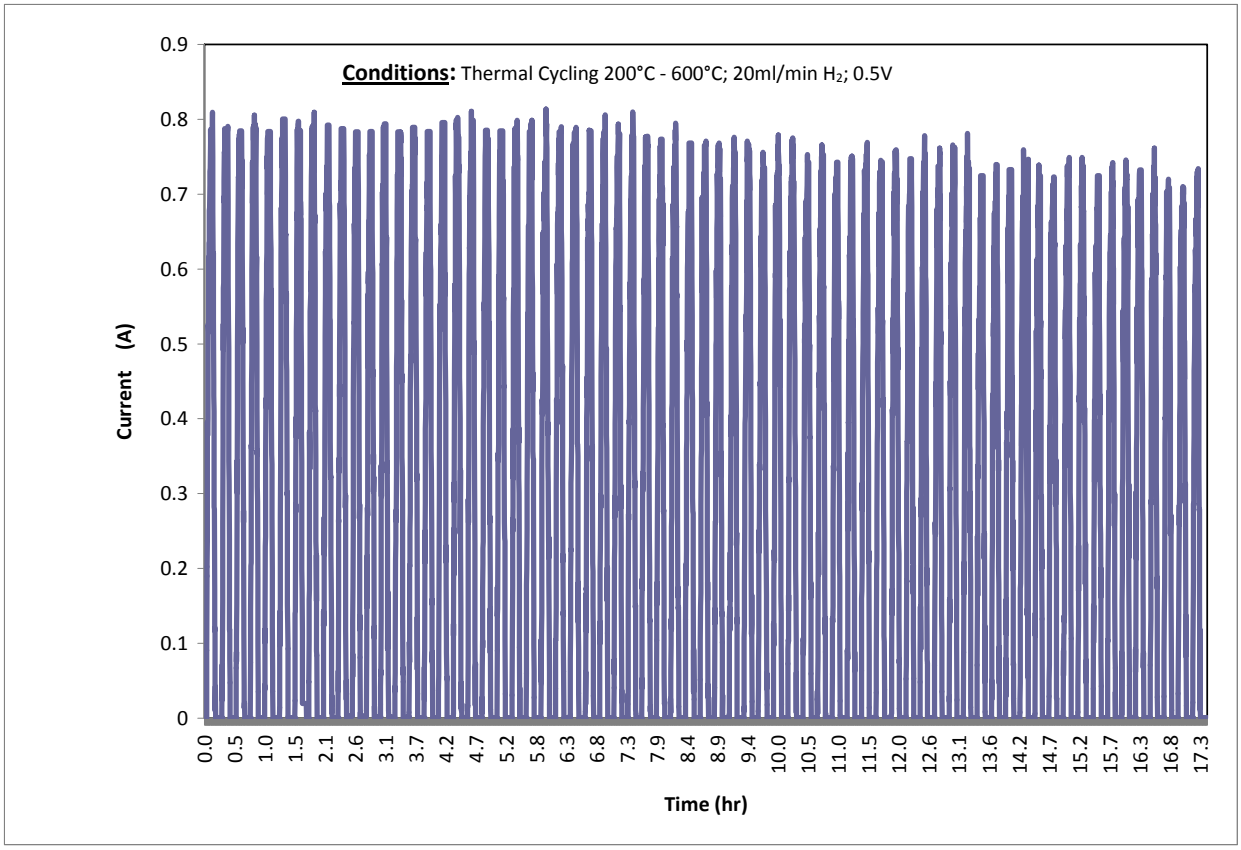

Figure 5.1. The results for thermal cycling between 200°C and 600°C

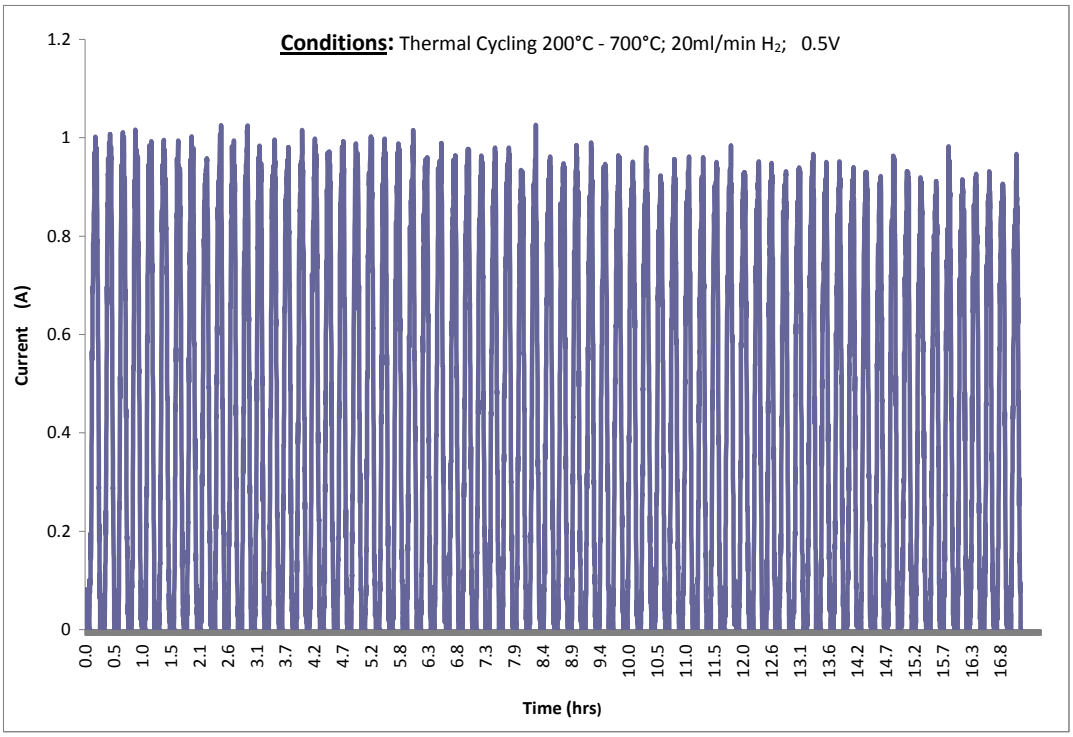

Figure 5.2. The results for thermal cycling between 200°C and 700°C

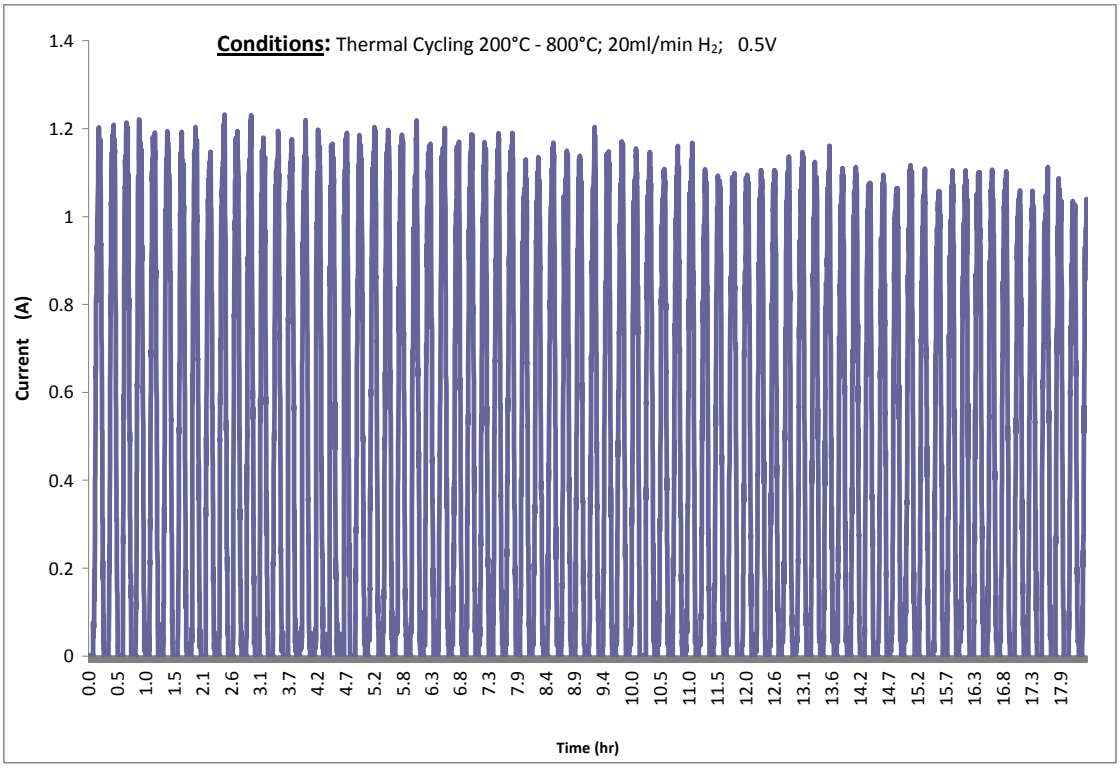

Figure 5.3. The results for thermal cycling between 200°C and 800°C

In Figure 5.2, the peak current was 1A; this gradually decreased as cycling proceeded giving a final current of 0.95A. The degradation observed was evaluated at 0.07%/cycle, while in Figure 5.3, an initial current of 1.2A was observed at the commencement of cycling, before it gradually decreased to 1.13A at the end of cycling. A degradation rate of 0.082%/cycle was evaluated in this case.

In all three cases, the trends and rates of degradation were similar. The general trend of degradation started with an initial high current, which decreased successively as cycling proceeded. Initially, it was thought that an increase in resistance of the electrodes due to micro-structural damage (micro-cracking) was responsible for the degradation, but post-mortem analysis (SEM) of the micro-tubes showed no micro-cracks or de-laminations. This finding indicates that perhaps thermal cycling only had a contributive effect to stresses accumulation in the cells but not macroscopic cracking. The stress accumulation arises mainly due to the temperature gradients, which exist during transient operation. In any case, under the conditions of thermal cycling for this project, the micro-tubes were found to show immense thermal cycling resilience.

However, it should be noted that stress accumulation in the PEN of cells is not capable of causing performance decrease, until physical degradation occurs. By critically analyzing the degradation trend, it was observed that the degradation during thermal cycling closely resembled that of iso-thermal operation where Ni sintering was found to dominate the degradation mechanism. Ni sintering is known to proceeds rapidly above 500°C and because of this; during thermal cycling micro-structural changes

occurred only when the cells were in the sintering regime i.e. above 500°C. This cyclic change in temperature between 200°C and the peak temperature meant that there were periods of time when sintering did not occur as against isothermal operation when the cells are held continuously in the sintering regime. Also, the rate of electro-chemical degradation during cycling between 200°C and 600°C was somewhat lower than reported for 200°C - 700°C and 200°C - 800°C because sintering proceeds at a lower rate at 600°C than at 700°C or 800°C. This is because when cycling between 200°C and 600°C, the cells had a shorter dwell time in the sintering regime than cycling between 200°C - 700°C or 200°C - 800°C

Figure 5.4, shows the comparison of electrochemical degradation during isothermal ageing and thermal cycling at 800°C, it can be seen that the degradation during thermal cycling was found to be only slightly higher than observed during isothermal operation. Initially a common degradation trend is observed for both isothermal operation and thermal cycling for the first 10hrs until further degradation is observed in the case of thermal cycling. The common degradation trend observed initially, points to the fact that the same degradation mechanism i.e. Ni agglomeration dominates the degradation during these early stages. Subsequently, the increase in degradation rate for thermal cycling signifies the commencement of another degradation mechanism. This degradation mechanism was identified as the melting of the silver interconnect. The silver current collecting structure was found to have creeped and melted leading to higher contact resistances. Thus, this is a common

finding in most thermal cycling studies; where researchers have reported frequent interconnect failure during thermal cycling[186].

Naturally, the differential expansion due to temperature gradients will cause steady stress induction in the inter-layers of the components, but what still needs to the investigated further is at what point the stresses become sufficient to drive micro-cracks and cause performance drop. It is common knowledge, that with progress in cycling, stress continues to build up in the material until sufficient energy is attained to propagate cracks but it is difficult to accurately decipher when one degradation mechanism sets-in or which degradation mechanisms in a bunch dominates the degradation, but degradation trends such as seen in Figure 5.4, where there is a change in the rate of degradation brings to light the complex nature of these degradation mechanisms.

Summarily, these micro-tubes degraded only slightly during thermal cycling, this has been corroborated by Bujalski et al[158] who achieved hundreds of thermal cycles using the same cells in the Adelan® hand held device without significant degradation in performance.

.

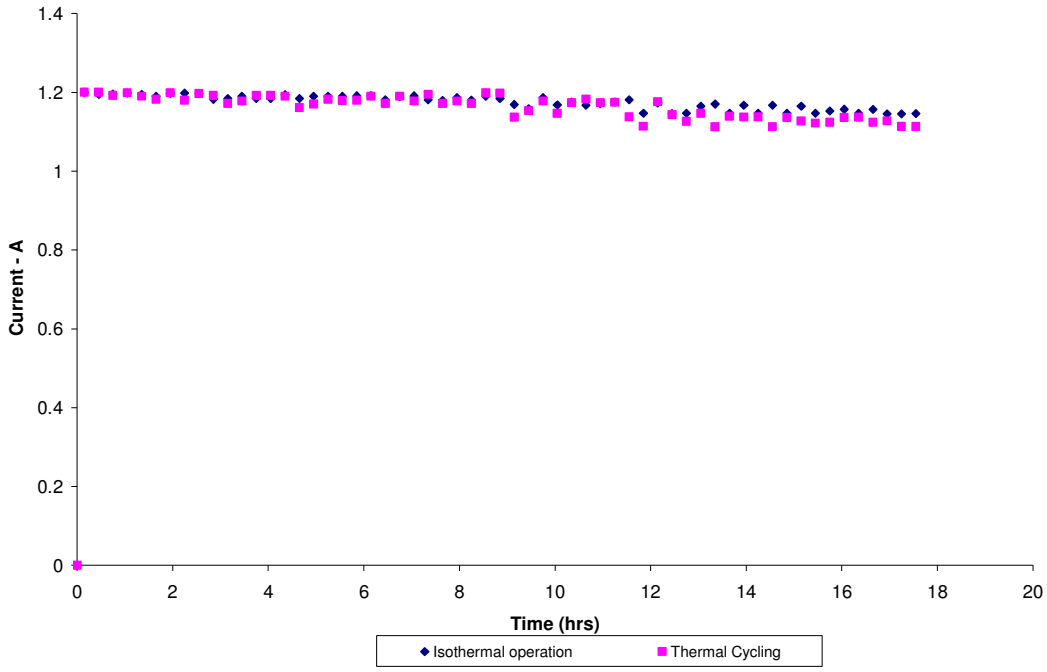

Figure 5.4 Comparison of isothermal operation and thermal cycling at 800°C.

5.3.3 The Effects of temperature gradients on the thermal cycling of micro-tubular SOFC.

Temperature gradients and hotspots are capable of causing micro-cracking and failure in SOFC. These could arise due to fuel leakage or fuel conversion gradient along a tube. Thermal stresses which arise due to temperature gradients during isothermal operation can be estimated for perfectly elastic bodies, to which many ceramics are a good approximation. For a perfectly elastic tube restrained in just one direction,

$$\sigma = -E\alpha(T_2 - T_1) \qquad (5.4)$$

Where σ is the stress induced, α is the CTE and (T_2 -T_1) is the magnitude of the thermal gradient.

For a tube, where thermal gradients develop during steady state heat flow, the thermal shock resistance of the material is given by

$$R_T = \frac{\sigma_f (1-\nu)}{E\alpha} K \qquad (5.5)$$

Where R_T is the thermal shock resistance, σ_T is the fracture stress, ν is the poisson ratio while K and E are the thermal conductivity and elastic modulus respectively. It should however be noted that because the tubes were subjected to transient conditions, this relationship can be applied only during the steady state segments.

To investigate the effect of thermal gradients during thermal cycling, 25% excess hydrogen flow was used in the micro-tubes to impose a gradient along the tubes by combustion at the outlet.

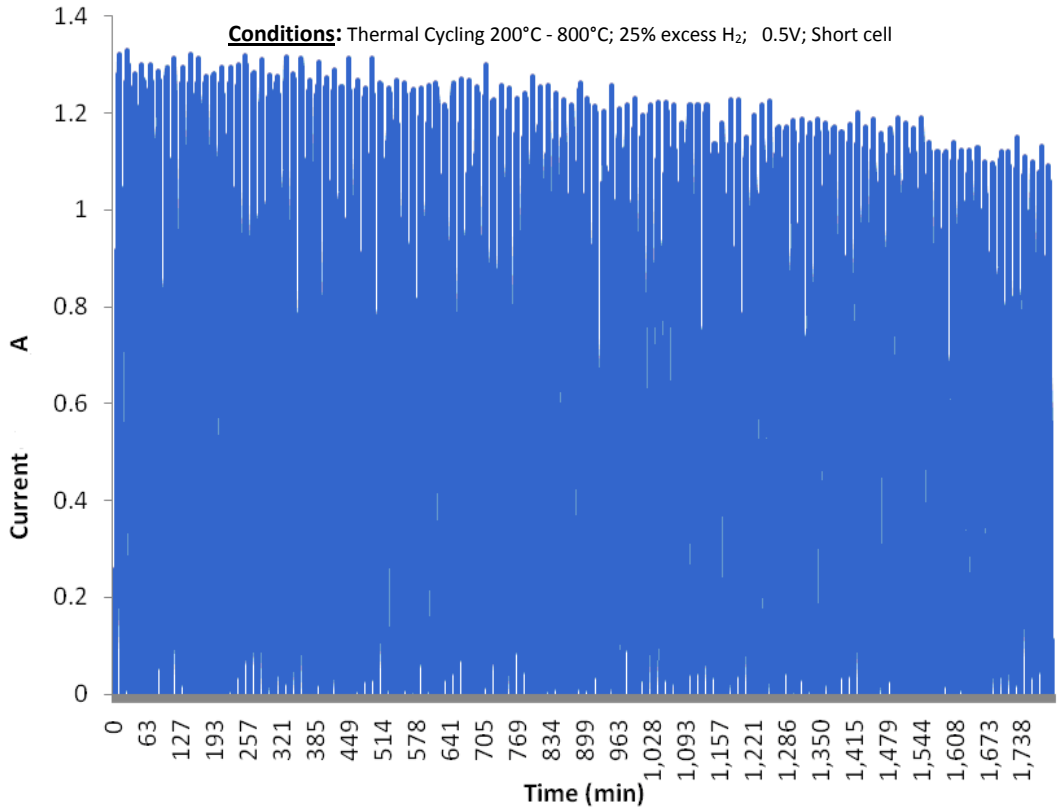

Figure 5.5 Thermal cycling of a short cell between 200°C and 800°C

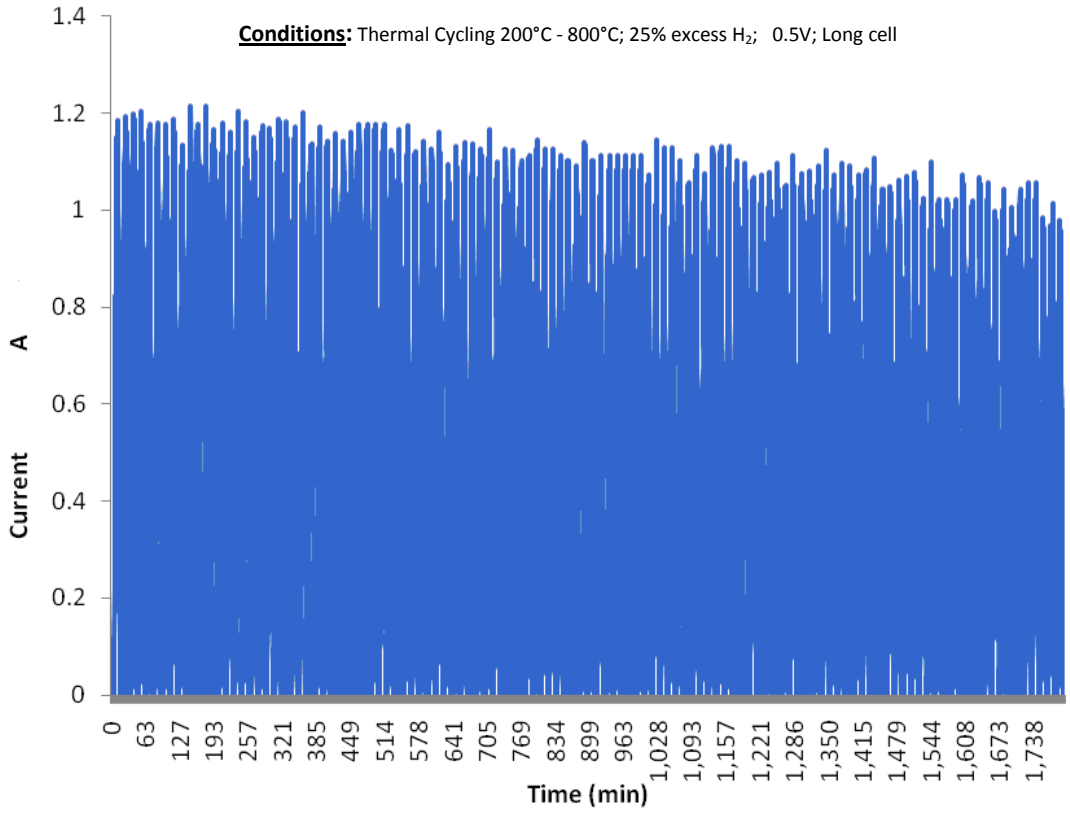

Figure 5.6 The thermal cycling of a long cell between 200°C and 800°C

The combustion at the outlet raised the temperature, thus imposing a gradient along the tube. Rapid thermal cycling was then performed between 200°C and 800°C on both short (25mm) and long (55mm long) tubes. Figure 5.5 and Figure 5.6 are thermal cycling results of a short and long cell respectively at 0.5V. The short cell presented an initial current of 1.32A at the commencement of cycling but as cycling proceeded the current is seen to decrease steadily, giving a final value of 1.16A after 110 thermal cycles. Similarly, the long cell presented an initial current of 1.2A and a final value of 1.03A after 110 thermal cycles.

In both cases, the rate of degradation was about 0.12%/cycle. This high degradation index is a resultant of several factors that all worked concertedly over the duration of thermal cycling. It is always difficult to isolate single degradation effects from others, especially when there are several transient conditions. In this case however, the degradation factors identified include; (1) Ni sintering (2) temperature gradients due to rapid heating and cooling during thermal cycling and (3) differential expansion along the tube due to the thermal gradient imposed.

Since each of these degradation effects occur simultaneously, isolating specific degradation trends is difficult. Impedance spectroscopy or modelling techniques might be required in order to understand and analyse specific degradation mechanism. For the purpose of this study however, the complex degradation phenomena is considered as a whole. Firstly, Ni sintering causes degradation by changing the micro-structure and decreasing the electro-active area necessary for oxidation, this happens mainly in the TPB layer of the anode functional layer and has been explained in greater detail in chapter 4. Secondly, the temperature gradients which arise due to rapid heating and cooling will induce stresses in the PEN due to localised expansions at different areas, leading to stress accumulation at material interfaces and layers. The thermal stresses induced in the PEN will have a greater effect along the radius due to the constraints imposed by other cell components[104]. This accumulation of stress is gradual as each thermal cycle induces further stresses until a certain critical stress value is exceeded, when it has sufficient energy to drive micro-cracks. However, thermal cycling alone has been shown not to cause micro-

cracking, see Figure 5.3. Finally, thermal gradients would accelerate material degradation by imposing an expansion gradient along the length of the tube. The tube outlet which is at a higher temperature expands more than the inlet, leading to an expansion differential which is capable of inducing further stresses.

The full extent of the interaction of these degradation effects is not fully understood, however this operation was found to cause micro-cracking and de-lamination as shown by SEM in Figure 5.15. It is postulated that during thermal cycling (with a temperature gradient imposed) the cell expansions were in all directions; radially (due to the constaint of other cell components) and length-wise (due to the temperature differential across the tube ends. Thus, these forces acting together will result in greater stress induction which can exceed the critical stress intensity for cracks to propagate. Usually, Tiny micro-cracks that open, would easily develop into large ones with further cycling because they become weak points in the structure. Such defects and faults compromise the integrity of micro-tubes, and lead to performance degradation as seen in Figure 5.5 and Figure 5.6, where a degradation of up 0.1%/cycle was reported. However, what remains to be investigated is the exact point when thermal cycling induces enough stresses to cause micro-cracking. And at what point the temperature gradient imposed starts to propagate cracks.

During thermal cycling, not only is the cell subjected to thermal stress accumulation but also the interconnecting materials that make up the cell. More often than not, the failure in micro-tubular SOFC in not due to degradation in the PEN, but failure of the interconnect materials. Figure 5.7 shows the failure of the silver interconnect of a

micro-tubular SOFC cycled in hydrogen. A degradation rate of 0.13%/cycle is observed before the silver interconnect started to melt, but as the structure started to melt a huge increase in degradation is observed before failure. SOFC interconnects such as silver, platinum etc are prone to stress induction during thermal cycling due to fatique and creep at high working temperature, making them prone to failure. Several researchers[9, 187] have reported failures in interconnects during operation at high temperature.

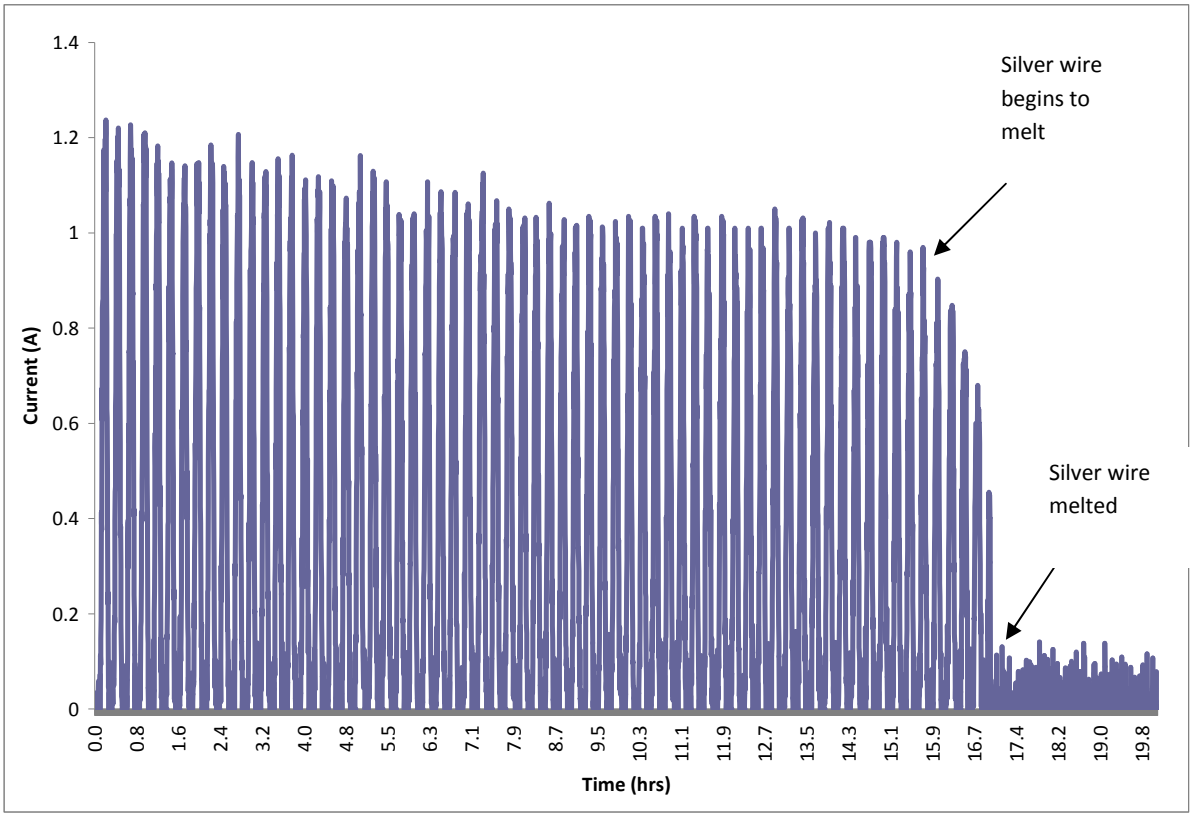

Figure 5.7. Showing interconnect failure in micro-tubular SOFC

5.3.4 Measurement of Expansions during Thermal Cycling

Dilatometry was used to characterize the mechanical behaviour of micro-tubular SOFC with respect to temperature. The bulk expansion of the samples was measured with respect to temperature. A coefficient of thermal expansion of 12.5 X 10^{-6}/^{o}C was evaluated.

Figure 5.8 and Figure 5.9 show the mechanical behaviour of an un-reduced and a fully reduced micro-tubular SOFC at 800°C respectively. Both are seen to present similar expansions i.e. 0.97% at 800°C indicating that the difference in porosity between the dense un-reduced NiO/YSZ sample and the reduced Ni/YSZ had little effect on the bulk expansion of the samples. This is important because it shows that both the reduced and unreduced tubes have similar behaviours at high temperature. The bold purple traces are the sample response while the thin dotted red line corresponds to the temperature profile. The blue dotted line corresponds to the first derivative of the sample expansion, this helps to show the onset of behaviour change in the sample with respect to temperature.

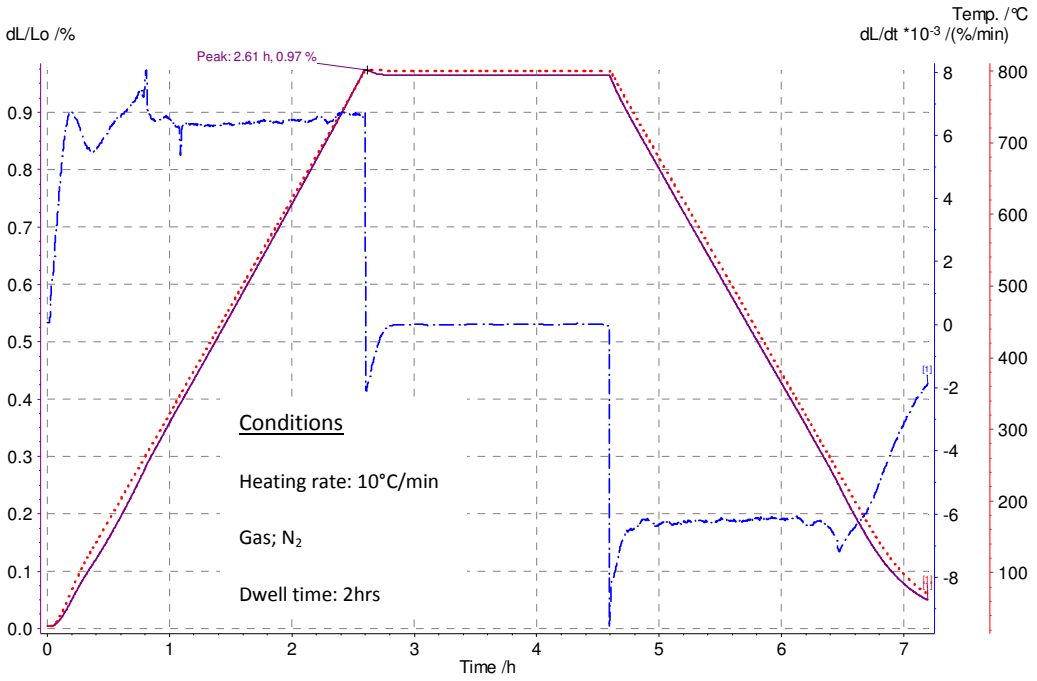

Figure 5.8. The expansion of an unreduced NiO/YSZ micro-tube at 800°C

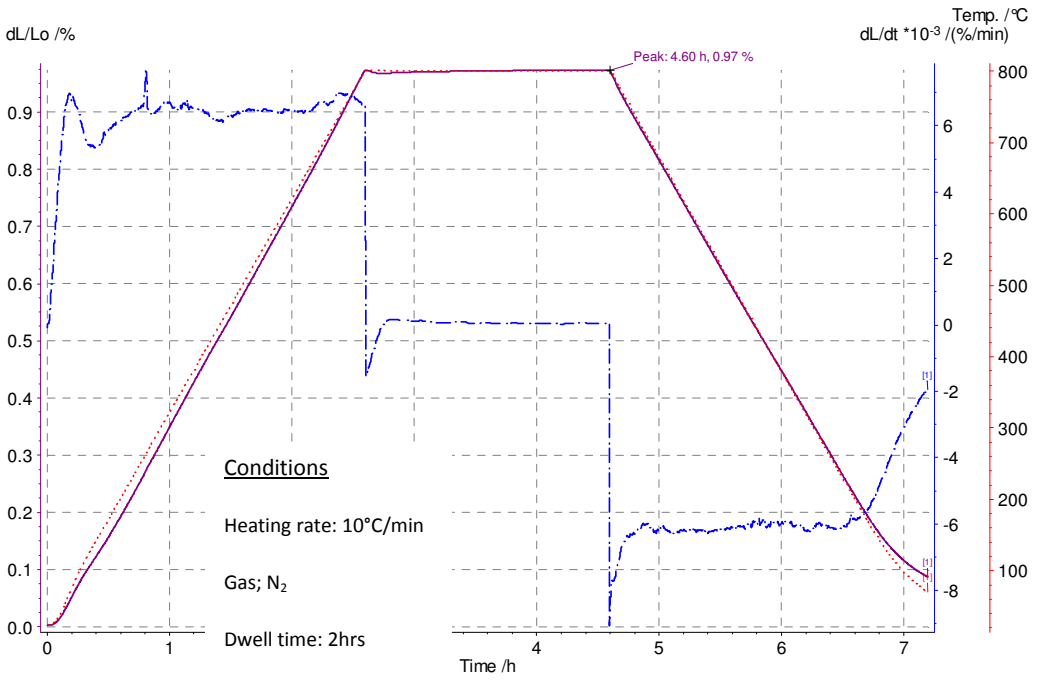

Figure 5.9. The expansion of a fully reduced Ni/YSZ micro-tube at 800°C

5.3.4.1 Expansion during Thermal Cycling

Figure 5.10 and Figure 5.11 show the results of fully reduced micro-tubes cycled between 200°C and 800°C. In Figure 5.10, a heating rate of 10°C/min and dwell time of 30 minutes was used and 9 thermal cycles were performed. Initially, an expansion of 0.94% was observed at 800°C but as cycling proceeded, an increase in the expansion is observed with each thermal cycle, giving a final expansion of 0.97% after 9 thermal cycles. Similar behaviour is seen in fig. 5.11 where a shorter dwell time of 10 minutes was used. At the commencement of cycling, an expansion of 0.96% is observed, but as cycling proceeded an increase in expansion is notice after each thermal cycle, giving an expansion of 0.99% after 9 thermal cycles and 1% after 22 thermal cycles, this implies that irreversible deformation occurs in the micro-structure of the tubes during thermal cycling.

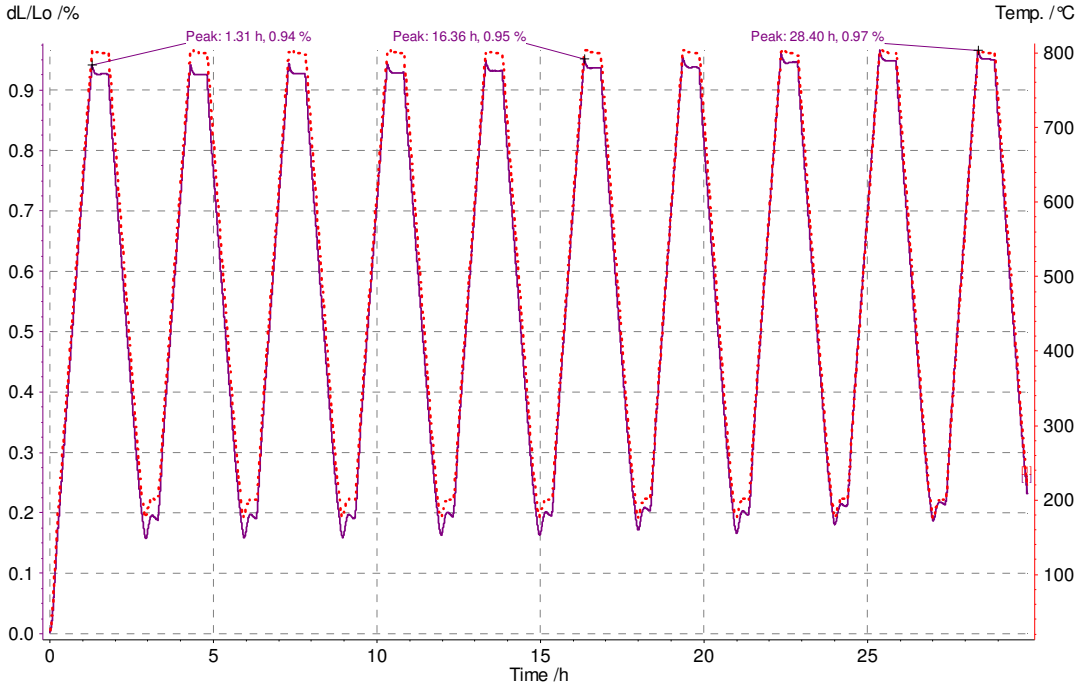

Conditions: Thermal Cycling, Heating rate: 10°C/min, Gas; N_2, Dwell time: 30 minutes

Figure 5.10. Showing the thermal cycling of a micro-tube between 200°C and 800°C

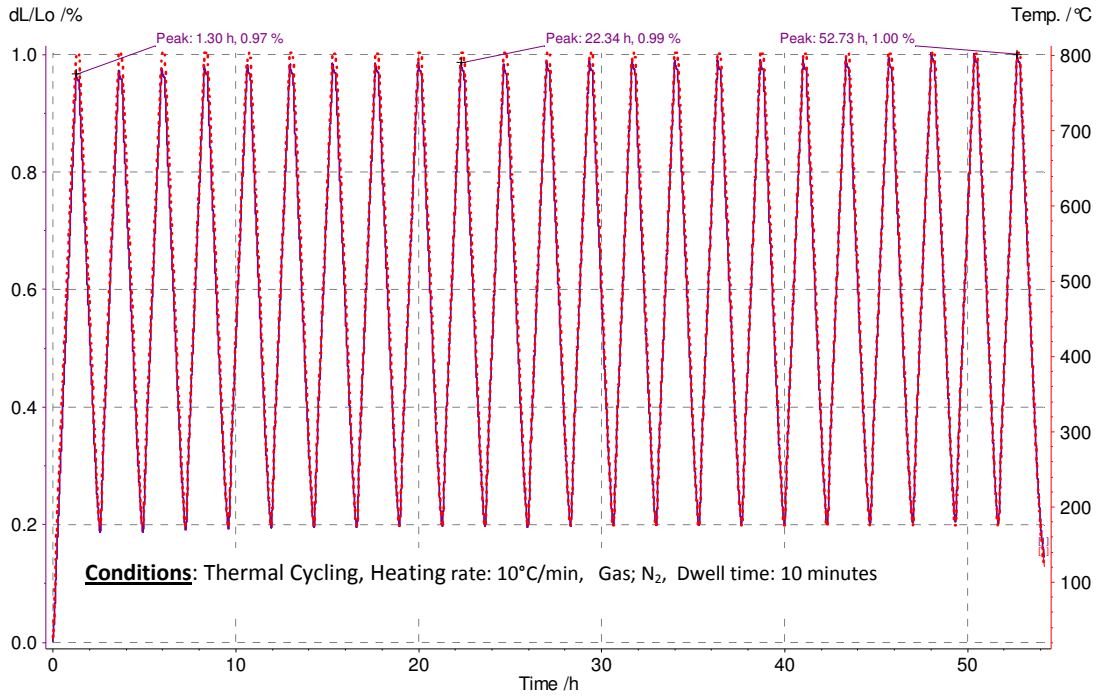

Figure 5.11. Showing irreversible deformation in a micro-tube with progress in thermal cycling

As explained previously in Figure 5.4, the irreversible deformation occurring at high temperature is due to the change in micro-structure (i.e. Ni sintering). At the commencement of thermal cycling, as the temperature is raised, the Ni particles become extremely mobile because of their low melting point (1453°C). This Ni mobility starts to occur at temperatures above 500°C, causing sample displacement and changing the micro-structure of the anode. As higher temperatures are approached, there is increase in the rate of sintering and consequently, bulk volume expansion and irreversible deformation. This high degree of sintering is sustained throughout the constant temperature hold at 800°C, until the cooling segment when the sintering rate is diminished. However, even though the sample contracts due to

the cooling, the irreversible deformation and micro-structural changes due to sintering of the Ni particles are not reversed. With further cycling, there is further sintering and bulk volume displacement until the Ni particles reach certain equilibrium when the Ni agglomeration is complete and the micro-structure assumes a definite configuration. Thus, sintering of the Ni anode proceeds rapidly at the onset but decreases with time because the anode agglomerates into a stable structure; at this stage, constant expansion is observed. Also, constant electrochemical performance will be observed since the surface area of the anode becomes constant as there are no further micro-structural changes beyond this point. The process of heating the cells at high temperature in order to achieved constant micro-structure is known as conditioning. With the Rolls Royce Fuel Cells Systems design, several tens or hundreds of hours are used for this initial conditioning. However, further thermal cycling might offset this steady performance by accumulating more stresses and propagating micro-cracks and de-lamination if the critical stress intensity is exceeded[156].

Further proof of Ni sintering during thermal cycling is presented in In Figure 5.12, where the irreversible deformation behaviour of a micro-tube was investigated under step-wise thermal cycling. The sample was heated to 200°C at 10°C/min and held for 10 minutes before heating again to 300°C and increased in similar steps to 800°C. Table 5.1 shows the irreversible deformation that occurred with cycling. At the commencement of thermal cycling, expansions of 0.2%, 0.33%, 0.46% and 0.58% are observed at 200°C, 300°C, 400°C and 500°C respectively giving average expansions of 0.13% between each step but above 500°C an increase in the average step-wise

expansion of 0.16% are observed. This is because above 500°C, the irreversible deformation due to the sintering of the Ni particles adds to the expansion due to the CTE to give a larger bulk expansion. At 800°C a peak expansion of 1.03% was observed but as the sample was cooled down and cycled again, expansion of 0.27%, 0.41%, 0.53%, 0.66%, 0.78% and 0.91% were observed at 200°C,300°C, 400°C, 500°C, 600°C and 700°C respectively. These higher expansions are evidences of the irreversible deformations that occurred in the samples due to thermal cycling. From the figure below, the bold purple trace corresponds to the sample response while the thin dotted red line associated with it is the temperature profile.

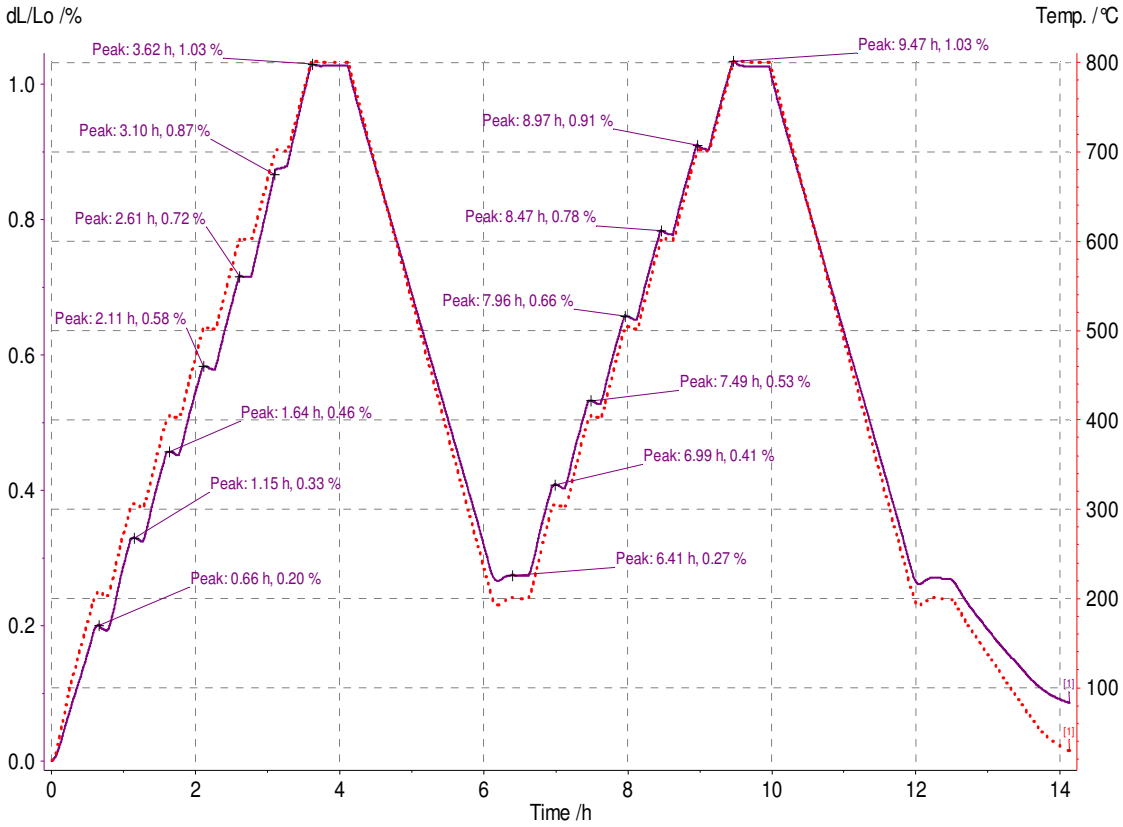

Figure 5.12. The irreversible deformation of a micro-tube under step-wise thermal cycling.

Temperature	Expansion (%) (Reference cycle)	Expansion (%) 1st Cycle
200	0.2	0.27
300	0.33	0.41
400	0.46	0.53
500	0.58	0.66
600	0.72	0.78
700	0.87	0.91

Table 5.1 The result of micro-structural change with thermal cycling.

5.3.5 Post Mortem Analysis

SEM was used to investigate the degradation in the micro-structure of the tubes after thermal cycling. The samples were prepared carefully so as to avoid micro-crack propagation during sample preparation; a thin cutting edge was used for this purpose.

No micro-cracking or delaminations were observed after thermal cycling between 200°C - 600°C, 200°C - 700°C or 200°C -800°C. Figure 5.13 is an SEM micro-graph showing the anode-electrolyte-cathode of a cell cycled 70 times between 200° - 800°C in 20ml/min of hydrogen while Figure 5.14 shows the anode of the same cell.

On the other hand, the cells which were cycled with a temperature gradient were found to show micro-cracking and delamination as shown in Figure 5.15.

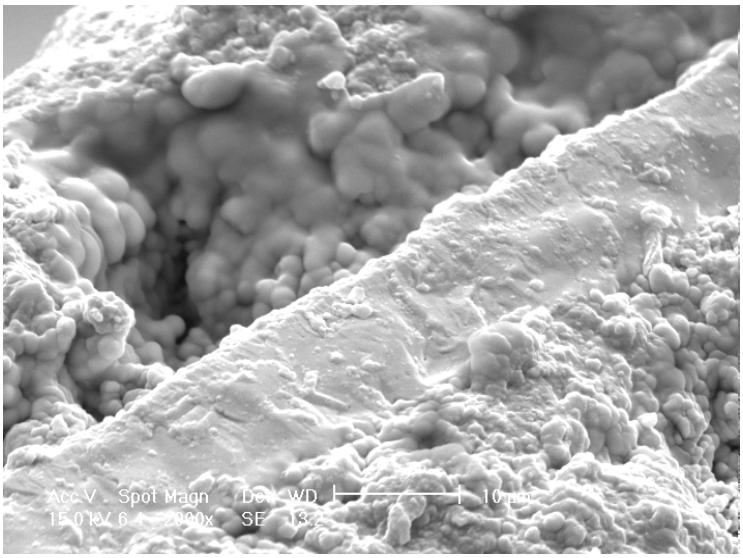

Figure 5.13. The micro-structure of a cell cycled between 200°C and 800°C

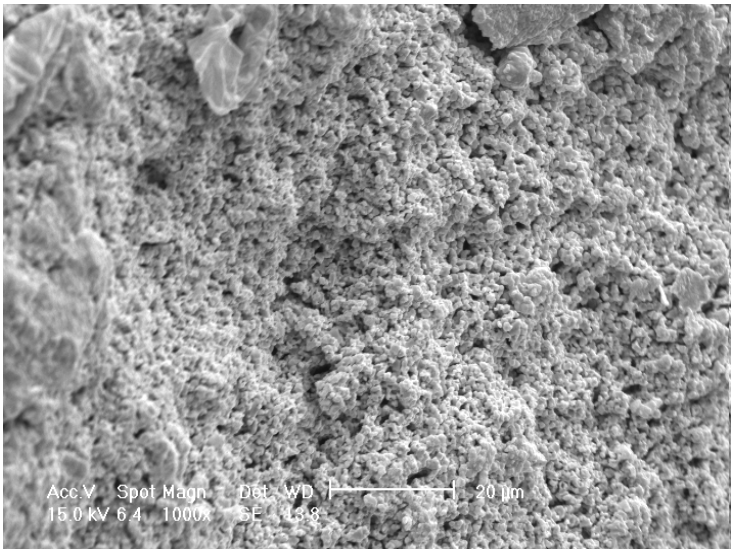

Figure 5.14. The anode of a cell cycled between 200°C and 800°C

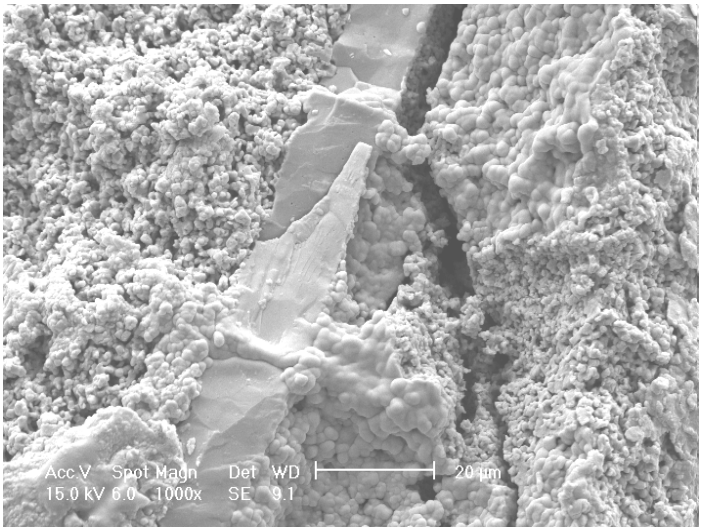

Figure 5.15. Micro-cracking and delamination in a tube cycled between 200°C and 800°C with a gradient imposed

5.3.6 Discussion of theory of Degradation during Thermal Cycling

Figure 5.16 shows the results for constant temperature operation of a micro-tube at 600^{o}C and 0.5V. The micro-tube current was 0.8A initially and this hardly decayed over the first 40 hours of operation. Long term degradation was not measured in detail but appeared to be less than 5% per 1000 hrs. The investigation showed that slight sintering of the micro-tube materials was occurring in this period, leading to small but noticeable decline in current.

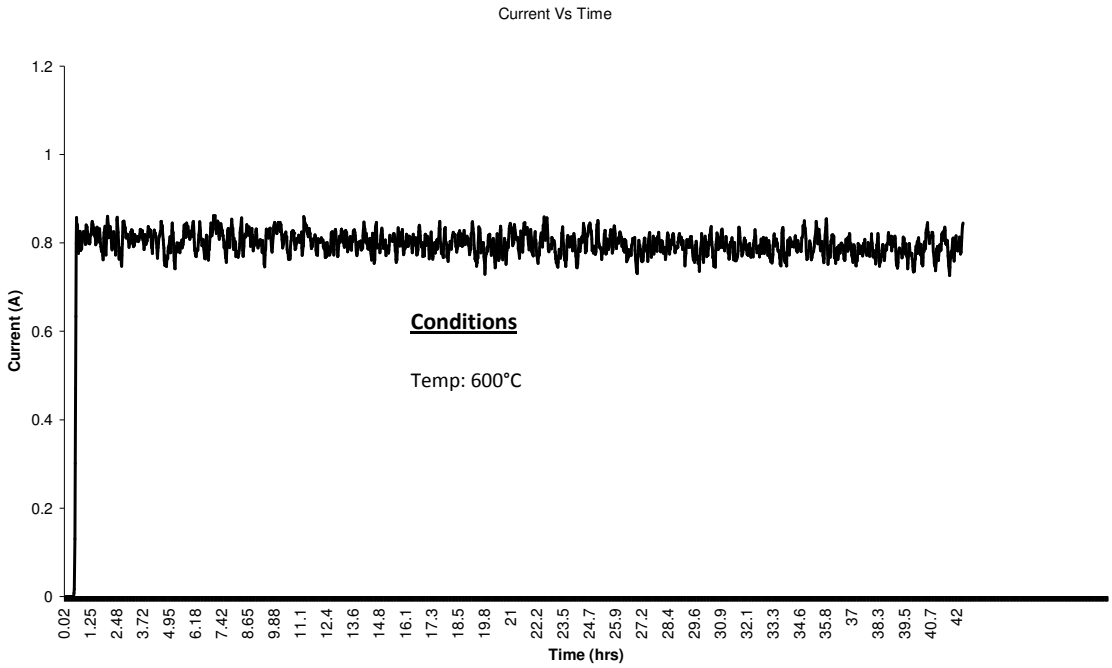

Figure 5.16 Constant temperature degradation of the microtube over 42hr

From Figure 5.1, where the rapid cycling of a micro-tube between 200^{o}C and 600^{o}C (i.e cycling range of 400^{o}C) is presented, It is clear that cycling caused much greater

degradation than the steady operating conditions. The current fell approximately linearly with the number of cycles. Initially, the output current was 0.83A, for this lower temperature of operation and the degradation was 0.056% per cycle. Increasing the temperature maximum from 600 to 700 then 800^{o}C (ie range from 400 to 500 then 600^{o}C) gave an increased degradation per cycle, 0.056% to 0.074% then 0.082% per cycle. From the theoretical argument, a change in temperature of 180°C is insufficient to cause damage because sufficient stress cannot be generated to propagate the cracks. Above this temperature range, an increase in micro-crack formation is observed, giving the linear prediction of degradation rate with cycling range K as shown in Figure 5.17.

$$C_R = 180 + 4630\ R_D \qquad (3)$$

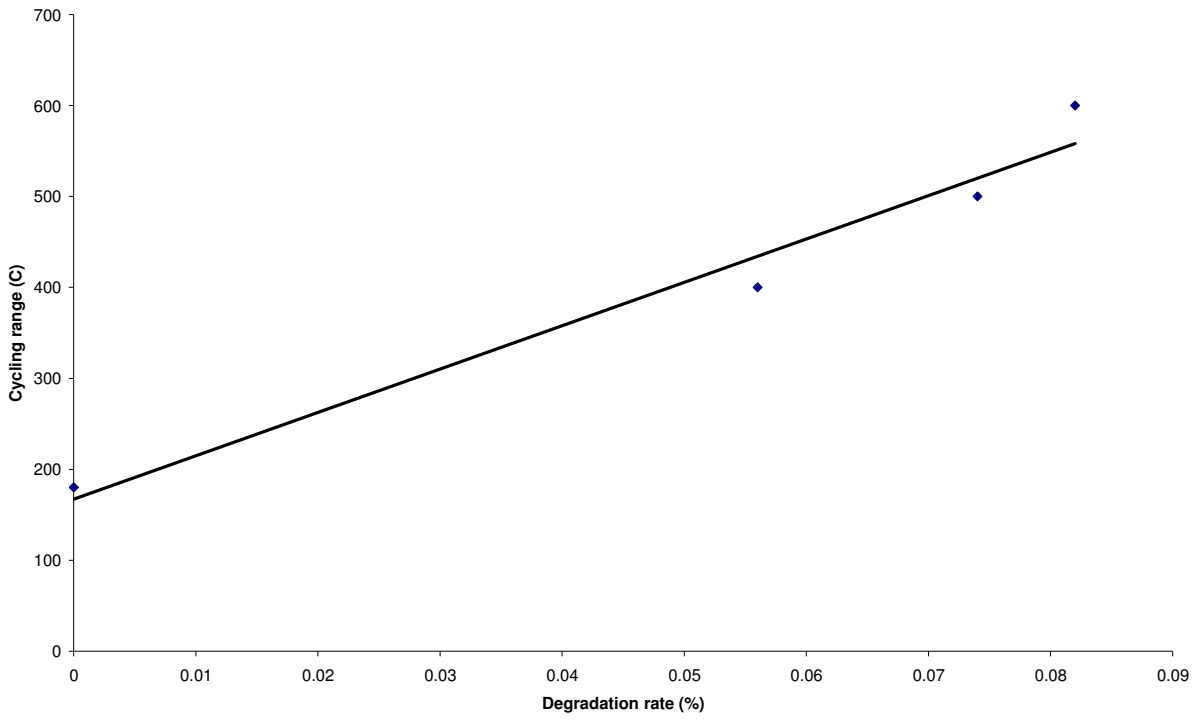

Figure 5.17 Relationship between thermal cycling range and degradation

5.4 Conclusion

Thermal cycling has been found to cause onlyslight degradation in micro-tubular SOFC, the degradation was mainly in the interconnecting silver wire which led to higher contact resistances. Cycling between 200°C - 600°C, 200°C -700°C and 200°C - 800°C all presented similar trends of degradation with Ni sintering progressing steadily once the cell was in the sintering regime (i.e. above 500°C) . Post mortem investigation by SEM showed the micro-tubes possessed good thermal cycling resilience by not cracking.

However, performing thermal cycling (with a gradient imposed) was found to cause micro-cracking and de-lamination in the PEN of the cells. This was principally because of several factors all working concertedly. These factors were identified as; Ni sintering, temperature gradients due to rapid heating and and differential expansion along the tube due to the temperature gradient imposed.

Also, dilatometry showed irreversible deformation occurring in the tubes because of the micro-structural changes that occur during sintering. This irreversible deformation was found to proceed rapidly initially and decrease with time as sintering diminishes. It should also be noted that even though the CTE mismatch in these tubes have been adjudged minimal, frequent starts-and-stop during operation can accumulate stresses due to this effect and cause degradation. To mitigate the effect of thermal cycling,

frequent start-and-stops during operation should be avoided or be performed in a very controlled manner.

Chapter 6

Redox Cycling

6 Redox Cycling

6.1 Objective

The objective of this chapter is to investigate and understand the redox behaviour of micro-tubular SOFCs. The investigation was performed by setting-up experiments to measure the physico-chemical changes and degradation that occur when Ni oxidizes to NiO. This is important because during SOFC operation, there is the probability of re-oxidation occurring due to leakages or blockages in the fuel delivery channel, system failure or emergency system shutdown[188].

The theory under investigation is that re-oxidation causes severe expansion in the anode, leading to micro-cracking, de-lamination and electrolyte channel cracking. Such degradation, will lead to increase in the resistance of the anode, thus causing performance drop. SEM is used to investigate degradation (micro-cracking, de-lamination and electrolyte channel cracking) in the micro-structure while thermo-gravimetric analysis is used to measure the rate of oxidation and reduction.

6.2 Experimental Methods

6.2.1 Electrochemical performance degradation Analysis

The electrochemical performance degradation of the micro-tubes was investigated by heating the micro-tubular SOFC at a constant rate (200°C/min) to the desired temperature (600^{o}C, 700^{o}C or 800^{o}C). The cell was then held at this temperature

while redox cycling was performed. Cycling was achieved by depriving the anode of hydrogen supply for a period of time (this was varied) to allow oxidation to occur and subsequently re-introducing hydrogen for reduction to occur. This was repeated several times in succession in order to observe the degradation in performance. Current was drawn at 0.5V all through the experiment.

The objective of these tests was to investigate the effect of redox cycling on the electro-chemical performance and durability of micro-tubular SOFCs. The degradation was characterized in terms of the decrease in electrochemical performance with progress in cycling.

6.2.2 Expansion and Contraction Measurements during Redox Cycling (Dilatomery)

Dilatometry was used in order to understand the mechanical behaviour of micro-tubular SOFC during redox cycling. A pushrod dilatometer (Netzsch^{TM} Dil 402C) was used to measure the sample expansion and contractions. For both oxidation and reduction, the samples were heated to the desired temperature (600^{o}C, 700^{o}C or 800^{o}C) in nitrogen before the reducing or oxidising atmosphere was introduced. The expansion and contraction in the samples are presented in terms of percentage (%) increase or decrease in sample length.

6.2.3 Thermo-gravimetric Analysis

Thermo-gravimetry was employed in order to measure the mass change during redox cycling. It was also used to determine the onset and end of oxidation and reduction. A

Netzsch™ TG 209C thermo-gravimetric analyser was used for this purpose. For constant temperature oxidation, the samples were heated to the desired temperatures in nitrogen (inert atmosphere) before oxidation or reduction was performed by using the appropriate atmosphere. The change in mass was presented as the % of the original mass.

6.3 Redox Cycling Results

6.3.1.1 Electro-chemical Measurements of degradation during Redox Cycling

In Figure 6.1 , a micro-tube is cycled in hydrogen at 800°C while current was being drawn at 0.5V. At the commencement of redox cycling, a current of 1.2A is observed, but as cycling proceeded this is seen to decrease slightly giving a final value of 1.15A after 9 redox cycles. This result is typical of SOFCs under redox condition[158], progressive degradation in performance has been reported with redox cycling. However, what still needs to be understood is the cause of this degradation and how it relates to the drop in performance. This is the subject of this chapter and will be looked at in great detail.

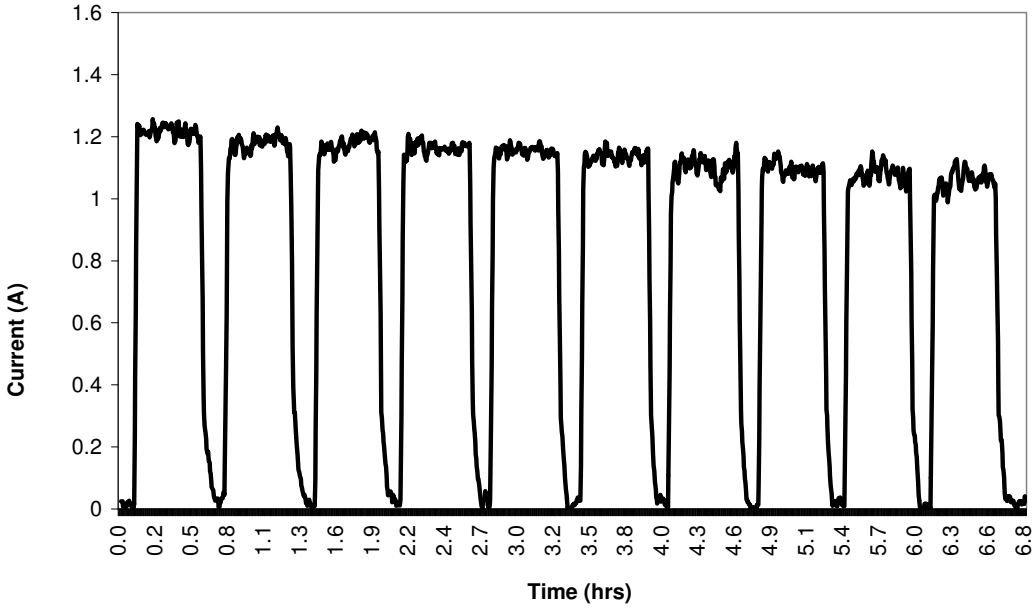

Figure 6.1 The degradation of a micro-tube with progress in redox cycling

6.3.2 Modes of oxidation during redox cycling

Two oxidation modes were utilized during redox cycling; oxidation due to oxygen diffusion through the tube from the atmosphere and electrochemical oxidation due to oxygen ion transfer through the electrolyte, which occurs due to fuel starvation. The later is only possible when current is being drawn from the cell during the redox operation, and it helps for complete oxidation to be achieved as oxidation due to diffusion is limited by the mass transfer effects and decrease in porosity when oxidation occurs. This phenomena has been discussed in detail in previous studies by Atkinson et al[189], where Anode substrate cracking and electrolyte channel cracking were reported as the main modes of degradation during electrochemical oxidation of

the anode. The modes of degradation due to these two oxidation modes are different and several researchers have reported numerous degradation pathways under these conditions[190, 191].

In any case, redox cycling has been reported to cause severe expansion and contraction in the micro-structure of SOFCs based on Ni/YSZ due to the conversion of the anode from Ni/YSZ to NiO/YSZ [104, 170, 192-194]. This conversion starts to occur at temperatures above 290°C for oxidation and 450°C for reduction as shown in Figure 6.2 and Figure 6.3. In Figure 6.2, the thick green trace is the % mass change of the sample as it was heated from room temperature to 800^{o}C, it can be seen from the dotted green line (i.e. the rate of mass change with time) that the change in mass started at about 290^{o}C. To investigate the minimum temperature required for reduction to occur, dilatometery was employed, see Figure 6.3. However, this is not the best technique for the investigation, because minute degree of reduction can occur without characteristic length change. However it was found that the minimum reduction temperature was 450^{o}C as shown by the bold purple trace. This value is similar to those reported in earlier studies by Dhir et al, where a value of approx. 460^{o}C was reported.

Waldillig et al studied the kinetics of oxidation and reduction and suggested that oxidation proceeded by parabolic kinetics at temperatures below 700°C with an activation energy of 87kJ/mol, while reduction proceeded by linear kinetic with an activation energy of 78kJ/mol[170].

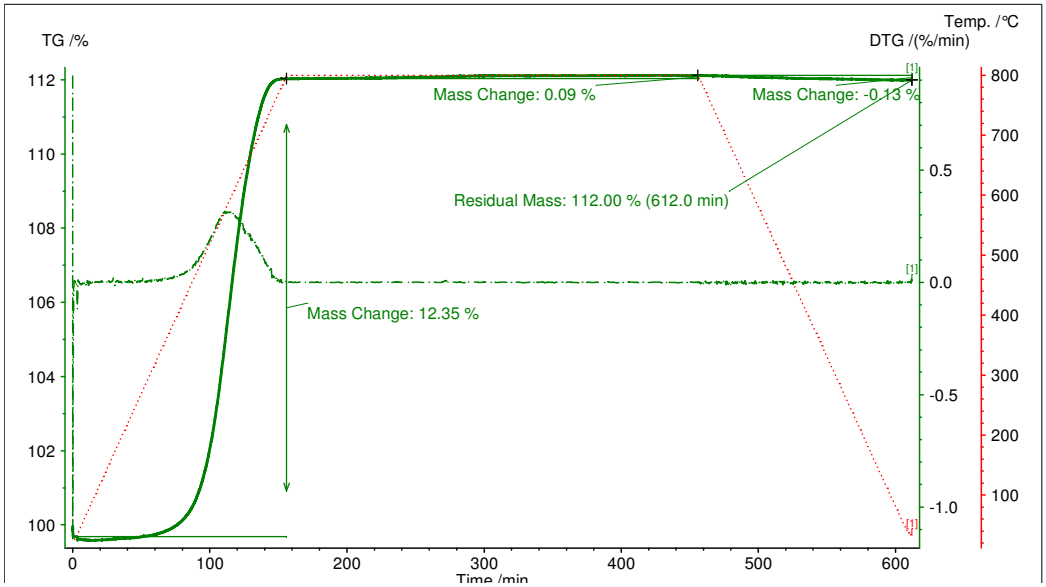

Figure 6.2 The minimum possible temperature at which oxidation proceeds

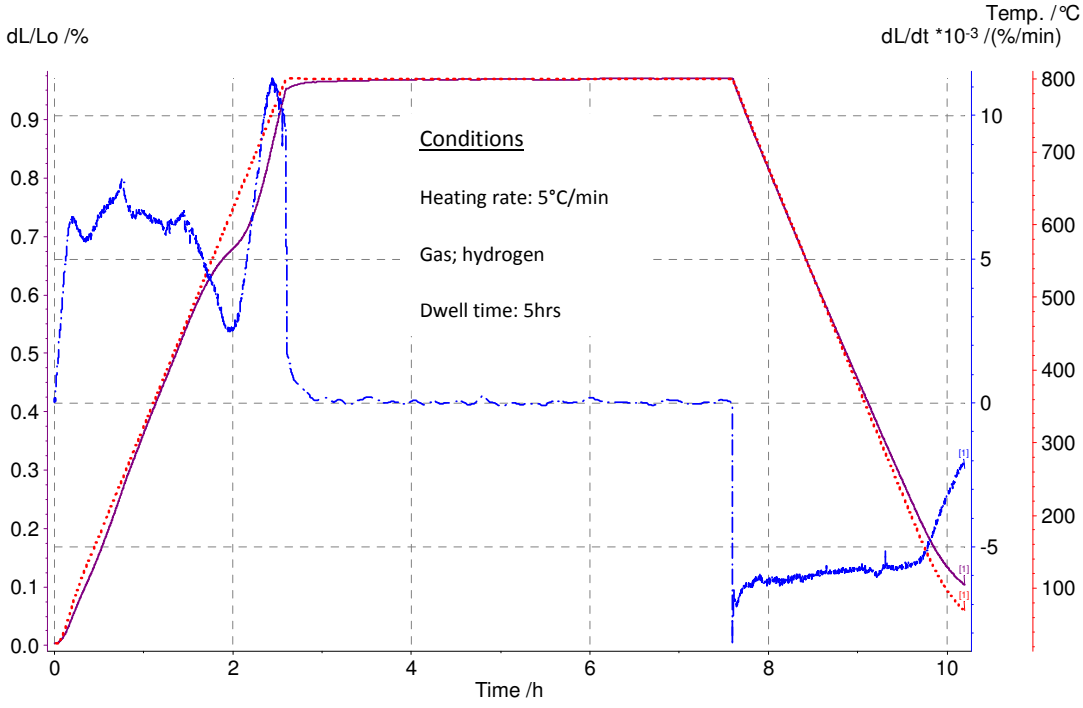

Figure 6.3. The minimum possible temperature at which reduction proceeds

6.3.3 Theory of degradation during Redox Cycling

As stated in section 6.3.2, two distinct oxidation methods were employed in order to characterize the redox behaviour of the tubes. They are;

- Oxidation by air diffusion: Air at atmospheric pressure is allowed to enter the anode compartment and oxidize the Ni particles. This oxidation technique has been used by quite a few researchers in the past and the mode of degradation is related to the anodic strain associated to the conversion from Ni to NiO.

- Oxidation by ionic current: This occurs due to fuel starvation or excessive fuel dilution in the anode. Very few researchers have looked into this phenomenon and its degradation mechanism is not well established. Ionic oxidation proceeds according to the reaction

  $Ni + O_2^- \rightarrow NiO + 2e^-$

6.3.3.1 Oxidation by Ionic Current

Electrochemical oxidation of the anode was investigated by switching the fuel flow from hydrogen to nitrogen and then drawing current. This was done in order to impose an oxygen flux across the anode TPB. Once this is done, the voltage is observed to fall instantaneously as the hydrogen in the anode compartment is consumed, until it reaches equilibrium value of 0.69V where the voltage is seen to be partially stable, see Figure 6.4. This value corresponds to the theoretical open circuit

potential for a NiO/Ni/H_2O system at the operating temperature i.e. 800°C. The open circuit potential under this condition is given by

$$OCV_{Ni+\frac{1}{2}O2\leftrightarrow NiO}=\frac{RT}{4F}\ln\frac{P_{O_2}^{air}}{P_{O_2}^{fuel}} \quad [189]$$

Where R is the universal gas constant, T is the operating temperature i.e. 800°C and P_{O2} are the partial pressure concentrations of fuel and air respectively. A similar oxidation potential has been reported by [189, 190]who used experimental and analytical techniques to calculate the open circuit potential under these conditions.

Since there is no-fuel on the anode side, the Ni present is used as fuel, with progressive conversion to NiO. As oxidation progresses, a steady decrease in the voltage is observed as the NiO conversion proceeds. This progressive decrease in performance is due to the growth of the NiO layer which increases the ohmic resistance of the anode. After 3 minutes of oxidation, the re-introduction of fuel for reduction showed an OCV of 1.09V, implying that no electrolyte cracking occurred during the oxidation process. Thus, the re-oxidation process might have given birth to micro-cracks and de-laminations in the anode, but it wasn't sufficient to cause electrolyte channel cracking. In the event of electrolyte cracking, severe voltage drop or even complete tube failure (in extreme cases) would be observed. Previous studies by Hatae et al reported that oxidation due to ion flux (i.e. < 5%) helps to relieve some of the residual stresses in the electrolyte. This implies that a small degree of ionic

oxidation might be beneficial to the cell, by helping to balance out some of the internal manufacturing stresses. This was however not verified in this study and will be looked at in future analysis.

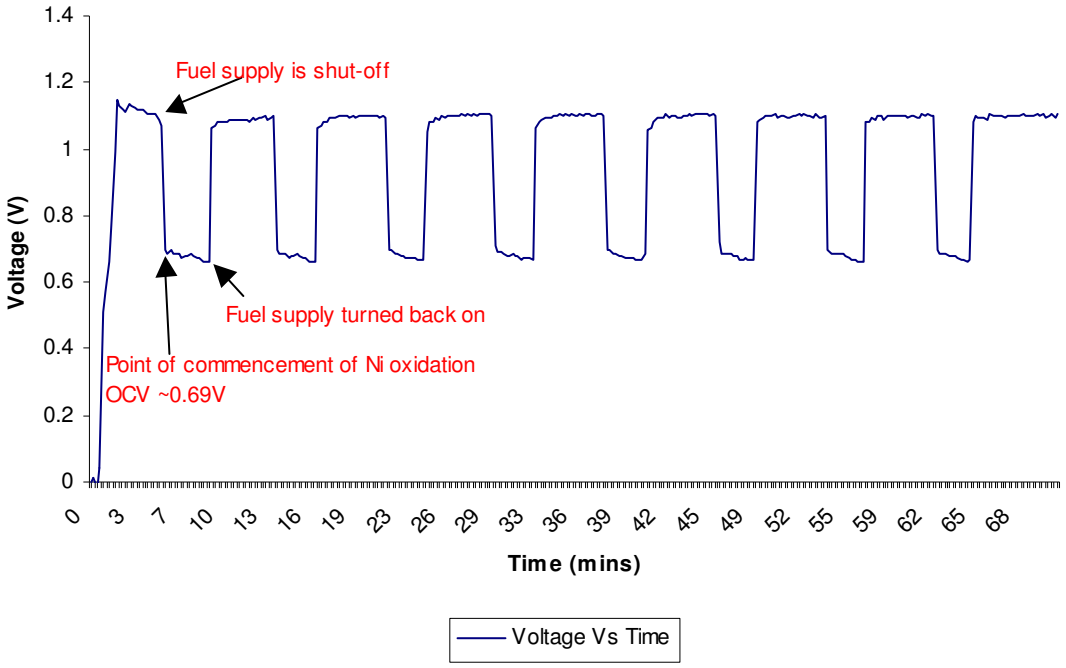

Figure 6.4 The voltage of a cell under electrochemical oxidation

6.3.3.2 Oxidation by air diffusion

Majority of the redox studies in the past have employed this technique, where an oxidizing atmosphere (usually air) is used in the anode side to convert the Ni present to its oxide i.e. NiO[167, 170, 195]. This method simulates a situation where a leakage

in the fuel delivery channel leads to the oxidation of the cermet. The degradation is a direct consequence of the macroscopic change that occurs in the structure when Ni oxidizes to NiO. This bulk expansion is dependent on the degree of expansion, Ni content and porosity in the cermet. The strain from the anode expansion induces stresses in the electrolyte and cathode causing cracking and flaking in severe cases. Sometimes even partial oxidation can lead to mechanical failure in the electrolyte[196]. Several analytical and modeling techniques have been used in the past to analyze and predict these degradation modes. It has been shown that the anode cracking occurs frequently but the electrolyte cracking starts to occur when the anodic strain reaches approximately 0.20% i.e. based on the Forchungzentrum Julich (FZJ) anode composition[190], this critical strain value has also been confirmed both experimentally and analytically by Atkinson et al [197] who performed redox investigations on the similar anode compositions. It was also established that the failure mode of SOFC under free standing oxidation is by electrolyte cracking.

In this study however, SEM micrographs (See Figure 6.5) have shown that electrolyte cracking was observed only after an oxidation strain ε_{ox} between 0.31 -0.42% corresponding to a degree of oxidation between 51 - 82%, see Figure 6.6. .This is slightly different from values reported by Laurencin et al [190], who reported a critical oxidation strain between 0.26% - 0.34% for electrolyte cracking. The reason for this difference may not be unconnected to the difference in anode thicknesses between the two geometries. The FZJ anode was 1.5mm thick while the electrolyte and cathode thicknesses were approximately 10µm and 50µm thick respectively. On the

other hand, the tubes used in this study had a 200µm thick anode supported by a 15µm thick electrolyte and a 50µm thick cathode. The FZJ anode was therefore 7.5 times thicker than the anode used in this study and its chemo-mechanical behaviour under redox condition would be significantly different from a thinner anode, because a thicker anode would see greater expansion and consequently a greater degree of micro-cracking Also, residual stress in micro-tubes are usually lower than planar cells because of stress concentration at the edges. The oxidation strain usually adds to the inherent residual stress from the manufacturing process to cause failure.

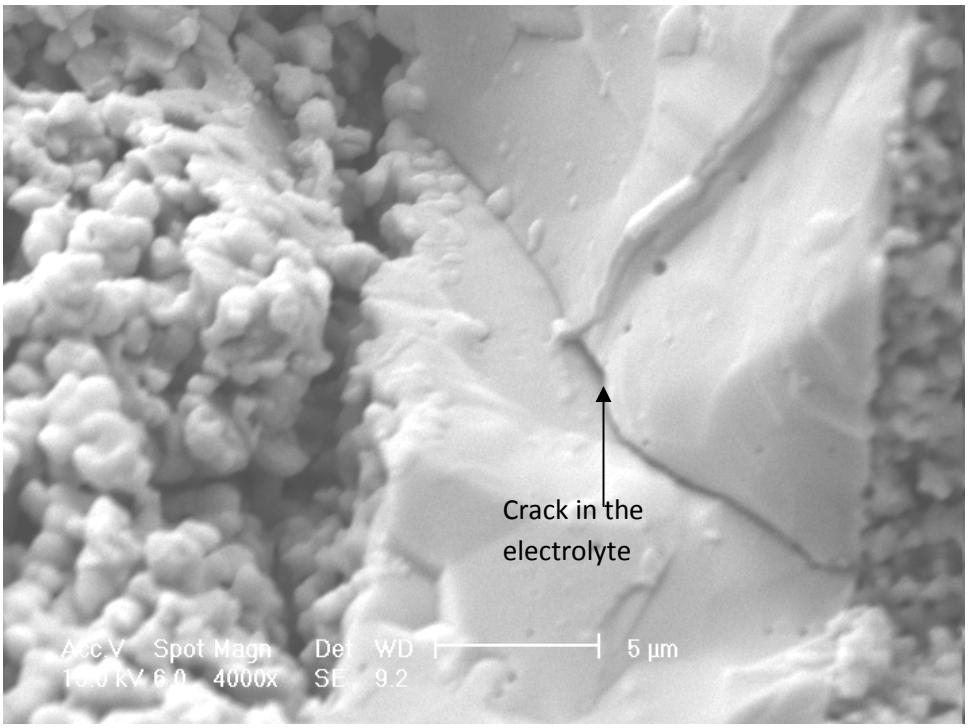

Figure 6.5 Showing a crack in the electrolyte

A crack in the electrolyte will lead to lower voltages and significant decrease in performance, due to fuel leaks across the electrolyte. Figure 6.6 shows the

macroscopic expansion in the anode with Ni conversion. It can be seen that the initial oxidation (i.e. 7 – 40%) proceeded by linear kinetics. Presumably, this corresponds to the oxidation of the surface Ni particles.

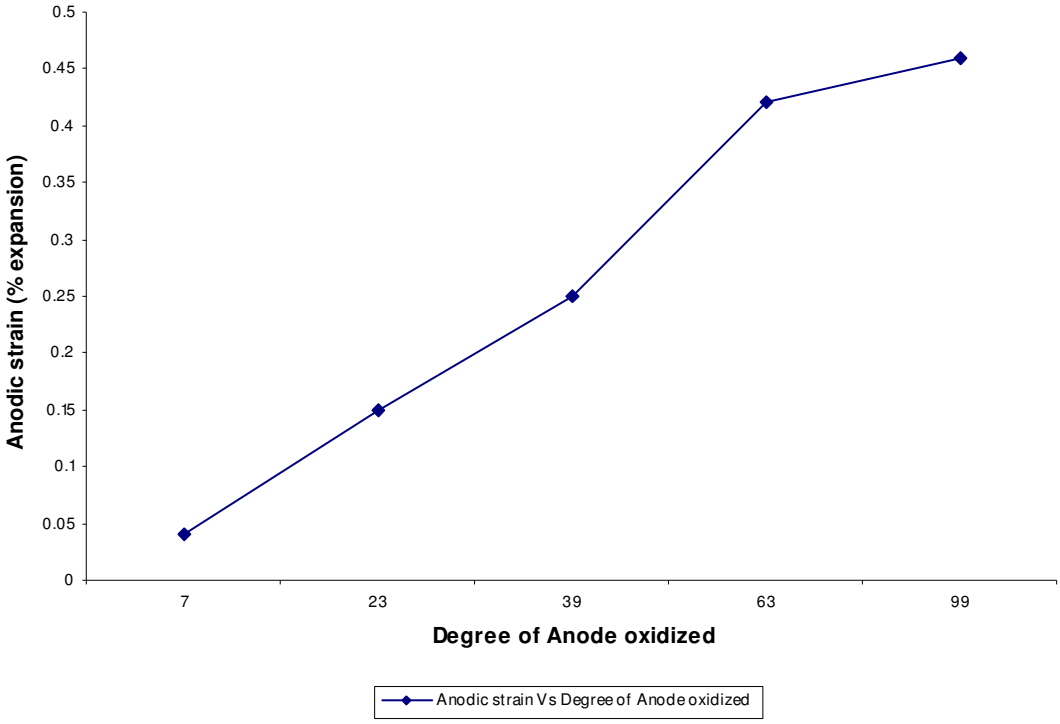

Figure 6.6 Showing the oxidation strain with degree of anode oxidized

6.3.4 Partial Oxidation and Reduction

In this section, the partial oxidation and reduction behaviour of micro-tubes is investigated. Partial reduction and oxidation simulates a situation where there are leakages in the fuel delivery channel, leading to anode oxidation by oxygen

entrainment from the air in the surrounding. This phenomenon occurs frequently during SOFC operation due to the failure of the interconnecting materials at high temperature. The ability of SOFCs to withstand some degree of oxidation during operation is very central to their operatability, because several SOFC manufacturers have reported re-oxidation of the anode during typical operation due to interconnect failures, thus SOFCs that can withstand a certain degree of oxidation without significant performance drop during operation are sought after

Figure 6.7, Figure 6.8 and Figure 6.9 show the results of the partial oxidation and reduction of micro-tubular SOFC at 600°C, 700°C and 800°C respectively. Partial oxidation was performed by shutting off the hydrogen supply for 5 minutes in order to allow oxidation by atmospheric oxygen to occur, while reduction was performed by opening the hydrogen supply valve for 5 minutes in order for reduction to proceed.

6.3.4.1 Partial Redox Cycling at 600^{o}C

In Figure 6.7 a peak performance of 0.81A is observed at the commencement of redox cycling, but as cycling proceeded a steady decrease is observed after each redox cycle, giving a final performance of 0.69A after 52 redox cycles. A degradation rate of 0.38%/cycle was estimated.

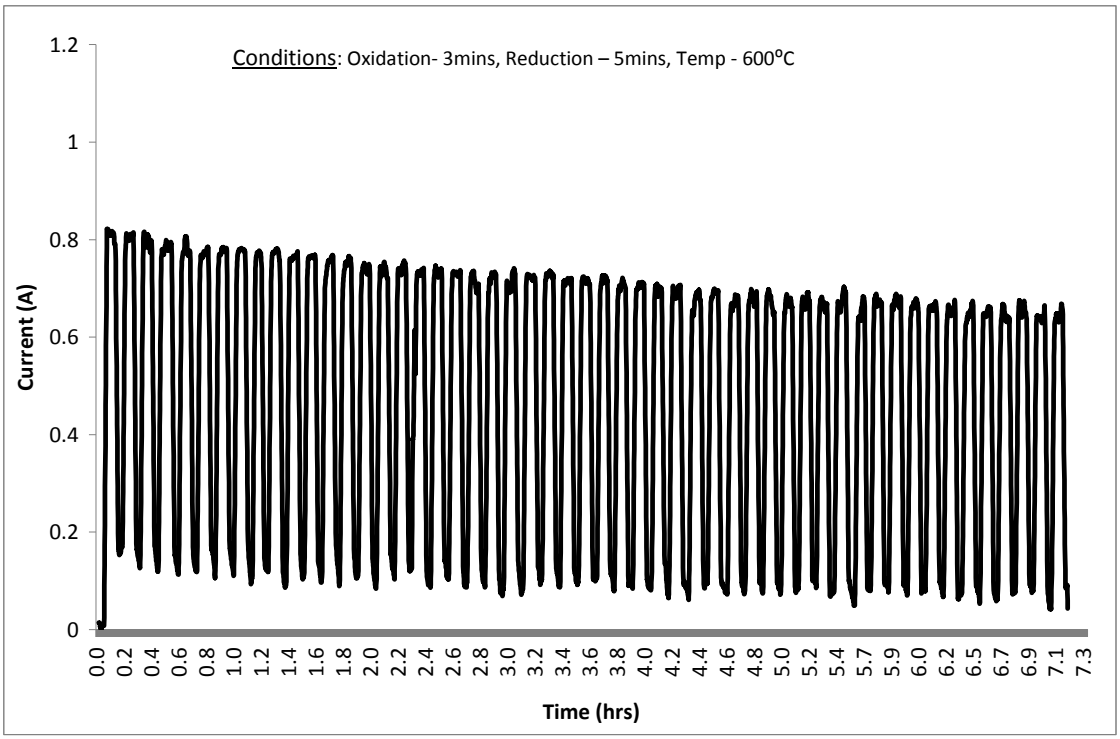

Figure 6.7. The partial redox performance of a micro-tube at 600°C

6.3.4.2 Partial Redox Cycling at 700°C

Figure 6.8 shows an initial peak performance of 1.04A at the commencement of cycling and a final current of 0.88A after 52 redox cycles, giving a degradation rate of 0.42%/cycle.

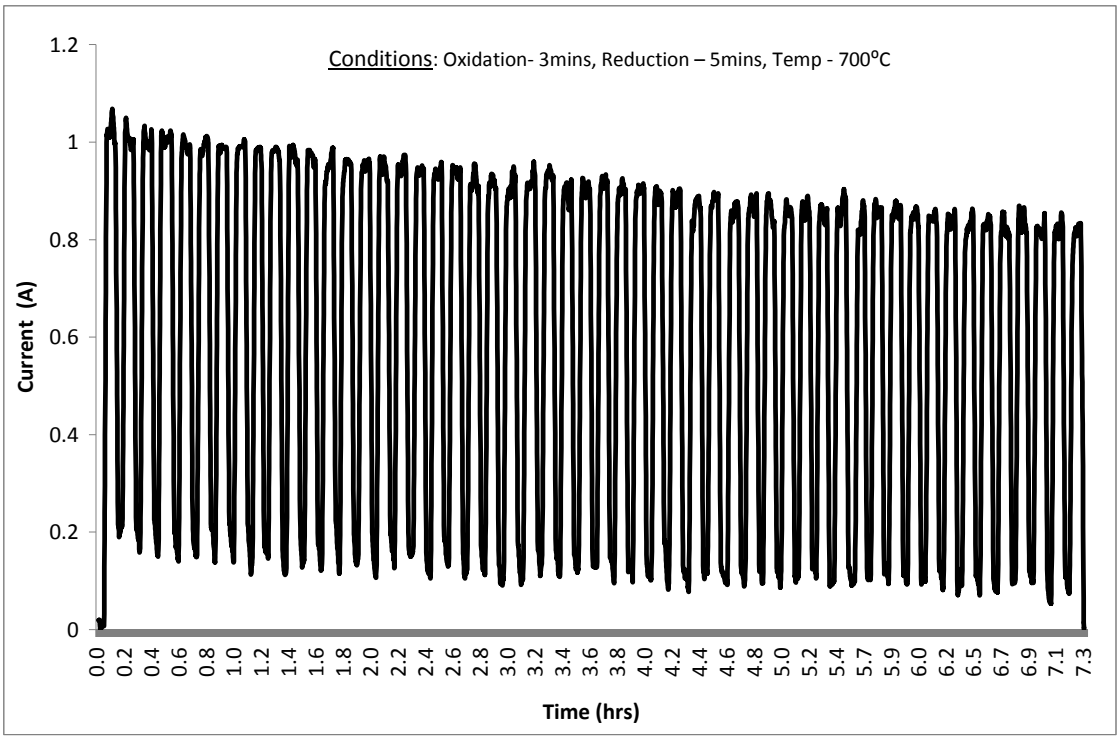

Figure 6.8. The partial redox performance of a micro-tube at 700°C

6.3.4.3 Partial Redox Cycling at 800°C

Figure 6.9 shows an initial peak performance of 1.21A which decreases to 1.02A after 52 redox cycles, giving degradation rate of 0.44%/cycle.

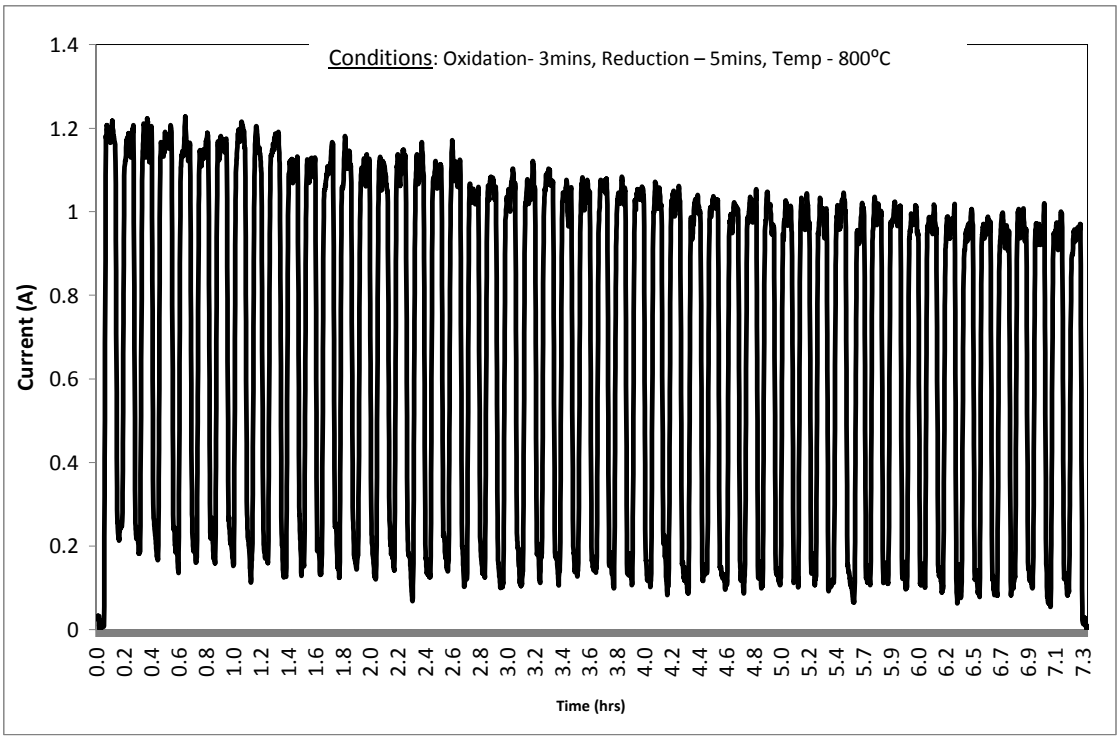

Figure 6.9. Showing the partial redox performance of a micro-tube at 800°C

6.3.4.4 Discussion of Partial Redox Cycling

In all three cases above, the percentage (%) of anode oxidized is seen to increase with temperature as portrayed in Table 6.1. The oxidized zones will experience severe expansions relative to the un-oxidized zones thereby creating a state of tension between these two zones. Also, an oxygen partial pressure gradient is bound to develop in the anode when the oxidation process commences because the oxygen enters at the open end of the tube and commences reaction with Ni there and gradually advances up the tube. Such conversion along the tube's length would give rise to a state of tension between the converted and unconverted areas. Stresses are likely to develop under this condition thereby enhancing degradation.

The oxidation of micro-tubes for such short periods as illustrated here does not cause gross cracking or instant failure in the micro-tubes as shown in the results. The degradation was however far more deleterious than observed during thermal cycling, where several thermal cycles only produced marginal degradation.

The use of inert purge gas to prevent the anode from re-oxidizing is sometimes employed in some SOFC devices but this increases the cost of the overall system. Thus, anode formulations with high redox tolerance and high electrochemical performance are mostly preferred.

Temperature	% Oxidation after 3 mins	% Reduction after 5 mins
600°C	4.5%	99%
700°C	6%	99%
800°C	7%	99%

Table 6.1 Showing the percentage of anode oxidized with temperature

6.3.5 Complete Oxidation and Reduction

In this section, the behaviour of micro-tubular SOFC under complete oxidation and reduction conditions is investigated. Complete redox simulates an extreme situation where a blockage in the fuel delivery channel leads to oxygen diffusion into the anode

and fully converting the Ni/YSZ cermet to a NiO/YSZ cermet. The possibility of this occurring is slim, but an investigation into the behaviour of the Ni anode under this condition is important considering the damaging effect of complete oxidation on SOFC anodes.

The redox behaviour of the micro-tubes under complete oxidation and reduction conditions are investigated at 600°C, 700°C and 800°C.Figure 6.10, Figure 6.15 and Figure 6.18 show their behaviour at 600°C, 700°C and 800°C respectively. Unlike partial redox conditions, only a few redox cycles have been performed here due to the severe degradation of the anodes with 100% redox cycling. For the purpose of elucidation, redox cycling at each of these temperatures will be considered individually.

6.3.5.1 Complete Redox operation at 600°C

Figure 6.10 shows the redox cycling of a micro-tube at 600°C, 2 complete redox cycles were performed with the flow of hydrogen changing between 20ml/min and 0ml/min. Current was drawn at 0.5V throughout the experiment and degradation was evaluated in terms of the decrease in electro-chemical performance. At 600°C, complete oxidation was achieved in 4.5 hrs as shown by thermo-gravimetry in Figure 6.11. While complete reduction was achieved in 4 hrs as shown in Figure 6.12. For both figures, the green trace corresponds to the mass change of the sample with oxidation while the red dotted line is the temperature profile. The blue dotted line is the first

derivative of the sample response with time, this shows the rate of mass change and the exact point in which the change started.

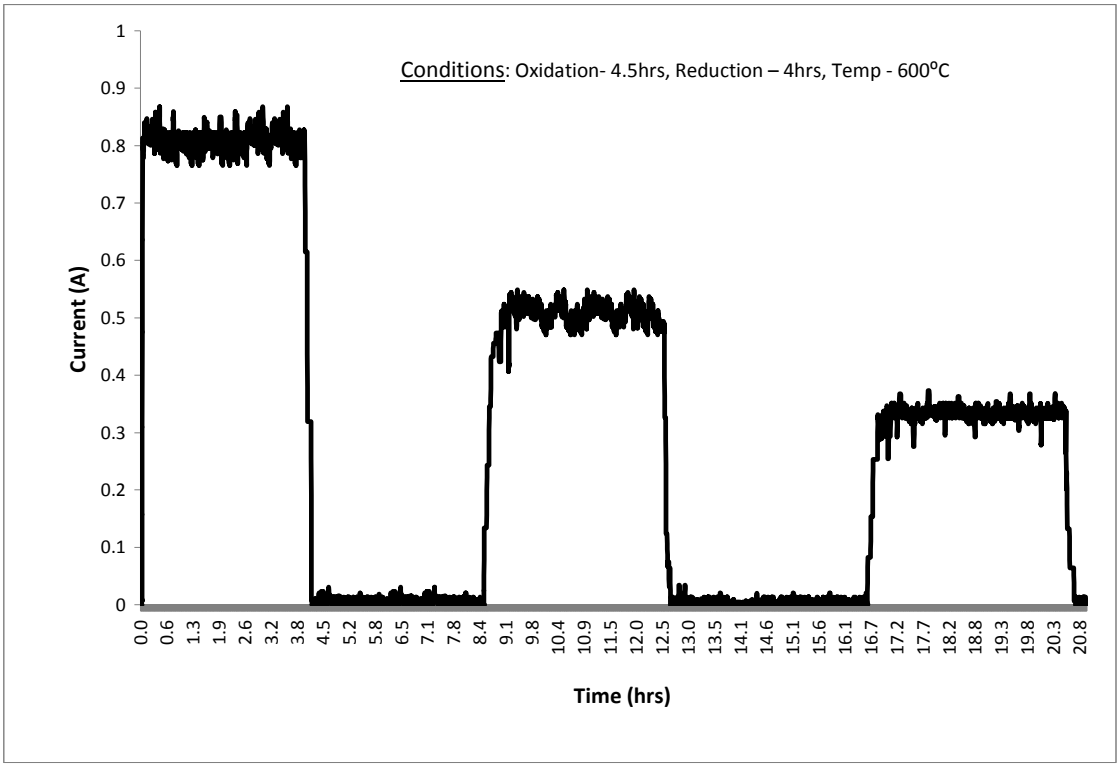

Figure 6.10. The redox cycling of a micro-tube at 600°C

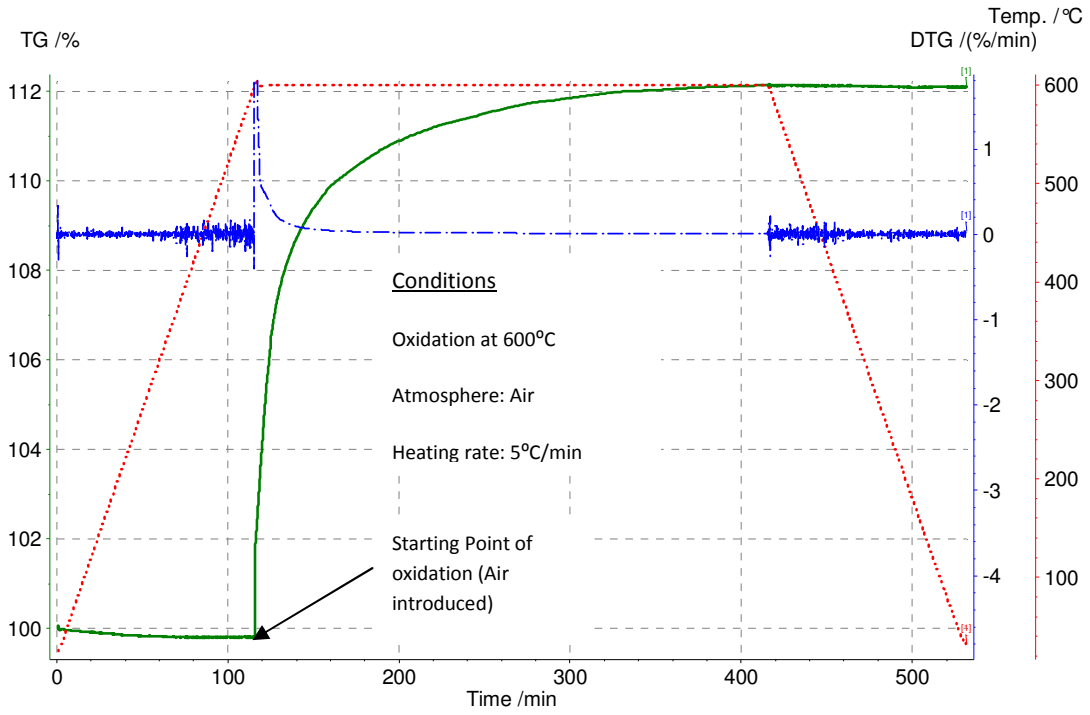

Figure 6.11. The complete oxidation of a micro-tube at 600°C under TGA

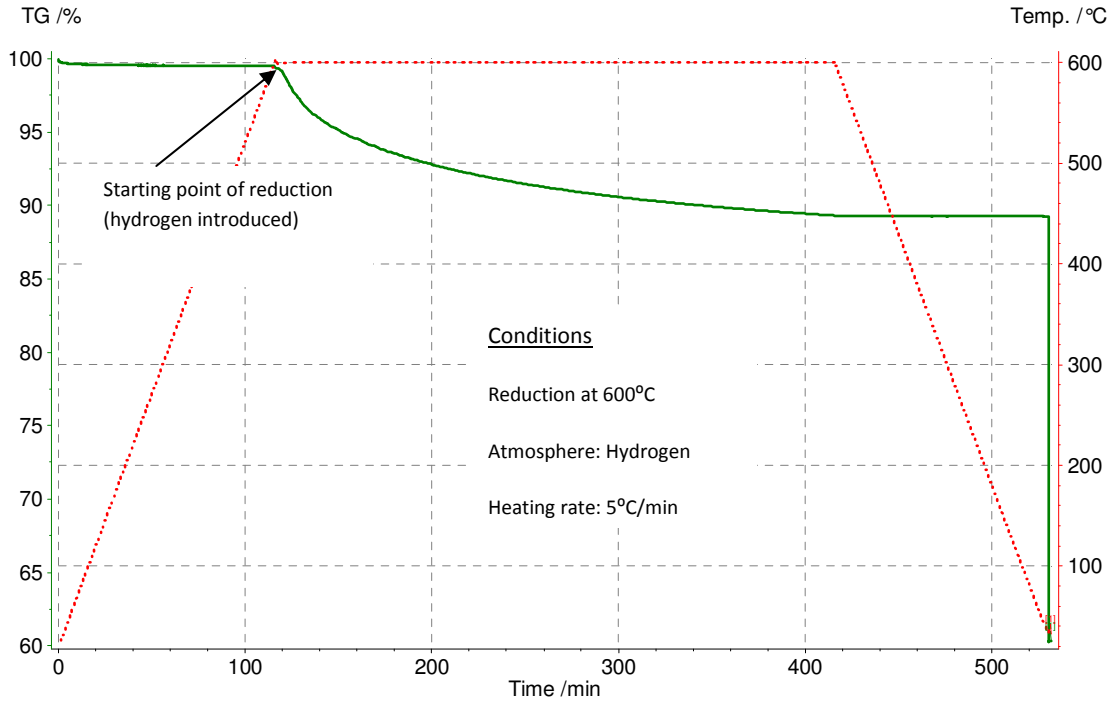

Figure 6.12. The complete reduction of a micro-tube at 600°C under TGA

At 600°C, oxidation was observed to proceed rapidly in the opening minutes, as the oxygen quickly oxidizes the surface Ni particles thereby converting them to NiO. The conversion of the surface Ni to NiO, decreases the surface porosity of the cermet making it difficult for the oxygen to access the sub-surface Ni in the anode. This decrease in oxidation rate is evident after 30 minutes as the % mass change begins to decrease until the % mass change become constant after 4.5 hrs, signifying the end of oxidation.

In the same vein, the reduction is seen to proceed gradually as the hydrogen began to reduce the surface NiO particles before gradually diffusing through the anode to reach the sub-surface NiO particles. Complete reduction was achieved in 4hrs. At this stage, the NiO/YSZ cermet has been fully converted to Ni/YSZ cermet and the anode is porous again.

From the redox cycling curve above, i.e.Figure 6.10, an initial current of 0.8A was observed as the micro-tube was held for 4 hrs at 600°C in order to achieve complete reduction. Subsequently, the hydrogen supply was shut off for 4.5 hrs in order to allow complete oxidation of the anode. With this first redox cycle, a current of 0.52 A was observed after the hydrogen supply was turned on; the degradation for this stage was 35%. The next redox cycle led to further degradation in the current from 0.52 A to 0.38 A′ giving a degradation of 26.9%.

It is very interesting to see that the first cycle led to a higher degradation compared to the second. This is because the first cycle caused the initial gross micro-cracking in the micro-structure while subsequent cycles only led to additional degradation and also increased the stresses in the bulk due to the expansion witnessed.

6.3.5.2 Complete redox operation at 700°C

To investigate the minimum time required for the 100% oxidation and reduction of micro-tubular SOFC at 700°C thermo-gravimetric analysis was performed. Figure 6.13 shows the result of the oxidation at 700°C. Initially, a very rapid oxidation is observed as the atmospheric oxygen attaches to the Ni in the anode. The initial rate of oxidation here is seen to proceed quicker than at 600°C. This is because the high temperature promotes the reaction. This segment is followed by a relatively lower rate of oxidation as seen by the gradual increase in mass. Oxidation is seen to attain completion after 3.4 hrs; this is significantly lower than the time for oxidation at 600°C because there is an increase in the rate of oxidation with temperature.

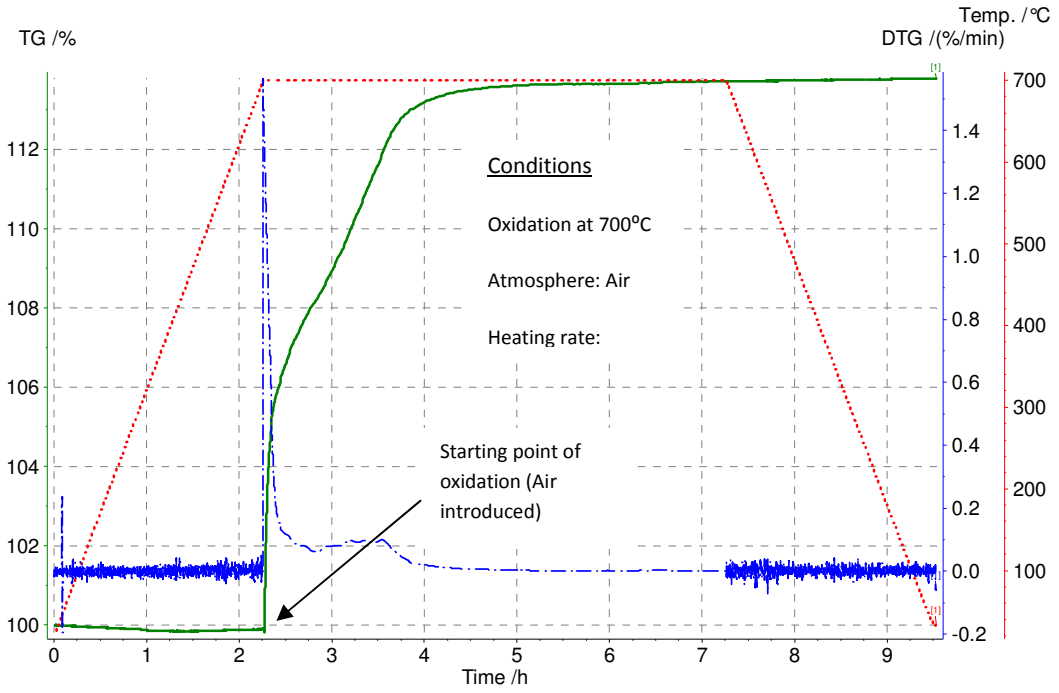

Figure 6.13. Showing complete oxidation of a micro-tube at 700°C

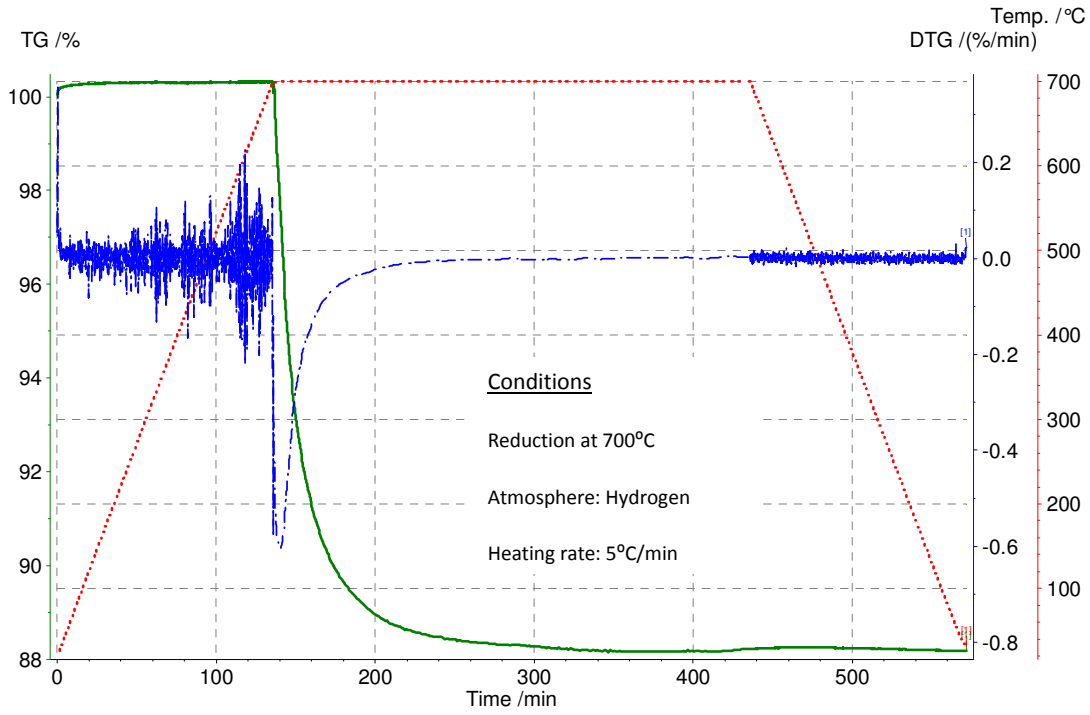

Figure 6.14. Showing complete reduction at 700°C

The reduction at 700°C is seen to proceed rapidly in the opening minutes by linear kinetics as shown by the Δ (TG%/min), see Figure 6.14. This linear rate is seen to change after 5 minutes as most of the Ni in the surface was reduced and the diffusion limitation comes into play. The maximum reduction rate was -0.5%/min which occurred after 5 minutes. 100% reduction was achieved after 3.3hrs.

Since the minimum times required for complete reduction and oxidation at 700°C are established, the electro-chemical performance of the micro-tubes under complete redox cycling was investigated at 0.5V as shown in Figure 6.15 below.

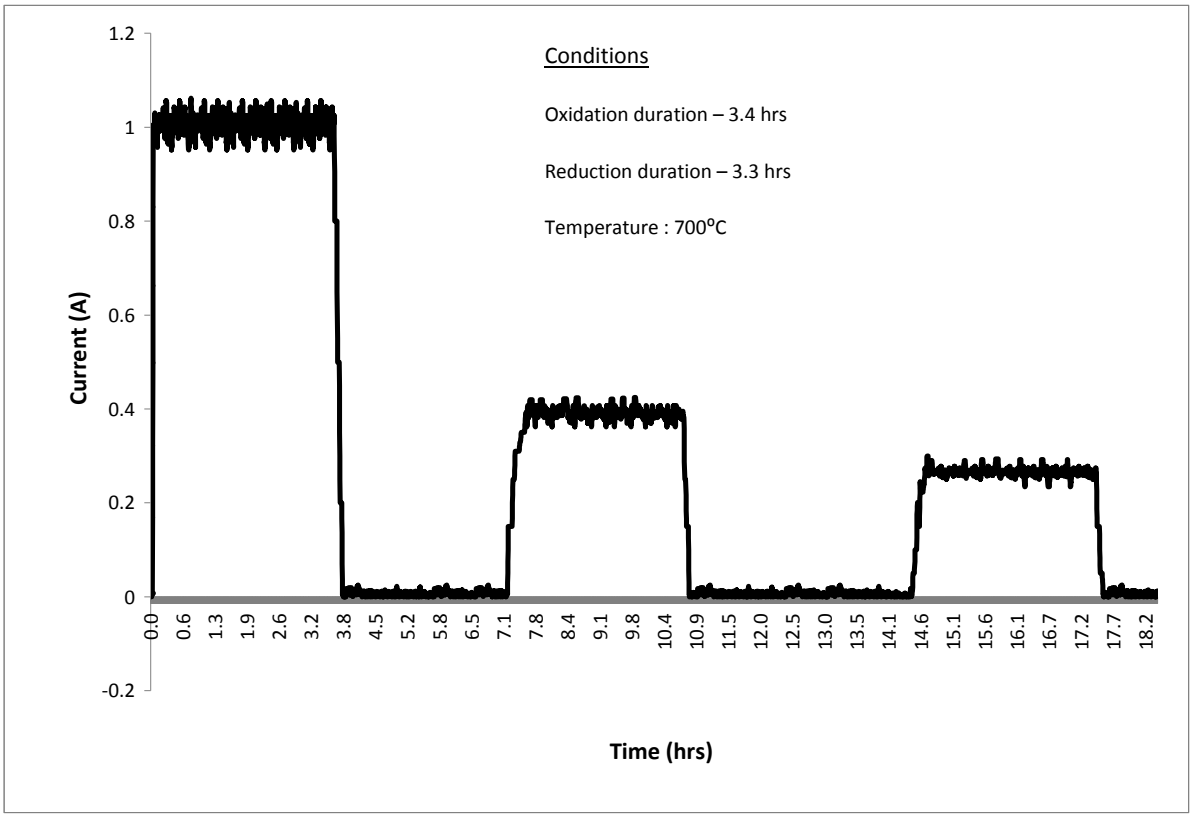

Figure 6.15. The complete redox cycling of a micro-tube at 700°C

Figure 6.15 shows the results for complete redox cycling at 700°C. Initially, a peak performance of 1 A is observed as hydrogen was fed but this was seen to decrease to 0.39 A after the first redox cycle. A degradation of 61% was calculated for this step. This large degradation rate is the result of micro-cracking caused by the severe expansion during oxidation at 700°C. During the second redox cycle, a decrease in performance from 0.39 A to 0.28A is observed, a degradation of 28% is estimated. As seen in the redox at 600°C, the first cycle had a greater degradation effect than the second cycle. This is mainly due to the gross micro-cracking caused by the first redox cycle which has a greater deleterious effect than the second cycle.

6.3.5.3 Complete redox operation at 800°C

Figure 6.16 shows the result of the oxidation of a micro-tube at 800°C. Just like the previous case i.e.redox at 700°C, the oxidation is observed to proceed rapidly initially as seen by the Δ (TG%/min) which showed a linear rate. This is mainly due to the oxidation of the surface Ni. The initial rate of oxidation in this case however is seen to proceed quicker than at 700°C, because the high temperature promotes this reaction.

This segment is followed by a lower rate of oxidation as seen by the gradual increase in mass. This lower rate of oxidation is again due to diffusion limitation, because oxygen atoms have to diffuse into the anode in order to reach the sub-surface Ni particles. Oxidation is seen to attain completion after 0.67 hrs; this is considerably lower than the time for oxidation at 700°C. This rapid oxidation rate will give rise to

sudden expansion in the micro-structure as the Ni particles are converted to NiO. This sudden expansion will lead to severe stress induction and gross micro-cracking.

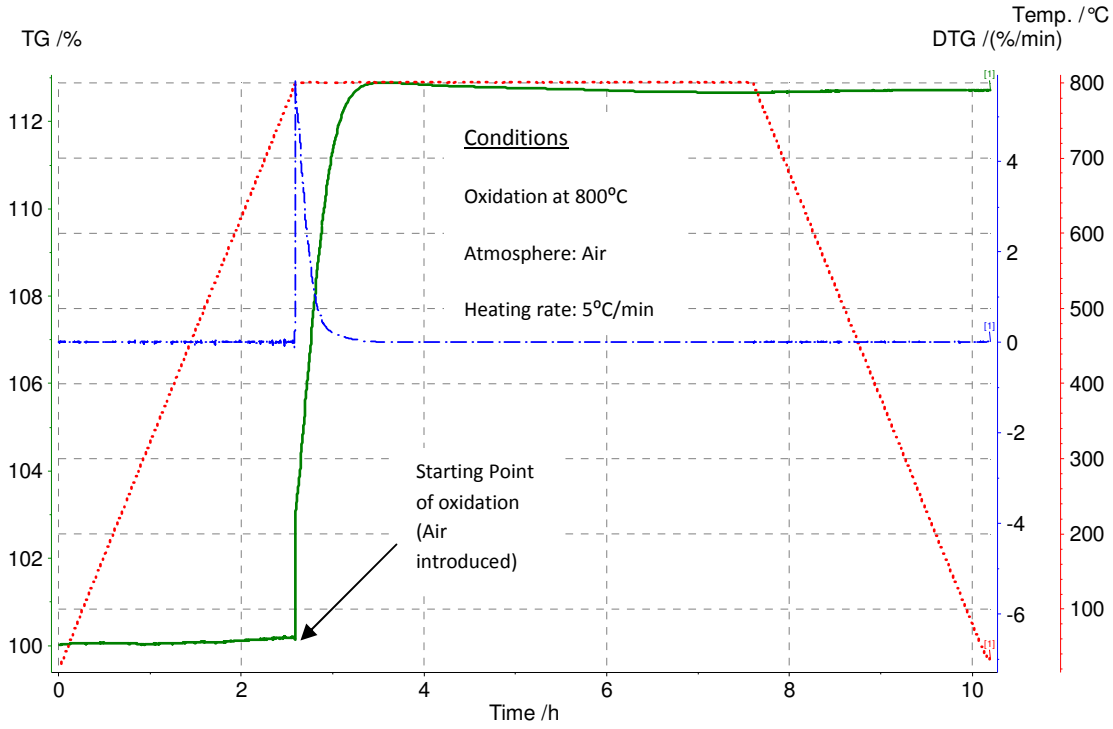

Figure 6.16. Showing complete oxidation of a micro-tube at 800°C

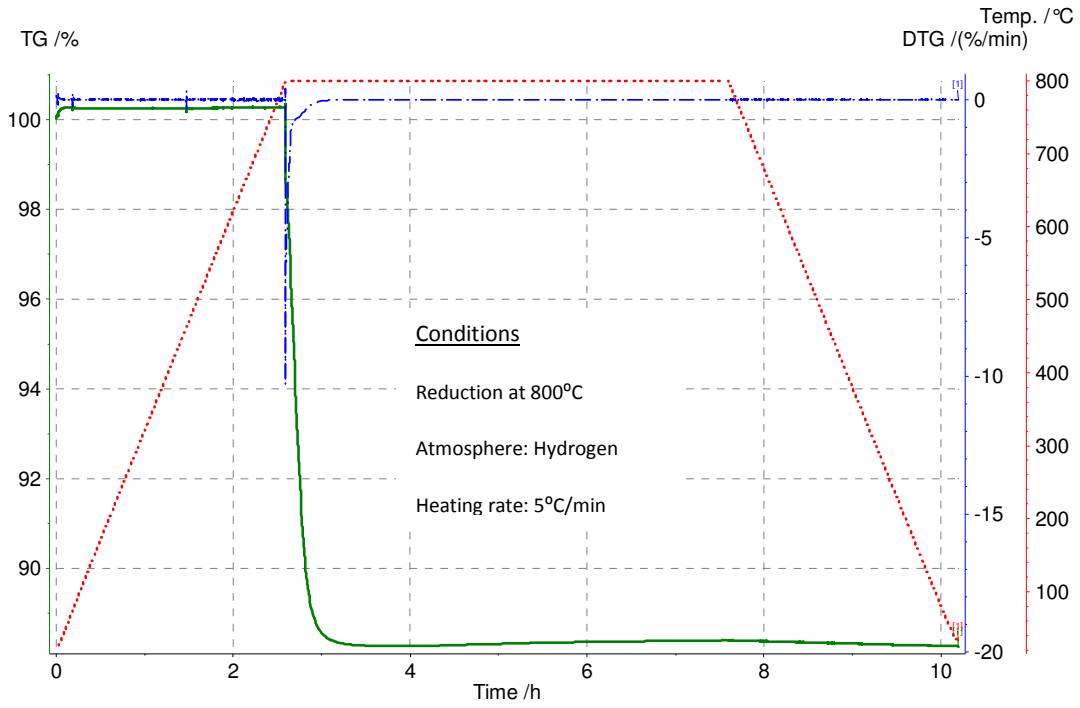

Figure 6.17. Showing complete reduction of a micro-tube at 800°C

As shown in Figure 6.17, reduction at 800°C is seen to proceed rapidly in the opening minutes by linear kinetics as shown by the Δ (TG%/min). This linear rate is seen to change after a few minutes as most of the Ni in the surface was reduced and the diffusion limitation comes into play. 100% conversion of NiO to Ni was achieved in 0.63 hrs.

With the minimum time required for complete reduction and oxidation at 800°C determined, the electro-chemical performance of the micro-tubes under complete redox cycling was investigated at 0.5V. Figure 6.18 shows the results for complete redox cycling at 800°C. Initially, a peak performance of 1.2 A is observed as hydrogen was flowed but this was seen to decrease to 0.34 A after the first redox cycle. A

degradation of 72% was calculated for this step. This large degradation rate is the result of micro-cracking caused by the severe expansion at 800°C.

During the second redox cycle, a decrease in performance from 0.34 A to 0.20 A is observed, giving a degradation of 41%. Just like the redox at 600°C and 700 ºC, the first redox cyle had a greater degradation effect than the second cycle. This is because the first cycle usually causes more damage, giving rise to the intial gross micro-cracking while the subsequent cycles merely add to the pre-existing degradation.

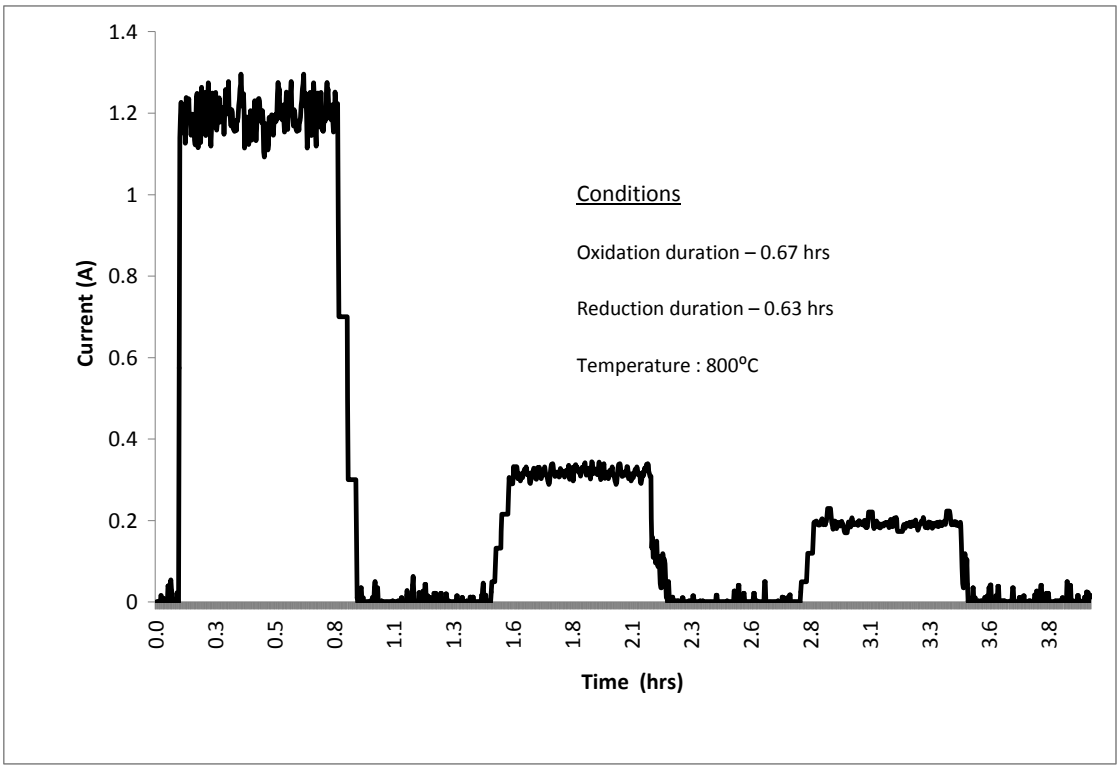

Figure 6.18**.** Showing complete redox cycling of a micro-tube at 800°C

6.3.5.4 Discussion of Complete Redox Cycling

As shown in table 6.2, operating the micro-tube at 600°C gave the best redox performance because the degradation rate was lower compared to the other temperatures. However, the current was also lower because of the high ohmic resistance due to a low ion transfer rate at this temperature. Thus in terms of redox performance, lower temperatures are better favoured for micro-tubes because the overall degradation due to redox cycling is low.The accelerated degradation rate at 800°C is mainly due to the rapid rate of oxidation at this temperature, which caused gross failure. The gross failure was because of severe cracking in the anode and the consequent electrolyte channel cracking. Electrolyte channel cracking is the most damaging degradation mechanism in SOFC, because it leads to lower operation voltages because of fuel cross over and electrons short circuiting. A degree of anode micro-cracking on the other hand, can be tolerated by the cells because it only affects the ohmic behaviour of the cells as against electrolyte cracking which affects the cell equilibrium and electrical behaviour.

These micro-tubes have shown immense redox cycling resilience, by their ability to somewhat withstand 100% oxidation and reduction. Previous studies by Bujalski et al[158] reported the gross cracking and splintering of a Forchungszentrum Julich (FZJ) cells after one partial redox cycle.

Temperature	Time to achieve Complete Oxidation	Time to achieve Complete Reduction	% Degradation after first Cycle
600°C	4.5hrs	4.0hrs	35%
700°C	3.4hrs	3.3hrs	61%
800°C	0.67hrs	0.63hrs	72%

Table 6.2 The redox durations and % degradation with respect to the various temperatures.

6.3.6 Expansion during Redox Cycling

The oxidation of Ni to NiO is known to cause severe expansion in the bulk of SOFCs[170]. As explained previously, this sudden expansion is responsible for the micro-cracking and failure in SOFC. In this section, the expansions of the micro-tubes at 600°C, 700°C and 800°C is discussed.

Figure 6.19, Figure 6.20 and Figure 6.21 show the expansion of micro-tubular SOFC during oxidation at 600°C, 700°C and 800° respectively. In all three cases, the cells were heated in a Nitrogen atmosphere, and once at the desired temperature 20 ml/min of air was fed into the cell in order to oxidize the anode.

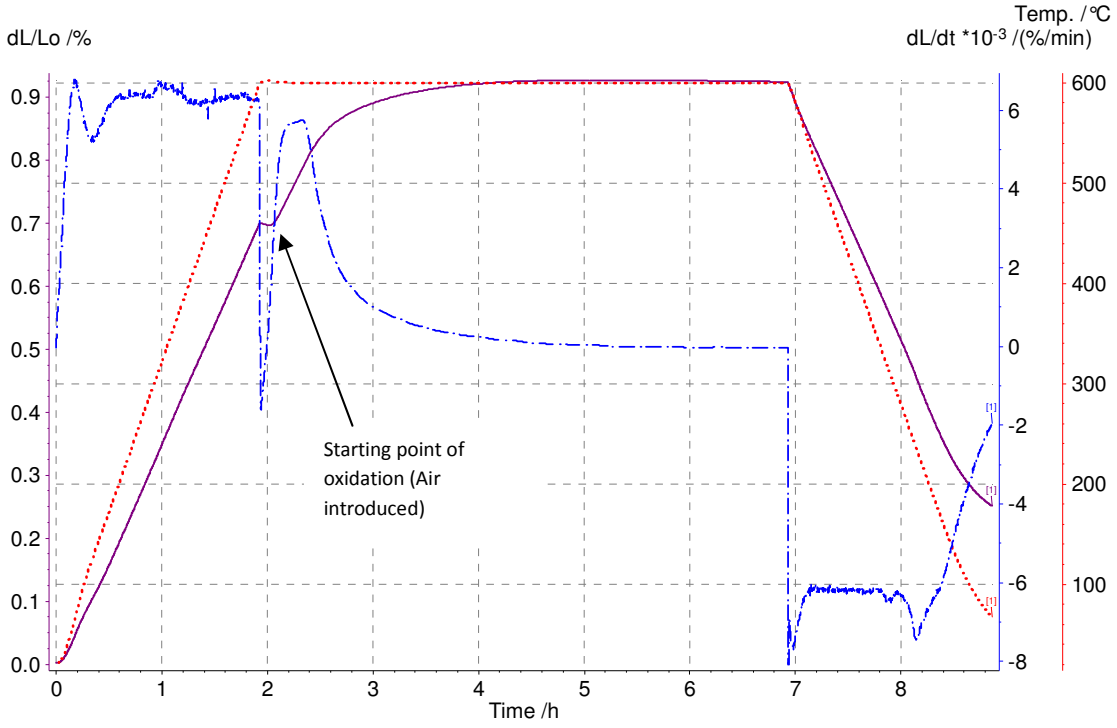

Figure 6.19. The expansion due to oxidation of a micro-tubular SOFC at 600°C

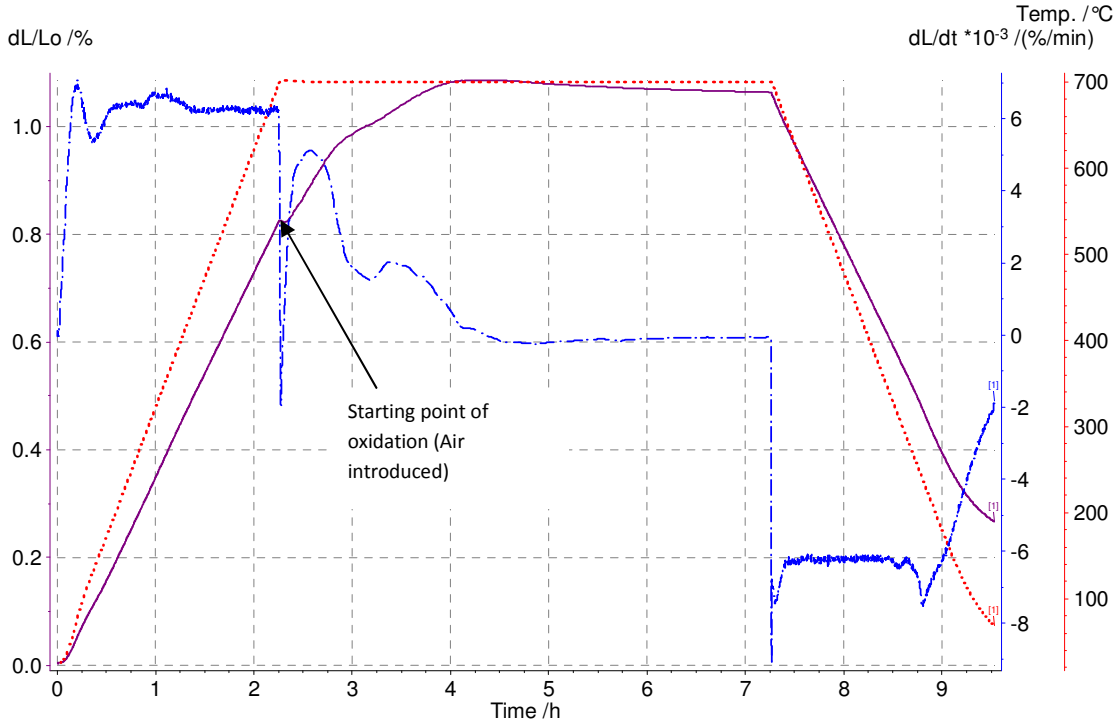

Figure 6.20**.** The expansion due to oxidation of a micro-tubular SOFC at 700°C

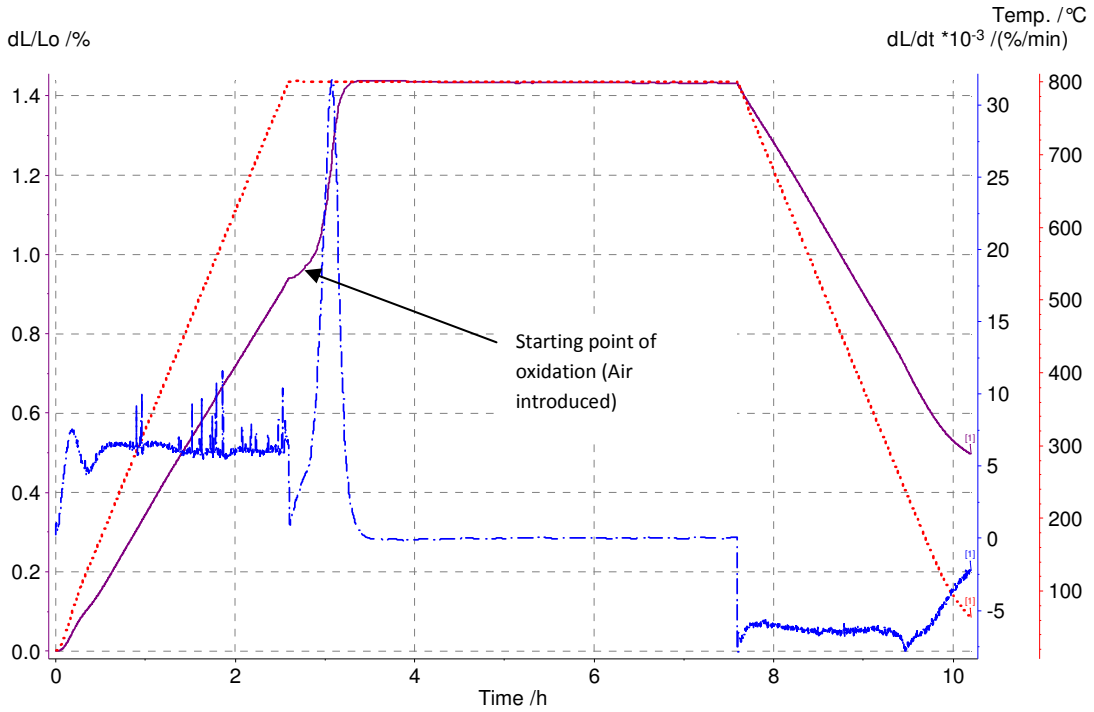

Figure 6.21. The expansion due to oxidation of a micro-tubular SOFC at 800°C

At 600°C, an expansion of 0.7% was observed before oxidation but with the onset of oxidation, a sudden expansion is observed giving a final expansion of 0.9%. The effective expansion due to oxidation was 0.2%. This sudden expansion will give rise to micro-cracking in the bulk of the micro-tube thereby leading to increased anode resistance. In the same vein, an expansion of 0.81% was observed at 700°C before oxidation but with the onset of oxidation, a sudden expansion to 1.14% was observed. The effective expansion due to oxidation was 0.33%. Finally, at 800°C an expansion of 0.96% was observed before oxidation while the expansion after oxidation was 1.42%. The effective expansion due to oxidation at 800°C was 0.46%. These sudden

expansions ripple through the anode and causes gross micro-cracking in order to relieve the expansive stresses. Once micro-cracking occurs, subsequent redox cycles are greeted by less cracking because most of the initial stresses have been relieved. It was interesting to see that the oxidation at the different temperatures produced different expansions. This was puzzling, because in theory, the expansion of the samples should be the same whether at 600^{o}C, 700^{o}C or 800^{o}C, because the Ni content in the anodes is the same. However, it was discovered that the difference in expansion with temperature was due to the rate of oxidation at the respective temperatures and consequently the severe cracking associated with the temperatures. At 800^{o}C, oxidation proceeded rapidly than at 600^{o}C and the delaminations and micro-cracking were more severe. So even though complete oxidation was achieved in all three cases, the larger micro-cracks developed at 800^{o}C, gave rise to bigger expansions. The conversion of Ni to NiO is followed by large volume change because of the difference in lattice size between a Ni atom and that of NiO.

Redox cycling is very deleterious because the expansion is mainly in the anode while the other cell components (i.e. electrolyte and cathode) do not expand. The other cell components which do not expand therefore act as constraints to the expansion thereby inducing further stress in the material interfaces. This might be one of the reasons why thermal cycling experiences less degradation than redox cycling because during thermal cycling all the cell components expand and contract relative to their CTE while redox sees the expansion of the anode relative to the others.

6.3.7 Confirmation of Theory of Micro-structural damage

Three distinct modes of micro-structural damage and failure were identified; one based on severe micro-cracking in the anode network due to the sudden expansion and contraction during redox cycling, the other based on the constraint imposed by the other cell components (electrolyte and cathode) during anode expansion thereby leading to stress accumulation in the anode-electrolyte interface causing de-lamination. And finally, electrolyte channel cracking due to the severe macroscopic expansion. These three degradation modes will be considered individually.

6.3.7.1 Micro-crack formation due to redox cycling

The sudden expansion in the anode due to oxidation of the Ni particles causes expansive stresses to accumulate between the Ni and YSZ particles leading to breakage and micro-cracking. Usually, the YSZ particle in the vicinity is displaced by the expansion of the Ni particle thus causing micro-cracking. Figure 6.22 is an SEM micro-graph showing micro-cracking in the anode due to redox cycling. The micro-crack is seen to propagate from the hollow interior of the anode towards the electrolyte. This crack is the result of stress build-up and fatigue due to continuous redox cycling. In theory, the bulk volume of a fully dense NiO sample should contract by 40.9% upon reduction and expand by 69.2% upon oxidation[170].

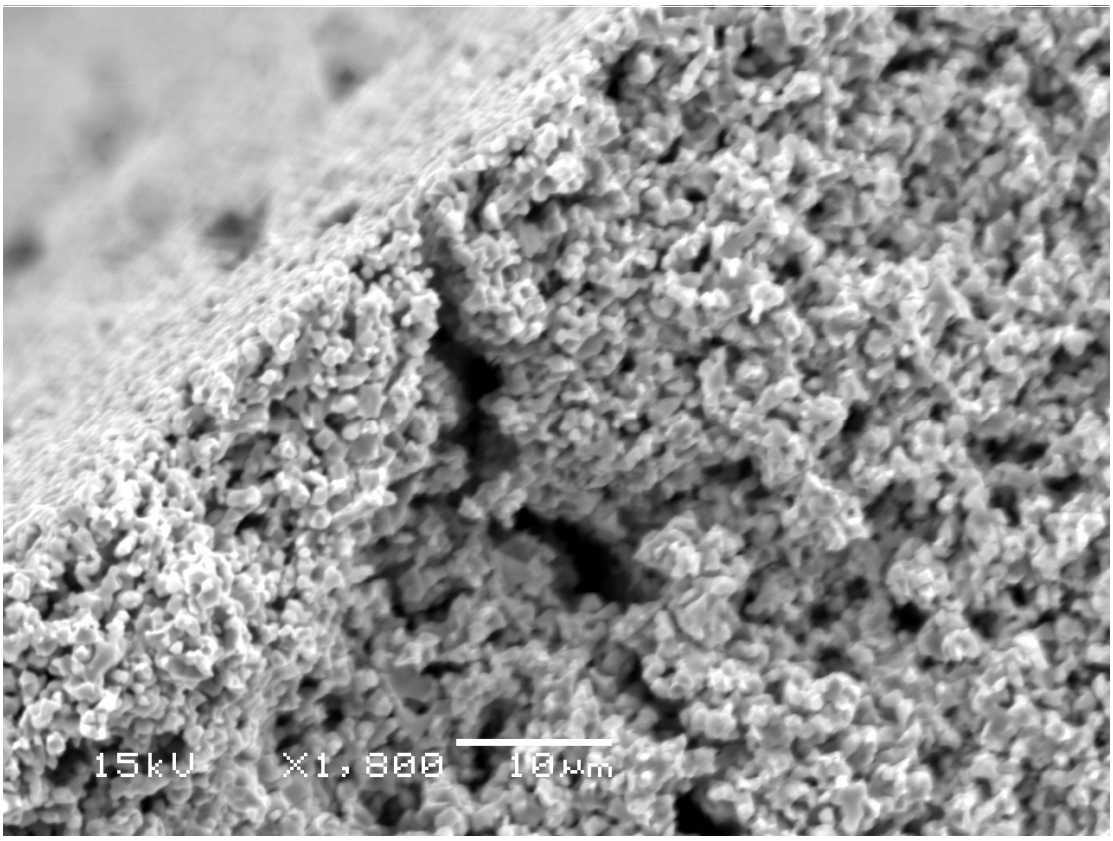

Figure 6.22. Showing micro-cracking in the anode of a micro-tube

These cyclic expansions and contractions are sufficient to drive cracks at the weakest points of the Ni/YSZ structure because they continually increase the residual stress of the cells until the critical stress intensity is exceeded in which micro-cracking becomes possible. Usually a small micro-crack would develop, but as cycling continues and more stress energy is accumulated in the crack, it begins to propagate and expand until a large crack propagates giving rise to an increase in electrode resistance. The overall resistance of the anode increases when there is an obstruction in the path of electron-flow such that the electrons would have to travel longer paths to arrive at their collection point. Micro-cracks exacerbate this phenomenon because they act as

barriers against electron flow. The generation and propagation of cracks is better explained via fracture mechanics, which is beyond the scope of this study.

Figure 6.23 is a schematic which seeks to elucidate the phenomenon of micro-cracking in the anode of micro-tubes.

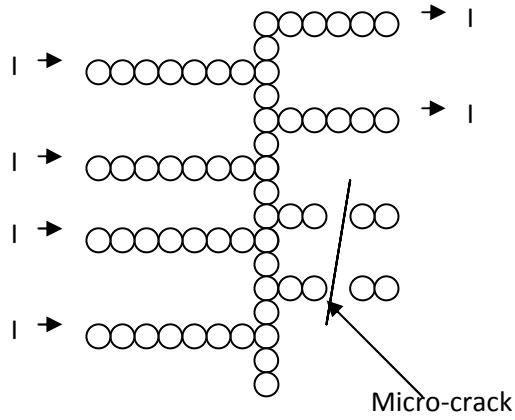

Re-oxidation → Expansion → Breakage → Increased resistance → Degradation

Figure 6.23. Schematic of the breakage in the Ni/YSZ anode network

6.3.7.2 De-lamination due to redox cycling

De-lamination in solid oxide fuel cells is not uncommon when solid oxide fuel cells are subjected to redox cycling. The constraint imposed by the other cell components which do not expand during redox cycling (i.e. electrolyte and cathode) is the main cause of de-lamination. When oxidation occurs, the expansion occurs mainly in the anode as the Ni is converted to NiO. The other cell components (i.e. electrolyte and

cathode) do not undergo any physico-chemical change and they act as constraints to the anode expansion. The result of this is severe stress induction in the anode-electrolyte interface leading to de-lamination.

The reduction of NiO to Ni is also known to subject the anode-electrolyte interface to further stress induction, because of the shrinkage associated with this operation. During reduction, the anode shrinks considerably thereby pulling itself away from the electrolyte and inducing further stresses. Thus cyclic oxidation and reduction leads to stress accumulation and subsequent de-lamination. Figure 6.24 shows a de-lamination crack in the anode-electrolyte layer.

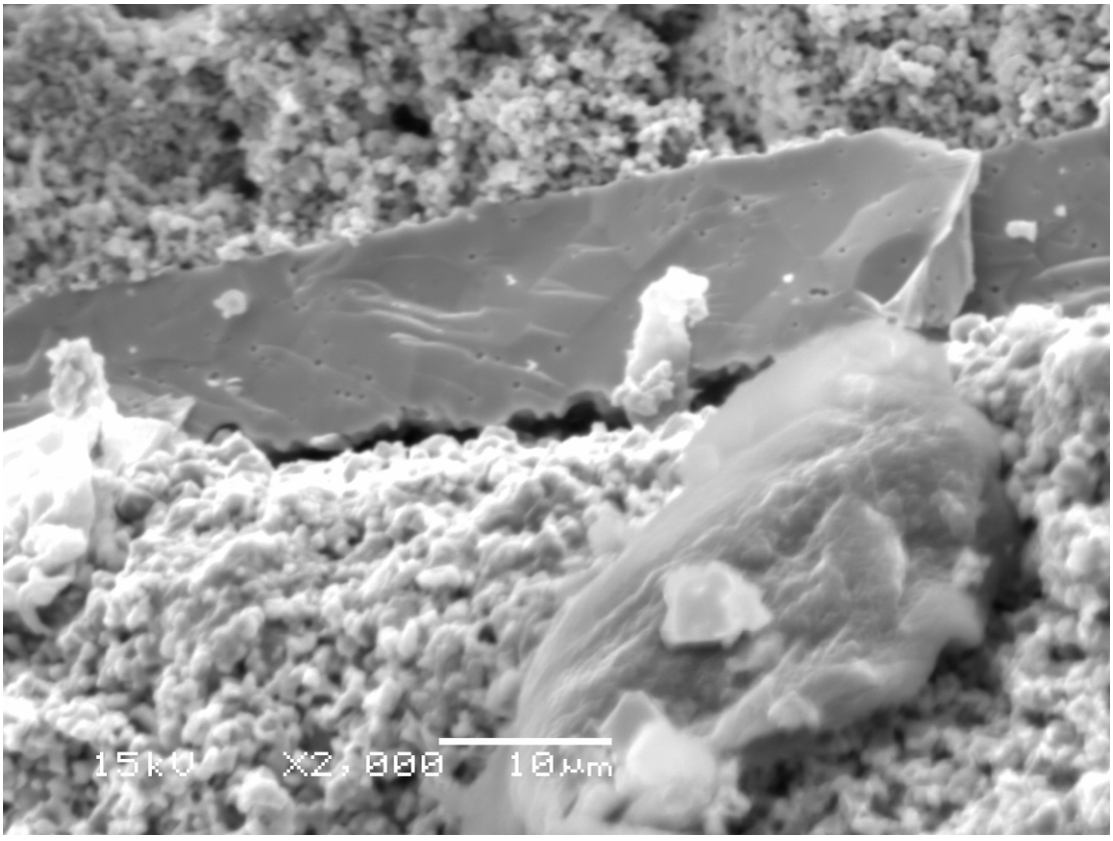

Figure 6.24. Showing a de-lamination crack in the anode-electrolyte interface

De-lamination cracks form insulative barriers that prevent ion exchange between electrolyte and electrodes. They act as obstructions that lead to the distortion of ions at the electrolyte-electrode interface. This distortion serves to lengthen transport paths and therefore increase the overall ohmic losses. For increasingly thin electrolytes, these ion-conduction distortions may lead to the effective loss of electro-active area at both the electrode and electrolyte interfaces[198].

For interfaces with no de-lamination and low electrolyte resistance, there is uniform ion flux density at the anode-electrolyte interface. In the event of de-lamination, the electro-active area of the interface becomes significantly reduced and an insulative void is created, see Figure 6.25. These voids serve to prevent ions from contacting the electro-active surfaces, thus leading higher ohmic polarization . The mode of transfer of ions in the electrolyte is however not fully understood and an in-depth analysis is required to fully understand the mode of transport of ions in the electrolyte and to provide insight into the effect of de-lamination cracks on the electrochemical performance of micro-tubular SOFC.

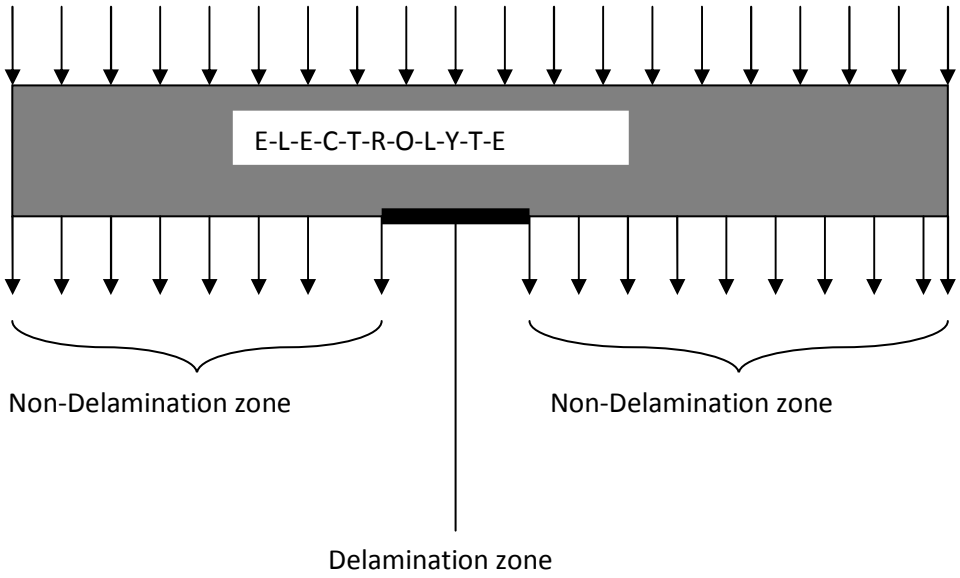

Figure 6.25. Schematic showing a de-lamination crack in the anode-electrolyte interface

6.3.7.3 Electrolyte fracture due to Anode re-oxidation

Electrolyte channel cracking is an extreme case of cell failure. This usually occurs after a micro-crack is propagated from the anode network. With the formation of a micro-crack in the anode, the crack becomes the natural weak point and stress concentration point for micro-damage. Further expansion during redox operation usually ripples through the structure, causing electrolyte fracture. This damage phenomena depends on the number of redox cycles performed, Ni content, duration of oxidation, porosity etc. It can be seen from Figure 6.5 that a micro-crack is propagated in the anode along side the micro-crack in the electrolyte. Electrolyte

cracking usually heralds the beginning of gross failure in a cell, because the voltage becomes significantly diminished due to fuel cross over.

To confirm the critical oxidation strain ε_{ox} for electrolyte channel cracking obtained from experiments (i.e. from Figure 6.6), an energetic modeling of fracture by Laurencin et al is employed. The model is based on the residual stresses during manufacture and the macroscopic expansion during anode oxidation. A fundamental assumption of the model is that an equi-biaxial stress field $\sigma_{equi\text{-}biaxial}$ is generally radially and circumfrentially in the electrolyte during anode oxidation. This means that the radial stress σ_{rr} is equal to the circumfrential stress $\sigma_{\theta\theta}$. The total stress generated in the micro-tube will be a sum of the residual stresses during manufacture $\sigma_{manufacture}$ [199, 200] and stresses induced due to the oxidation $\sigma_{oxidation}$.[200] Assuming the contraint imposed by the cathode layer is negligible, the equi-biaxial stress in the electrolyte is estimated using the expression by Laurencin et al [190], as

Total stress on the electrolyte $\sigma_{equi\text{-}biaxial} = \sigma_{residual} + \sigma_{oxidation}$

Where $\sigma_{oxidation} = \frac{E_{YSZ}}{(1-\nu_{YSZ})}\varepsilon_{ox}$

$$\sigma_{manufacture} = \frac{(\alpha_{NiO/YSZ} - \alpha_{YSZ})(T_{oxidation} - T_{manufacture})}{((1-\nu_{YSZ})E_{YSZ} + (h_{electrolyte}/h_{anode})(1-\nu_{NiO/YSZ})/E_{NiO/YSZ}}$$

Where α and E are the poison ratio, thermal expansion coefficient and the young's modulus with the respective subscripts either denoting the electrolyte or anode

layers. $T_{oxidation}$ denotes the oxidation temperature, $T_{manufacture}$ is the anode-electrolyte co-sintering temperature i.e.1350^{o}C while ε_{ox} is the oxidation strain.

The energy release rate G, which is the energy available for channel cracking through the electrolyte is given by

$$G = \frac{1-\nu_{YSZ}}{E_{YSZ}} \times Z \times \sigma^{2}_{equi-baxial} \times h_{electrolyte} \quad [190]$$

Where Z is a dimensionless parameter which depends on the elastic properties of both the NiO/YSZ anode and the electrolyte. For a NiO/8YSZ anode and 8YSZ electrolyte the value of Z is approximately 2.5 [201]

Using the above equations, an energy release rate of 6.74J/m^2 was calculated at a strain of 0.36%. Since the fracture toughness G_c of 8YSZ is 6.70J/m^2, this strain is established as the critical oxidation strain for fracture. This validates the experimental value obtained and shows that catastrophic electrolyte channel crackingwill only occur when over 49% of the anode is oxidized.

6.4 Conclusion

The effect of partial and complete redox cycling has been examined at three different temperatures; 600^{o}C, 700^{o}C and 800^{o}C. Partial oxidation did not cause gross micro-cracking or instant failure but successive drop in performance with progress in redox

cycling was experienced. It was also established that after 3 minutes of re-oxidation, only a small portion of the anode was oxidized and because of this, expansive stresses developed between the oxidized and un-oxidized regions causing micro-cracking and de-lamination.

Complete oxidation was found to cause gross micro-cracking and electrolyte cracking in the micro-structure, the degradation was found to increase with temperature. 600^{o}C showed the lowest redox degradation and was adjudged the best temperature at which to operate the micro-tubes.

Three theories of micro-structural damage based on sudden expansion/contraction, electrolyte and cathode constraints and electrolyte channel cracking were propounded. The first was based on severe expansion, due to rapid oxidation thus, leading to micro-cracking in the anode. While the second was based on the constraint imposed by the other cell components to the expansion in the anode, thereby causing de-lamination.

The critical oxidation strain necessary to cause electrolyte channel cracking was also established by experiments and verified by analytical techniques.

Chapter 7

Thermal and Electrical Shock Analysis

7 Introduction

In this section, the thermal and electrical shock behaviours of micro-tubular SOFCs are investigated. The micro-tubes were subjected to extreme thermal and electrical shock conditions in order to understand stress accumulation, failure/micro-cracking and also to establish the critical temperature difference for failure (ΔT_c) and minimum energy required for micro-cracking to occur. A three-point-bend test was employed to measure the decrease in fracture strength of the tubes after thermal and electrical shock testing.Shock can occur during SOFC operation due to rapid heating or due to hotspots which arise when there is a leakage that gives rise to fuel combustion on the cell surface. Shock is one of the main culprits of stress induction in the PEN of SOFC, as such an investigation into its effects is of great importance.

7.1 Theory of thermal shock

If a body undergoes a sudden change in temperature (thermal shock), the rate of heat transfer from the surface is high, and the surface reaches the new temperature instantaneously. However, the sub-surface and inner layers remain at the previous temperature. The surface (if free) would contract due to the heat loss, but it remains constrained by the sub-surface layers which are still at the previous temperature. This sudden contraction of the surfaces causes tensile stresses to be induced. For stress equilibrium to be attained, the tensile stress from the surface must be balanced by an equal amount of compressive stresses from the sub-surface layers. The stress induction at any given point on the fuel cell depends on the temperature difference

between the two points. The temperature differential gives rise to an associated strain, which if not uniform leads to stress induction. The fracture stress due to an instantaneous change in temperature can therefore be characterized by the expression

$$\sigma = \frac{E}{1-\nu}\alpha\theta \qquad (7.1)$$

Where E is the young modulus, α is the CTE, ν is the poisson ration and θ is the critical temperature difference for fracture to occur.

For a micro-tube under thermal shock, the maximum tensile stress at the surface occurs at the instance when the temperature differential exist i.e. Time = 0. This is at the instance when the surface temperature is at the new temperature whereas the temperature of the sub-surface materials is still at the previous temperature.

The effect of thermal shock and stress induction in these micro-tubes depends not only on the shock duration, residual stress level, shock medium and stress distribution but also on the properties of the materials such as defects, homogeneity and porosity. In view of these, it is difficult to propose a thermal shock resistance parameter that works in all conditions. However from equation 5.1 above the critical fracture temperature is given by

$$\theta_C = \frac{\sigma_1(1-\nu)}{E\alpha} \qquad (7.2)$$

For other geometries other than tubes, the equation can be re-written as

$$\theta_c = \frac{\sigma_f (1-\nu)}{E\alpha} S \quad (7.3)$$

Where S is the shape factor and σ_1 is the fracture stress. The equation can be re-written as

$$\theta_c = R_a S \text{ , Where } R_a = \frac{\sigma_f (1-\nu)}{E\alpha} \quad (7.4)$$

R_a is a constant that is unique to every material and can be described as the material's resistance to thermal shock. Based on this relationship, a material will exhibit good thermal shock resistance when it has high fracture stress, low modulus of elasticity and low thermal expansion coefficient.

7.2 Experimental Methods

7.2.1 Thermal shock Test

Thermal shock analysis was performed on two different types of micro-tubes; anode-supported and electrolyte-supported micro-tubes. The anode supported tubes were 2.3mm in diameter, with an electrolyte thickness of approximately 20µm and anode thickness of 200µm while the electrolyte supported tubes were 2.8mm in diameter, with an electrolyte thickness of 220µm. Both SOFC types were approximately 55mm in length. The anode supported and electrolyte supported tubes are shown in Figure 7.1 and Figure 7.2 respectively.

7.2.1.1 Thermal Shock Procedure

Thermal shock was performed by heating the tubes to the shock temperature and holding for ten minutes, before shocking in bowl of water at ambient temperature. The tubes were then dried and prepared for strength analysis using a three-point-bend machine. Thermal shock was performed between temperature ranges 100^{o}C - 300^{o}C.

Figure 7.1**.** An anode supported micro-tube

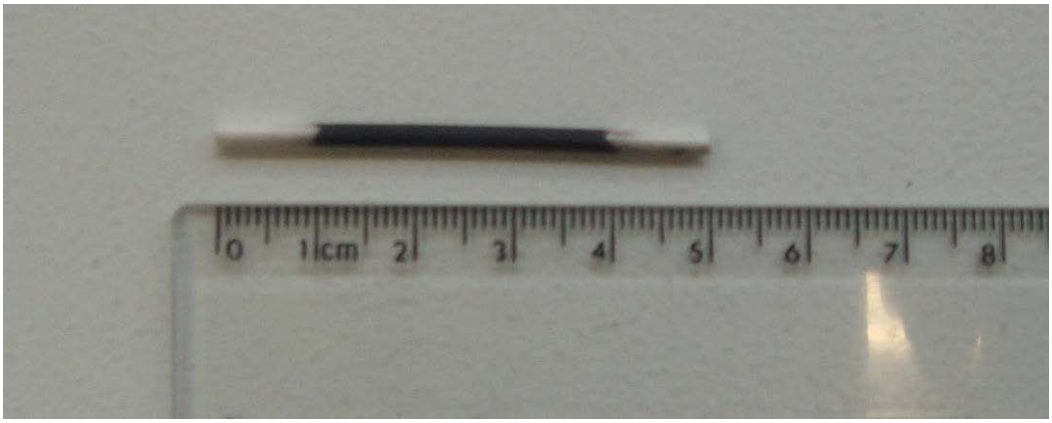

Figure 7.2. An electrolyte supported micro-tube

7.2.2 Electrical shock Test

7.2.2.1 Electrical shock equipment and Cell preparation

Electrical shock was performed only on the anode supported micro-tubes. Initially, the tubes were reduced in 20ml/min of hydrogen in order to convert the NiO/YSZ anode to Ni/YSZ. The tubes were subsequently prepared by polishing-off the electrolyte on both ends to expose the anode. Silver wires were then wound on these ends so that current can be passed through the anode. Cement was then used to cover the wires to prevent atmospheric oxygen from oxidizing these portions at high temperature. Figure 7.3 shows a tube made using this technique. A power supply (Manson® EP - 925) was used to pass current though the anode of the tube and temperature measurement was achieved using K-type thermo-couples. Figure 7.4 is a picture of this set-up

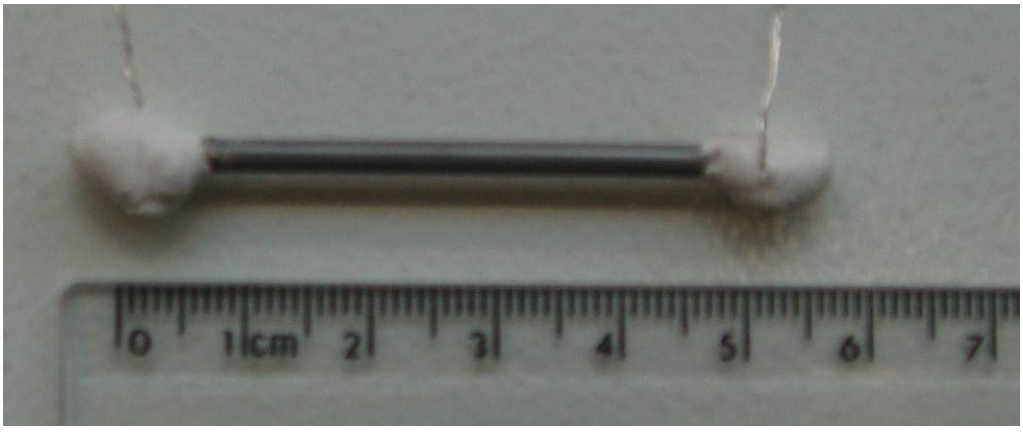

Figure 7.3. A tube prepared for electrical shock testing

Figure 7.4. Showing the electrical shock set-up

7.2.2.2 Electrical shock method

Electrical shock was performed by passing current through the anode of a micro-tube while using the inherent resistance of the tube to heat it to the desired temperature. Once at this temperature, the cell was held for a specified time before the sequence was repeated again.

In addition, a constant temperature hold electrical shock test was performed, where current was passed and the cell was held at high temperature (800^{o}C) until it failed.

7.2.3 Mechanical Strength Test

A three-point-bend-test was performed on the tubes that were previously shocked either thermally or electrically in order to determine their strength. The tubes were

suspended on a two point contact frame while a third point, which was attached to a force sensitive transducer, was lowered on to the middle of the tube by a motor, the test setup is shown schematically in Figure 7.7. The third point exerted force on the middle section until the sample failed; the transducer measured this minimum failure force. The force at failure is proportional to the strength of the sample.

7.3 Results

7.3.1 Thermal Shock Analysis

The behaviour of micro-tubular SOFC under thermal shock was investigated. Two types of micro-tubes were tested; 2.3mm anode supported and 2.8mm electrolyte supported micro-tubes.

7.3.1.1 Thermal shock of the anode supported micro-tubes

Table 7.1 shows the thermal shock results of the anode-supported micro-tubes. The tubes were heated to the desired shock temperature in a carbolite® furnace before being quickly removed and shocked in a bowl of water at ambient temperature.

The fracture force of the un-shocked micro-tubes was approximately 11.40N. With progress in thermal cycling however, the cells that were shocked at 150^{o}C were found to increase in strength. It is not fully understood why this is the case, but it is hypothesized that at this shock temperature, some of the residual stresses in the material are presumably relaxed, thus further investigation into the grain size and microstructure of the tubes after shock at this temperature is proposed. In any case,

further heating and thermal shock led to a steady decrease in the strength of the tubes until they shattered in the 255^{o}C - 265^{o}C regime, as seen in Figure 7.5.

Shock Temperature (^{o}C)	Force (N) (After first Shock)	Force (N) (After Second shock)	Force (N) (After Third shock)
Ambient	11.4	11.5	11.3
100	10.3	7.44	7.05
150	16.13	11.62	10.59
200	15.2	11.1	9.5
250	10.51	6.45	3.22
255	10.22	8.54	Shattered
260	4.13	Shattered	Shattered
265	Shattered	Shattered	Shattered

Table 7.1 The minimum force of fracture of anode supported tubes after thermal shock

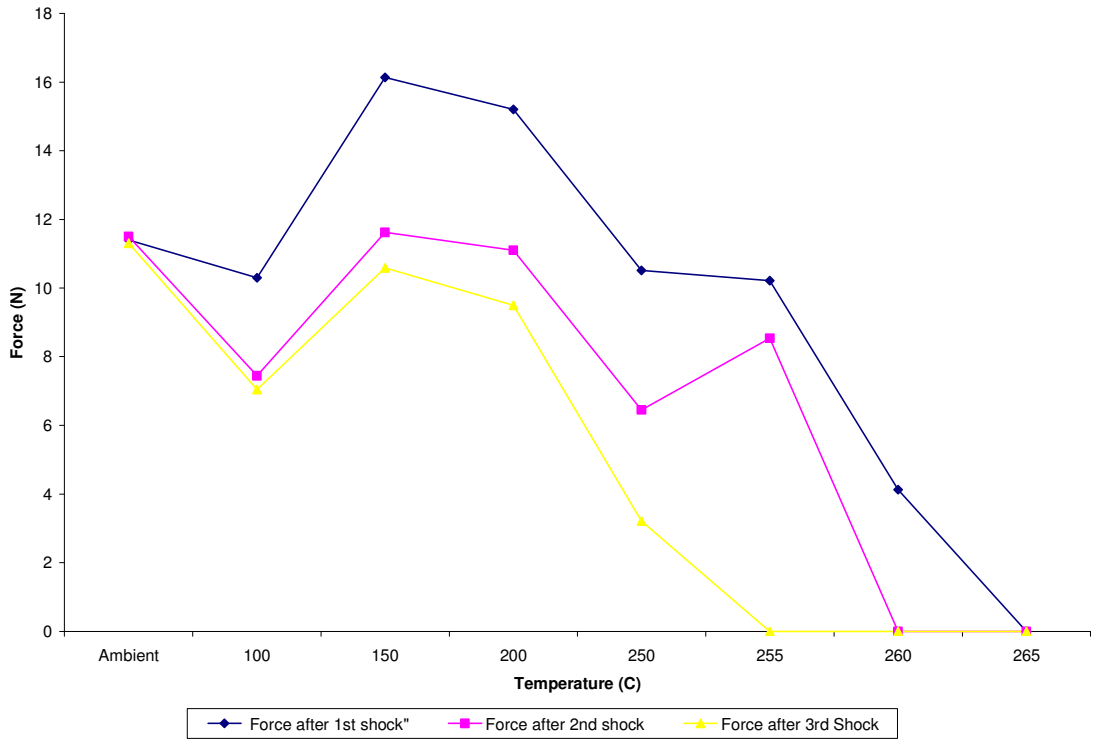

Figure 7.5. The fracture force of an anode supported micro-tubes after thermal shock

7.3.1.2 Thermal shock of electrolyte supported micro-tubes

Table 7.2 shows the results of the repeated thermal shock of electrolyte-supported micro-tubes. The fracture force of the tubes at room temperature was 39.0 N, this is significantly higher than the fracture force observed for anode supported tubes. This is presumably because of the uniform preparation technique which led to fewer defects and thick zirconia electrolyte (220µm), which is known for its characteristic strength.

As seen in Figure 7.6, the tubes exhibited similar behaviour to anode-supported tubes; they showed their greatest strength when shocked at 150^{o}C, and decrease steadily as

the temperature was increased. The tubes however failed in a lower temperature regime (250^{o}C – 255^{o}C) regime than anode-supported tubes. Thus, even though these tubes exhibited higher strengths initially, they were more prone to stress induction and failure.

Shock Temperature (^{o}C)	Force (N) (After first Shock)	Force (N) (After Second shock)	Force (N) (After Third shock)
Ambient	38.8	39	39
100	43.75	39.84	31.04
150	49.24	41.87	33.93
200	33.77	19.46	9.29
250	8.45	4.34	Shattered
255	Shattered	Shattered	Shattered

Table 7.2 The minimum force of fracture of electrolyte supported tubes after thermal shock

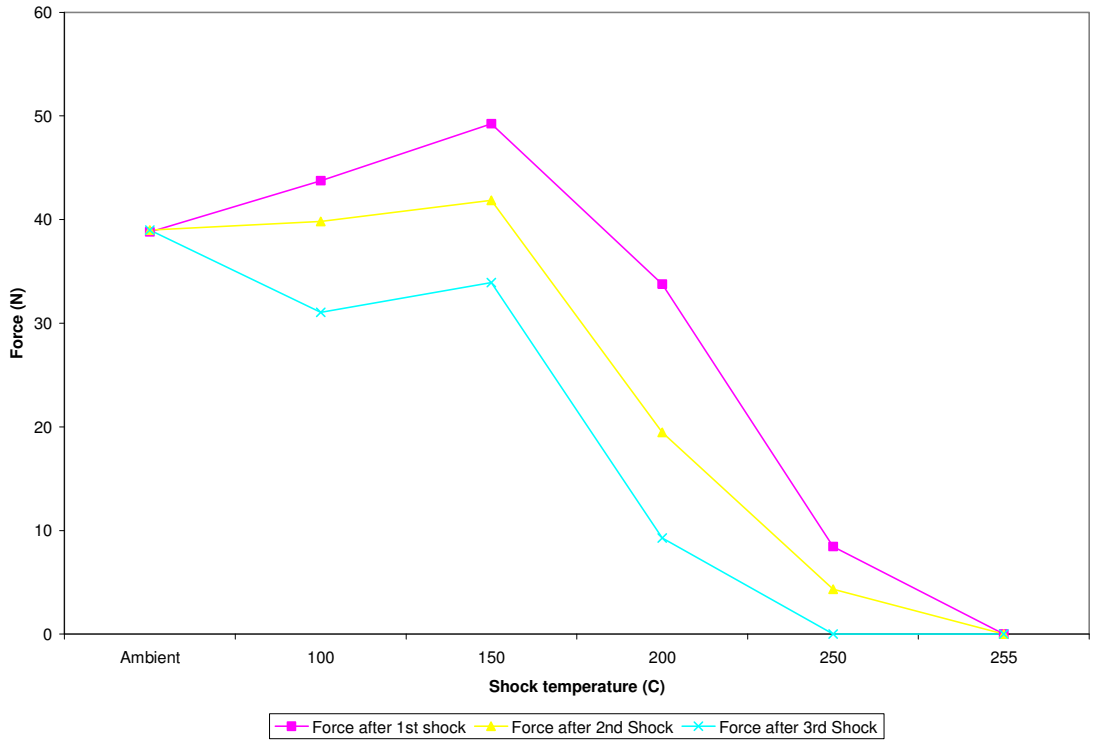

Figure 7.6. The fracture force of electrolyte supported micro-tubes after thermal shock

7.3.2 Strength of the Micro-tubes after Thermal Shock Test

The decrease in strength of the tubes due to thermal shock was evaluated from the yield stress (strength) of the tubes. This was calculated from the minimum fracture force, which is known. The yield stress is the force acting on a unit area of material

causing it to fail or break. The force used in this case was applied through a single contact point.

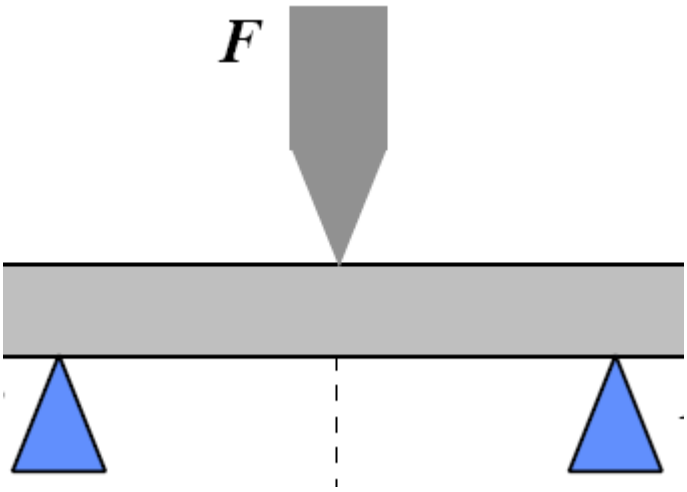

Figure 7.7 Three-point-bend test setup

Figure 7.8 shows the plot of the strength of the anode-supported tubes with respect to the shock temperatures. The strength of the tubes before thermal shock (i.e. the un-shocked tubes) was approximately 205MPa. With the commencement of thermal shock, the tubes that were shocked at 150^{o}C showed the highest strength, reaching a maximum of 270Mpa. As stated earlier, this is presumably due to the relaxation of some of the residual stresses at this temperature. However, as the thermal shock temperature was increased progressively, the strength was found to decrease beyond this point until failure occurred in the 255C – 260C regime.

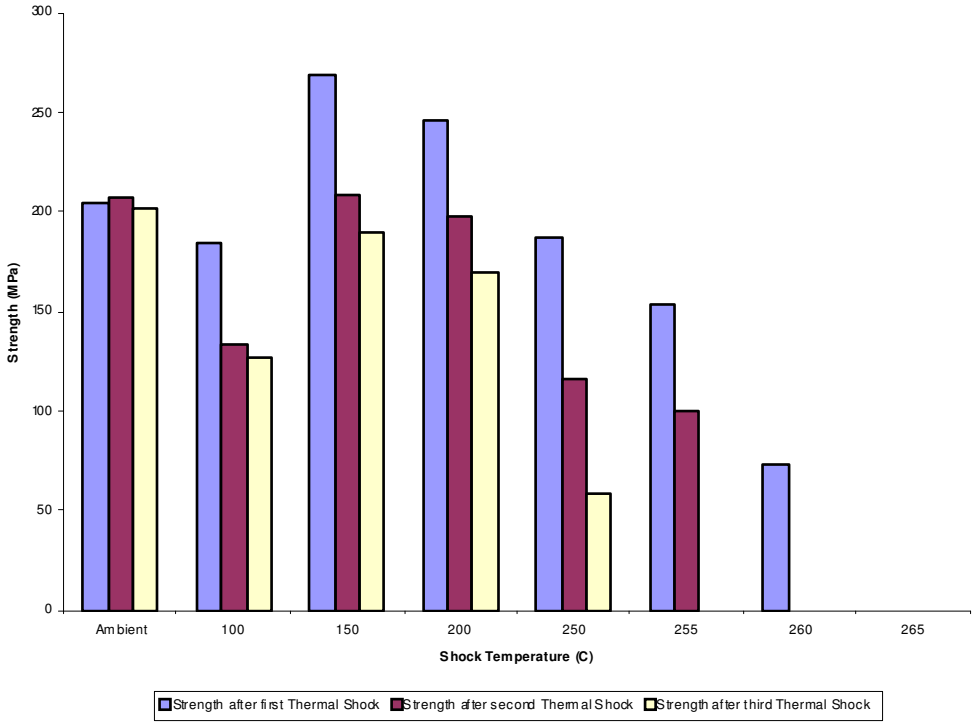

Figure 7.8. The change in yield strength of the anode supported micro-tubes with thermal shock

Figure 7.9 below shows the results of the repeated thermal shock of electrolyte-supported tubes. A similar trend to anode-supported tubes is observed; initially the strength before thermal shock was approximately 240MPa but as more thermal shock proceeded, a maximum strength of approximately 290MPa was observed at 150^{o}C after which a steady decrease was observed until failure in the 250C – 255C regime. The electrolyte supported tubes showed superior strengths to anode-supported tubes.

Atkinson et al[203, 204], also studied the fracture strengths of laminated GDC/YSZ layers at high and room temperatures and reported higher fracture strengths for

laminated GDC/YSZ layers than for single GDC layers. It was also reported that fracture always initiates at the region of maximum tensile stress i.e. at surface defects for single layer and at interfaces for laminate structures.

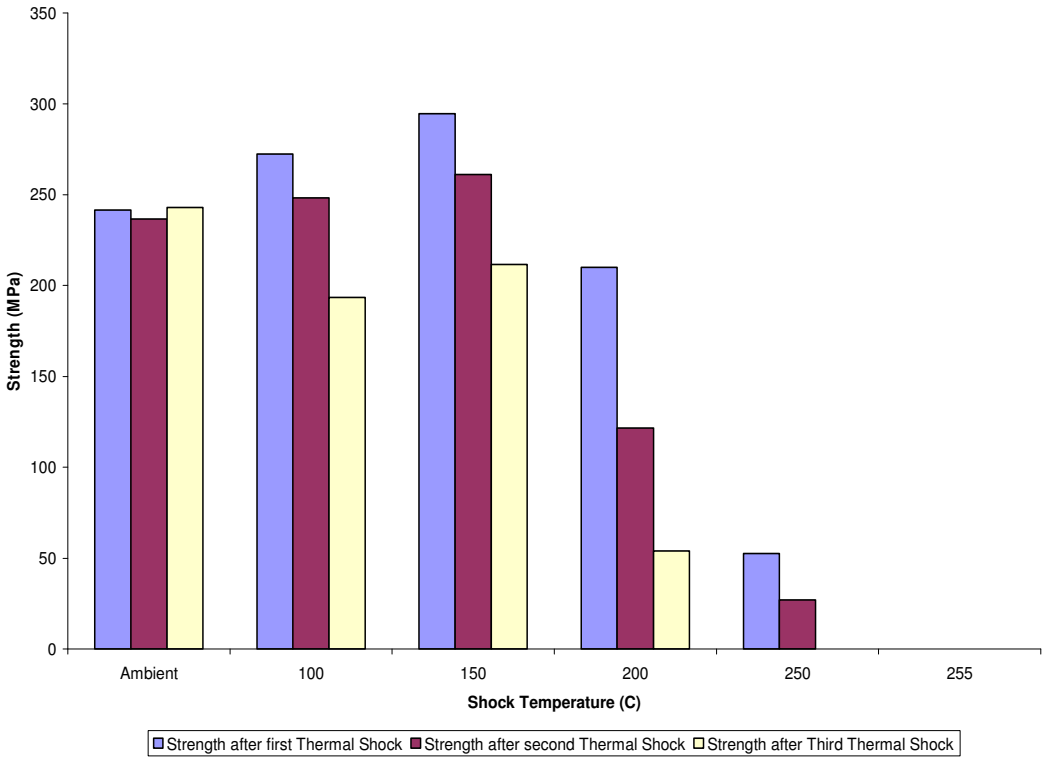

.

Figure 7.9. The change in yield strength of the electrolyte supported micro-tubes with thermal shock

7.3.3 Electrical Shock test

7.3.3.1 Electrical shock Cycling

Electrical shock tests were performed only on the anode-supported tubes. It was performed by passing an electric current though the anode of the tubes and utilizing the inherent resistance of the tubes to heat them to high temperatures. Electrical

shock was performed at three different temperatures; 600^{o}C, 700^{o}C and 800^{o}C in order to quantify the amount of stress necessary to cause failure at each of these temperatures. A universal shock procedure where the tubes were raised up to the desired temperature and held for 30 seconds before being cooled down to ambient temperature in air was used. This was repeated several times until the tubes failed, the results are present in tabular form in Table 7.3.

To raise the tube to 600^{o}C, a voltage of 1.8V and current of 9.0A was passed through the tube and 16 electrical shock cycles were achieved before failure. For 700^{o}C, the voltage and current were 2.0V and 11A respectively. At 800^{o}C, the voltage and current were 2.0V and 12A respectively while the number of electrical shocks to failure was 13, see Figure 7.10. This decrease in strength with cycling is due to an increase in stress induced with temperature. As electrical shock proceeds, stress continues to build-up in the tube due to the non-uniform heating profile across the tube and the huge difference in temperature between the tube and the surroundings. This stress build-up will cause failure once it exceeds the critical stress value.

Number of cycles	Strength after shock at 600^{o}C	Strength after shock at 700^{o}C	Strength after shock at 800^{o}C
0	202.1	204.25	202.1
2	184.9	178.45	178.45
4	172	167.7	159.1

6	159.1	152.65	139.75
8	146.2	122.55	120.4
10	129	124.7	107.5
12	118.25	94.6	88.15
13	109.65	86	0
14	90.3	0	0
15	79.55	0	0
16	0	0	0

Table 7.3 The change in strength of the anode supported tubes after electrical shock

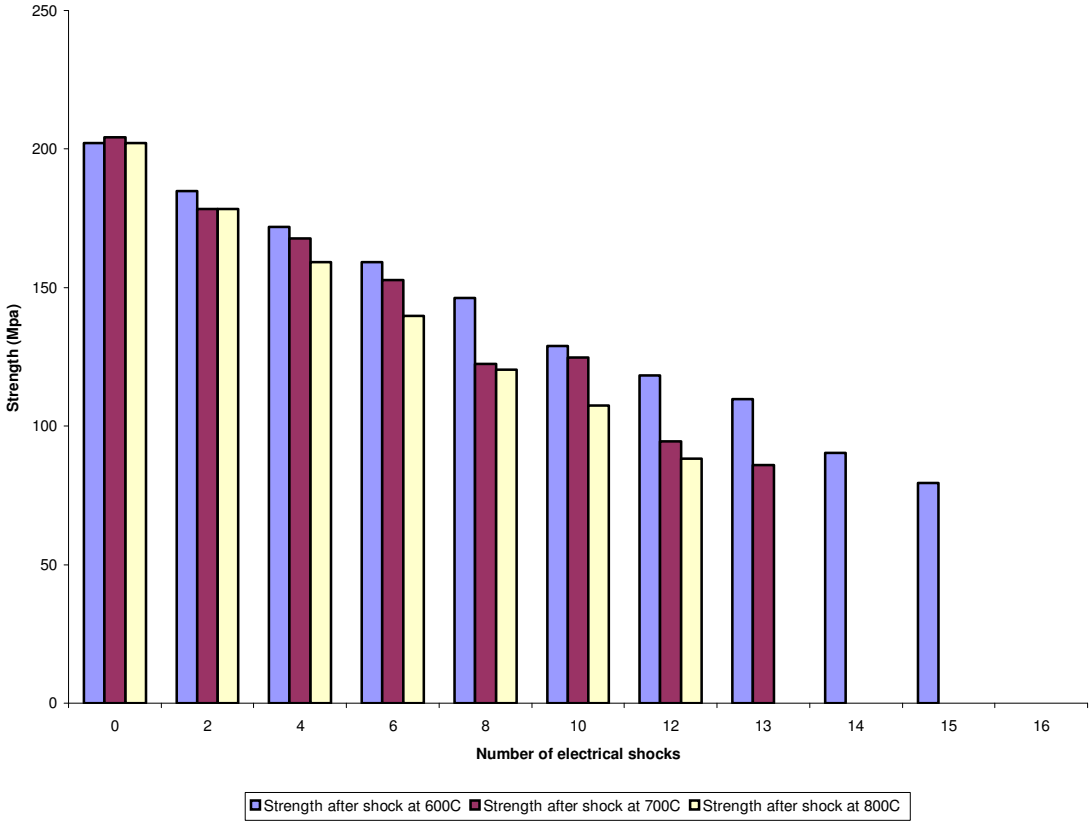

Figure 7.10. The change in yield strength of the anode supported micro-tubes with electrical shock

7.3.3.2 Constant Temperature hold Electrical shock test

In this test, a micro-tube was held at a constant temperature of 800^{o}C until failure occurred. The current passed through the tube was 12A and the voltage applied was 2V. The current was continuously adjusted manually in order to avoid exceeding this temperature.

As expected, a uniform glow (red hot) was noticed all across the tube as it was held at constant temperature, see Figure 7.11. This uniform glow was sustained for 6 minutes until a more intense (bright white) glow was observed at one of the tube ends, see Figure 7.12. This bright light became brighter with time until the tube failed after 6.75 minutes, see Figure 7.13. The bright light signified the commencement of micro-cracking through the electrolyte which led to the oxidation of the Ni anode. This oxidation gave rise to a more intense light as more Ni was converted to NiO

The energy required to cause total failure in the tubes was calculated from the current drawn, voltage and the duration of fracture at 2.7Whr.

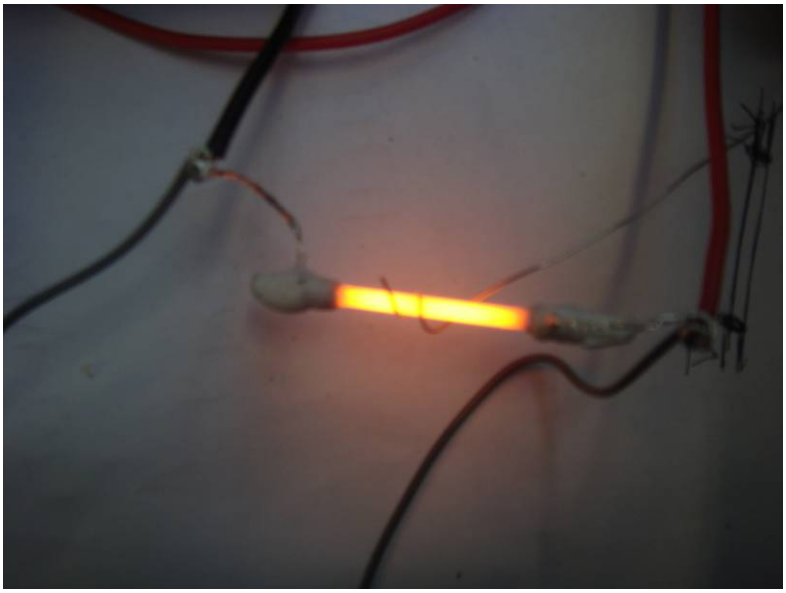

Figure 7.11. A tube held at constant temperature during electrical shock

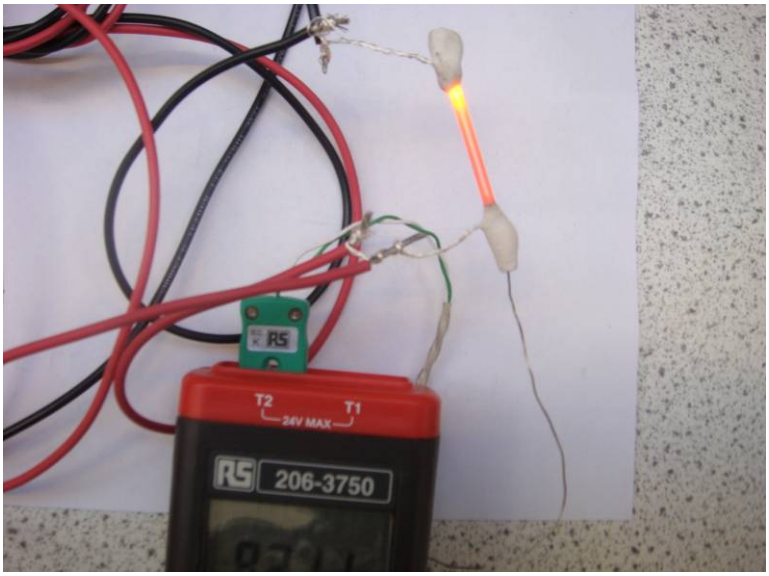

Figure 7.12. Showing the commencement of failure (bright spot) in a micro-tube held at constant temperature.

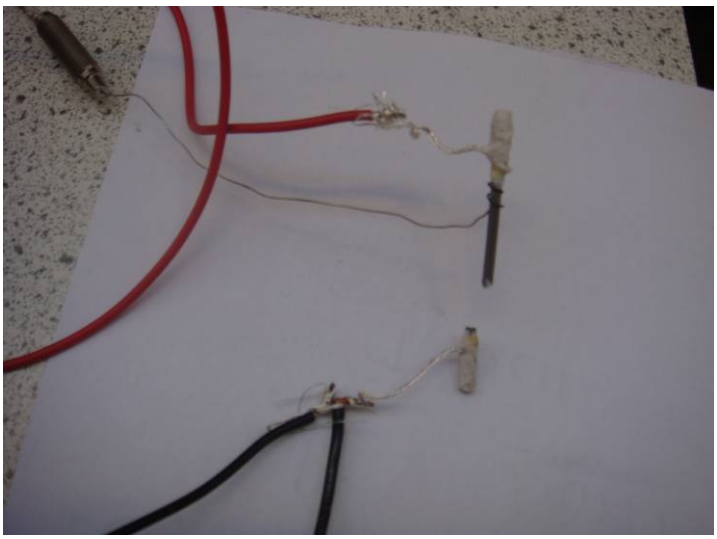

Figure 7.13. A tube that had failed under electrical shock testing

7.4 Discussion of results

7.4.1 Thermal shock Test

When thermal shock occurs, considerable amount of thermal stresses are induced in the bulk of the tubes due to the sudden change in temperature. These stresses cause the weakening of the bonds in the microstructure thereby making them prone to failure. As more and more thermal stresses are induced due to repeated thermal shock, the bonds in the material continue to weaken causing the overall strength to decrease until the critical stress intensity of the material is exceeded and failure becomes evident as shown in figs. 7.12. According to Zhou et al [205], thermal shock occurs when the total elastic strain energy of the material (W) is greater than the total energy dissipated in the formation of N micro-cracks (U_1) and the energy dissipated by the extension of the N micro-cracks until failure (U_2)

i.e. $W > U_1 + U_2$

From the above theory, it can be noted that thermal shock depends on the quantity of stress induced, thermal expansion coefficient of the material and the residual stresses of the materials. If the stress induced in the material is below the energy required for crack propagation and extension then stresses will be locked in the body of the tube as strain energy, otherwise micro cracking would occur.

The electrolyte-supported tubes showed greater strength than anode supported ones; the fabrication technique and thick electrolyte (220µm) was responsible for this

immense strength. Ceramics usually posses high yield strengths because of their strong bonds however their high yield strength gives rise to their brittle nature, where there is sudden failure or fracture upon exceeding this yield strength. From fig. 7.8, the electrolyte supported tubes failed suddenly in the 250^{o}C - 255^{o}C regime as against 260^{o}C - 265^{o}C for anode supported ones, so even though they posses higher strengths, they were more prone to thermal stress induction and failure than the anode supported tubes. Ahmad et al, [206] have done extensive study on the failure and fracture mechanics of these micro-tubes and findings reported corroborate the results reported here.

7.4.2 Electrical shock test

The mechanism of electrical shock is very similar to thermal shock i.e. both of them arise due to temperature differences. Electrical shock gives a more realistic representation of temperature gradients than thermal shock because of the crude method of shocking the tubes in water. However, thermal shock in the manner it was performed helps to present a case of extreme stress induction in the tubes.

In any case, using the electrical resistance of the tube to heat it up to high temperature gives rise to non-uniform heat distributions in the tube because of the inherent manufacturing defects, e.g. changes in material thickness along the tube and variable resistances. These non-uniform heat distributions lead to differential expansion along the tube, where the hotter parts expand by a greater index than the other parts. Differential expansion such as these will lead to severe stress induction.

As shocking proceeds, stresses continue to build up in the body of the tubes until they exceed the critical stress intensity when micro cracking becomes evident. Usually, a small micro-crack develops but as shocking proceeds the micro-crack continues to expand because of the accumulated stresses. This crack propagation will lead to increased resistance in the anode and can extend to the surface of the electrolyte. Once a micro-crack opens up at the surface, oxidation of the Ni begins to occur instantaneously. With the conversion of Ni to NiO the overall resistance of the anode increases and the spot of conversion show a bright white glow because it is at a higher temperature due to the higher resistance. This leads to further stress induction because of its high temperature compared to the other areas. This spot usually becomes the failure point as shown in fig 7.12.

The difference in temperature between the fuel cell and its surrounding also induces severe stresses in the bulk of the tubes due to the huge temperature difference.

7.4.3 Theory of Micro-structural Damage

7.4.3.1 Thermal shock

In the event of thermal shock, there is sudden shrinkage in the tube due to the difference in temperature between the tube and the shock medium (water at ambient temperature). This differential expansion leads to severe stress induction. Stresses become locked up in the body of the micro-tube thereby making the bonds of the material weak. The accumulation of stress and consequently the weakening of the bonds in the material lead to a decrease in the overall strength of the tube.

The quantity of stress induced in a tube during thermal shock, depends on the temperature difference (ΔT). If ΔT is < ΔT_c (critical temperature difference sufficient to cause failure), then the stress will accumulate in the tube. The theory of micro-structural damage is depicted below.

Thermal shock → Severe shrinkage → Stress induction → Micro-cracking or Instant failure

7.4.3.2 Electrical Shock

Temperature gradients which occur due to varying resistances across the tube's length (see fig. 7.13) leads to a state of tension between the various areas. The areas that are at a higher temperature expand by a higher index than those at a lower temperature, leading to stress induction. The accumulated stress leads to micro-cracks which tend to grow with time, until a large crack opens up at the surface. In the event of this occurring, oxidation of the Ni in the anode begins to occur thereby increasing the resistance of the anode. Oxidation is evident by the bright white light, which can be seen visibly. The point of oxidation is usually at a higher temperature due to the higher resistance of this point. This high temperature, coupled with the difference in temperature between the tube and surrounding lead to failure at this point. The theory of micro-structural damage during electrical shock testing is depicted below;

Electrical shock → Differential expansion → Stress induction → Micro-cracking → Oxidation → Increased resistance → Additional stress induction → Failure

7.5 Conclusion

The thermal and electrical shock behaviours of micro-tubular SOFCs was Investigated. Thermal shock was performed on anode supported and electrolyte supported micro-tubular SOFCs. Electrolyte supported tubes showed considerably greater strength but their thermal shock resilience was lower than anode supported tubes; they failed in the 250^{o}C - 255^{o}C regime as against 260^{o}C - 265^{o}C for the anode supported micro-tubes. The theory of micro-structural damage during thermal shock test was based on severe shrinkage due to the sudden change in temperature between the tube and the shocking medium (water at ambient temperature). The shrinkage led to stress induction that accumulated to cause failure.

Electrical shock tests were performed only on the anode-supported micro-tubes. The inherent resistance of the anode was used to heat the tube to high temperatures by passing electric current. However, hotspots were found to develop along the tube due to manufacturing and fabrication defects. These hotspots caused temperature gradients to develop across the tube's length thereby inducing stresses. As more stresses accumulate, tiny micro-cracks begin to propagate. Initially the cracks open up in the anode before they propagate through the electrolyte. In the event of this occurring, the Ni in the anode oxidizes to NiO thereby increasing the local resistance

at that point. This increase in resistance further exacerbates the temperature gradient.

In the same vien, further studies are proposed in order to understand the increase in strength of micro-tubes shocked at 150^{o}C.

Chapter 8

Conclusions and Future Work

8 Summary of Conclusions

8.1 Overview

The degradation of micro-tubular SOFCs were studied under isothermal conditions, thermal cycling, redox cycling and electrical load cycling, in order to understand the effects of these on electro-chemical performance. Thermal analysis (thermo-gravimetry and dilatometry) was also used to characterize the mechanical behaviours of these micro-tubes at high temperature.

Finally, thermal and electrical shock test were preformed in order to understand micro cracking and failure. Post mortem analyses of the tubes were performed by SEM in order to observe any changes in microstructure.

8.1.1 Isothermal Ageing

It was found that Ni sintering was responsible for most of the initial degradation during isothermal ageing. Sintering proceeded rapidly for the first 10 hours, the Ni particles agglomerated into a dense structure leading to decreased TPB and lower electro-chemical performance however after this period the rate of sintering was found to diminish considerably because the structure assumes a more stable configuration giving steady electro-chemical performance.

Irreversible deformation was also found to occur as the micro-tubes were raised to high temperature and cooled down. Dilatometry showed that the sample failed to

recover back to its original length upon cooling. This irreversible deformation was the combined effect of severe stress induction at high temperature due to temperature gradients and sintering.

Furthermore, the effect of temperature gradients on the electro-chemical performance of micro-tubes was investigated by flowing 25% excess fuel through the tubes for combustion at the cell outlet. No degradation or micro cracking was observed and their effect was adjudged to be marginal.

8.1.2 Thermal Cycling

Thermal cycling was found to cause only slight degradation during SOFC operation. The tubes showed immense thermal cycling resilience as no micro-cracking or de-laminations due to differences in the CTE of the materials were observed. Even though no physical damage was observed, the cycling between high and low temperature induced thermal stresses in the bulk of the tubes. However, the slight degradation observed was due to sintering of the Ni particles at high temperature. The sintering observed during thermal cycling was less than during isothermal ageing, because of the change between high and low temperatures during thermal cycling.

Passing 25 % excess fuel (in order to impose a temperature gradient) across the tube was found to cause micro-cracking and de-lamination. The degradation was mainly due to combination of stresses induced radially (due to difference in CTE) and across the ends of the tube (due to the temperature gradient).

Also, Irreversible deformation was observed to occur progressively as thermal cycling proceeded. Figure 5.11 showed an expansion of 0.97% initially and 1% after 21 thermal cycles. This irreversible deformation is the result of stress build-up in the tube, which is locked in the tube as strain energy.

8.1.3 Redox Cycling

Re-oxidation of the Ni/SZ anode was found to cause significant expansion in the anode microstructure; expansions of up to 0.2% were observed at 800^{o}C. This expansion caused severe stress induction or de-lamination in the tube because of the constraint imposed by the electrolyte and other cell components. Rapid oxidation also caused micro-cracking in the anode due to the rapid expansion in the anode.

Partial redox cycling showed a steady decrease in performance with cycling. Each redox cycle caused micro-cracking thereby increasing the overall resistance of the anode leading to electro-chemical performance degradation. Complete redox cycling on the other hand showed severe degradation in performance, with 72% degradation observed after the first cycle at 800^{o}C. Gross micro-cracking and de-lamination were observed after complete oxidation due to its severe nature. Redox cycling was therefore adjudged the most deleterious form of cycling, giving the most damaging effect during SOFC operation.

8.1.4 Electrical load Cycling

This was found to have a very marginal effect on the electro-chemical performance of the micro-tubes. Cyclic loading between OCV and 0.5V caused an increase in the temperature of the tube, especially when the cell was loaded at 0.5V. This was mainly because of the ohmic resistance of the material to the flow of electrons.

8.1.5 Thermal and Electrical Shock test

Electrolyte supported tubes were found to be considerably stronger than anode supported tubes. They were however found to be more prone to thermal stress induction as they failed in the 250^{o}C - 255^{o}C regime as against 260^{o}C - 265^{o}C for the anode supported micro-tubes.

Electrical shock tests provided better understanding of temperature gradients and shock in SOFC. The tubes were found to be plagued mainly by the temperature gradients and hotspots which develop because of the variation in resistance along the tube. These differences in resistance led to several hotspots across the tube, causing fracture and eventual failure.

8.2 Future work

8.2.1 Cycling with Hydrocarbon fuels

The cycling studies reported in this project were largely performed with hydrogen as fuel. This is very idealistic because hydrogen is not yet the primary energy vector in today's society however it provided a baseline for assessing the electro-chemical

performance of these tubes. Cycling with commercially available fuels like methane, propane and butane will provide valuable information about the durability and reliability of fuel cells for the present market. Dhir et al [172] performed a few cycles using hydrocarbon fuels but further studies are required in order to effectively characterize the effects of carbon deposition as it relates to performance and sintering of the Ni particles.

8.2.2 Cycling of micro-tubular SOFC Stacks

In this project, only single micro-tubes were tested. The design, fabrication and testing of SOFC stacks will provide valuable insight into other factors like inter-connect degradation and failure, overall system efficiency etc. The cycling performance of each cell in a stack depends on the others; also the temperature gradients across them would vary. A few stack manufacturers have reported interconnect failure and short-circuiting during operation of stacks[207]. Thus, extensive study is required.

8.2.3 Shorter Cells

During the course of this work, I have been able to show that shorter micro-tubes (25mm long) demonstrated superior cycling performance to longer (55mm long) micro-tubes. They were also found to give similar electrochemical performance to longer tubes[156]. This needs to be investigated in greater detail because of the several advantages that shorter tube present, including lower cost of fabrication, more compact designs, ease of stacking and decreased degradation.

Also temperature gradients across these tubes were found to be smaller, thus giving smaller degradation indexes.

8.2.4 Thermal and Electrical shock test

During the thermal shock of the micro-tubes at 150^{o}C, a characteristic increase in strength was observed as against a decrease at other temperatures. This is not fully understood, so further investigation into the behaviour of these micro-tubes and their fracture mechanics is essential.

9 References

1. *The EU Green paper: A European Strategy for Sustainable, Competitive and Secure Energy*. Annex to the green paper. 2008, Brussels: The Commission of the European Communities.

2. *The scientific case for setting a long term emmisions reduction target*. 2004, Washington DC: Department for Environment, Food and Rural affairs (DEFRA).

3. *A summary of the Kyoto Protocol*. Framework document. 1997, Kyoto: United Nations Framework Convention on Climate Change.

4. *Wind Power overview, UK*, ed. W. Cahill. 2003, London: British Wind Energy Association (BWEA).

5. *Annual World Solar PhotoVoltaic report*. 2005, Houston, Texas: World Solar Agency.

6. *Biomass Task Force Report to Government*. 2005, London: Biomass Task Force.

7. Jacobs, T., *Introduction to fuel cells*. FHI - Seminar. 2004, London.

8. Srinivasan, S., *Fuel Cells, From Fundamentals to Applications*. 2006: Springer.

9. Larminie, D., *Fuel Cells Systems Explained*. Vol. 2nd ed. 2003: John Wiley and Sons.

10. R. L. Borup, J.R.D., F. H. Garzon, D. L Wood, P. M. Welch and K. More, *Polymer Electrolyte Membrabe (PEM) Fuel Cell Durability.* Materials Research Highlights, 2006. **108**.

11. Beckel, D., et al., *Micro-hotplates--A platform for micro-solid oxide fuel cells.* Journal of Power Sources, 2007. **166**(1): p. 143-148.

12. Damm, D.L. and A.G. Fedorov, *Reduced-order transient thermal modeling for SOFC heating and cooling.* Journal of Power Sources, 2006. **159**(2): p. 956-967.

13. Gariglio, M., et al., *Analysis of the cooling transient of a large SOFC generator.* International Journal of Hydrogen Energy

2nd World Congress of Young Scientists on Hydrogen Energy Systems, 2008. **33**(12): p. 3204-3208.

14. Weil, K.S. and B.J. Koeppel, *Thermal stress analysis of the planar SOFC bonded compliant seal design.* International Journal of Hydrogen Energy

TMS07: Symposium on Materials in Clean Power Systems, 2008. **33**(14): p. 3976-3990.

15. Stutz, M.J., et al., *Fast and exergy efficient start-up of micro-solid oxide fuel cell systems by using the reformer or the post-combustor for start-up heating.* Journal of Power Sources
Selected papers from the International Workshop on Degradation Issues in Fuel Cells, 2008. **182**(2): p. 558-564.

16. Lee, T.J. and K. Kendall, *Characterisation of electrical performance of anode supported micro-tubular solid oxide fuel cell with methane fuel.* Journal of Power Sources
FUEL CELLS IN A CHANGING WORLD SELECTED PAPERS FROM THE TENTH GROVE FUEL CELL SYMPOSIUM, 2008. **181**(2): p. 195-198.

17. Selimovic, A., et al., *Steady state and transient thermal stress analysis in planar solid oxide fuel cells.* Journal of Power Sources
Selected papers presented at the Fuel Cells Science and Technology Meeting, 2005. **145**(2): p. 463-469.

18. Kronemayer, H., et al., *A direct-flame solid oxide fuel cell (DFFC) operated on methane, propane, and butane.* Journal of Power Sources, 2007. **166**(1): p. 120-126.

19. Gupta, G.K., et al., *Comparison of conversion and deposit formation of ethanol and butane under SOFC conditions.* Journal of Power Sources, 2006. **158**(1): p. 497-503.

20. Hotz, N., et al., *Disk-shaped packed bed micro-reactor for butane-to-syngas processing.* Chemical Engineering Science. **In Press, Corrected Proof**.

21. Lisbona, P. and L.M. Romeo, *Enhanced coal gasification heated by unmixed combustion integrated with an hybrid system of SOFC/GT.* International Journal of Hydrogen Energy. **In Press, Corrected Proof**.

22. Haseli, Y., I. Dincer, and G.F. Naterer, *Thermodynamic modeling of a gas turbine cycle combined with a solid oxide fuel cell.* International Journal of Hydrogen Energy. **In Press, Corrected Proof**.

23. Guo, W. and J. Liu, *The effect of nickel oxide microstructure on the performance of Ni-YSZ anode-supported SOFCs.* Solid State Ionics
Solid State Ionics 16: Proceedings of the 16th International Conference on Solid State Ionics (SSI-16), Part II, 2008. **179**(27-32): p. 1516-1520.

24. Gao, H., et al., *The effect of Fe doping on the properties of SOFC electrolyte YSZ.* Solid State Ionics

Solid State Ionics 16: Proceedings of the 16th International Conference on Solid State Ionics (SSI-16), Part II, 2008. **179**(27-32): p. 1620-1624.

25. Vladikova, D.E., et al., *Impedance studies of cathode/electrolyte behaviour in SOFC.* Electrochimica Acta
7th International Symposium on Electrochemical Impedance Spectroscopy, 2008. **53**(25): p. 7491-7499.

26. Lee, D., et al., *Performance of strontium- and magnesium-doped lanthanum gallate electrolyte with lanthanum-doped ceria as a buffer layer for IT-SOFCs.* Journal of Power Sources, 2008. **185**(1): p. 207-211.

27. Ni, M., D.Y.C. Leung, and M.K.H. Leung, *An improved electrochemical model for the NH3 fed proton conducting solid oxide fuel cells at intermediate temperatures.* Journal of Power Sources, 2008. **185**(1): p. 233-240.

28. Lee, C., S.-W. Baek, and J. Bae, *Cathodic behavior of La0.8Sr0.2Co1 - xMnxO3 - [delta] perovskite oxide on YSZ electrolyte for intermediate temperature-operating solid oxide fuel cells.* Solid State Ionics
Solid State Ionics 16: Proceedings of the 16th International Conference on Solid State Ionics (SSI-16), Part II, 2008. **179**(27-32): p. 1465-1469.

29. Bi, L., et al., *A novel anode supported BaCe0.7Ta0.1Y0.2O3-[delta] electrolyte membrane for proton-conducting solid oxide fuel cell.* Electrochemistry Communications. **In Press, Corrected Proof**.

30. Joo, J.H. and G.M. Choi, *Open-circuit voltage of ceria-based thin film SOFC supported on nano-porous alumina.* Solid State Ionics, 2007. **178**(29-30): p. 1602-1607.

31. Xie, Y., et al., *Measurement of the interface adhesion of solid oxide fuel cells by indentation.* Journal of Power Sources, 2006. **162**(1): p. 436-443.

32. Hussain, M.M., X. Li, and I. Dincer, *Mathematical modeling of planar solid oxide fuel cells.* Journal of Power Sources, 2006. **161**(2): p. 1012-1022.

33. Chen, K., et al., *Performance of an anode-supported SOFC with anode functional layers.* Electrochimica Acta, 2008. **53**(27): p. 7825-7830.

34. Chaisantikulwat, A., C. Diaz-Goano, and E.S. Meadows, *Dynamic modelling and control of planar anode-supported solid oxide fuel cell.* Computers & Chemical Engineering, 2008. **32**(10): p. 2365-2381.

35. Lin, B., et al., *A cathode-supported SOFC with thin Ce0.8Sm0.2O1.9 electrolyte prepared by a suspension spray.* Journal of Alloys and Compounds, 2008. **465**(1-2): p. 285-290.

36. Jung, H.-G., et al., *Investigation of anode-supported SOFC with cobalt-containing cathode and GDC interlayer.* Solid State Ionics
Solid State Ionics 16: Proceedings of the 16th International Conference on Solid State Ionics (SSI-16), Part II, 2008. **179**(27-32): p. 1535-1539.

37. Han, M.-F., et al., *Fabrication and properties of anode-supported solid oxide fuel cell.* Solid State Ionics
Solid State Ionics 16: Proceedings of the 16th International Conference on Solid State Ionics (SSI-16), Part II, 2008. **179**(27-32): p. 1545-1548.

38. Wang, Z.R., et al., *Improvement of anode-supported solid oxide fuel cells.* Solid State Ionics
Solid State Ionics 16: Proceedings of the 16th International Conference on Solid State Ionics (SSI-16), Part II, 2008. **179**(27-32): p. 1593-1596.

39. Kawano, M., et al., *Steam reforming on Ni-samaria-doped ceria cermet anode for practical size solid oxide fuel cell at intermediate temperatures.* Journal of Power Sources
Selected papers from the International Workshop on Degradation Issues in Fuel Cells, 2008. **182**(2): p. 496-502.

40. Kishimoto, H., et al., *Anomalous transport property at surface and interface of metal/rare earth doped ceria.* Solid State Ionics
Solid State Ionics 16: Proceedings of the 16th International Conference on Solid State Ionics (SSI-16), Part II, 2008. **179**(27-32): p. 1343-1346.

41. Kendall, S.S.K., *High Temperature Solid Oxide Fuel Cells; Fundamentals, Design and Applications.* Elsevier Advanced Technology. 2-20.

42. Hsiao, Y.C. and J.R. Selman, *The degradation of SOFC electrodes.* Solid State Ionics, 1997. **98**(1-2): p. 33-38.

43. Esfakur Rahman, A.H.M., et al., *Microstructure characterization and electrical conductivity of electroless nano Ni coated 8YSZ cermets.* Surface and Coatings Technology, 2008. **202**(10): p. 2182-2188.
44. Kim, S.-D., et al., *Ni-YSZ cermet anode fabricated from NiO-YSZ composite powder for high-performance and durability of solid oxide fuel cells.* Solid State Ionics, 2007. **178**(21-22): p. 1304-1309.

45. Zhu, H. and R.J. Kee, *The influence of current collection on the performance of tubular anode-supported SOFC cells.* Journal of Power Sources, 2007. **169**(2): p. 315-326.

46. Kong, J., et al., *Ni-YSZ gradient anodes for anode-supported SOFCs.* Journal of Power Sources, 2007. **166**(2): p. 337-342.
47. You, H., et al., *Reactions of low and middle concentration dry methane over Ni/YSZ anode of solid oxide fuel cell.* Journal of Power Sources
IBA - HBC 2006 - Selected papers from the INTERNATIONAL BATTERY ASSOCIATION & HAWAII BATTERY CONFERENCE 2006 Waikoloa, Hawaii, USA 9-12 January 2006, 2007. **165**(2): p. 722-727.

48. Han, K.R., et al., *Fabrication of NiO/YSZ anode material for SOFC via mixed NiO precursors.* Materials Letters, 2007. **61**(4-5): p. 1242-1245.

49. Ding, J. and J. Liu, *An anode-supported solid oxide fuel cell with spray-coated yttria-stabilized zirconia (YSZ) electrolyte film.* Solid State Ionics
Solid State Ionics 16: Proceedings of the 16th International Conference on Solid State Ionics (SSI-16), Part I, 2008. **179**(21-26): p. 1246-1249.

50. Liu, M., et al., *YSZ-based SOFC with modified electrode/electrolyte interfaces for operating at temperature lower than 650 °C.* Journal of Power Sources, 2008. **180**(1): p. 215-220.

51. Chinnan M. Dikwal, W.B., K. Kendall, *Investigation of the Thermal Cycling Behaviour of Micro-Tubular SOFC.* 8th European Solid Oxide Fuel Cell Conference, Lucerne, 2008.

52. Zhao, X.-Y., et al., *Studies on the carbon reactions in the anode of deposited carbon fuel cells.* Journal of Power Sources, 2008. **185**(1): p. 104-111.

53. Shiratori, Y., T. Oshima, and K. Sasaki, *Feasibility of direct-biogas SOFC.* International Journal of Hydrogen Energy. **In Press, Corrected Proof**.

54. Nikooyeh, K., et al., *Effect of hydrogen on carbon formation on Ni/YSZ composites exposed to methane.* Applied Catalysis A: General, 2008. **347**(1): p. 106-111.

55. Slinn, M., et al., *Steam reforming of biodiesel by-product to make renewable hydrogen.* Bioresource Technology, 2008. **99**(13): p. 5851-5858.

56. Nikolla, E., J.W. Schwank, and S. Linic, *Hydrocarbon steam reforming on Ni alloys at solid oxide fuel cell operating conditions.* Catalysis Today
Reforming of Liquid Hydrocarbon Fuels for Fuel Cell Applications, 2008. **136**(3-4): p. 243-248.

57. Tolchard, J. and T. Grande, *Physicochemical compatibility of SrCeO3 with potential SOFC cathodes.* Journal of Solid State Chemistry, 2007. **180**(10): p. 2808-2815.

58. Hornés, A., et al., *Catalytic properties of monometallic copper and bimetallic copper-nickel systems combined with ceria and Ce-X (X = Gd, Tb) mixed oxides applicable as SOFC anodes for direct oxidation of methane.* Journal of Power Sources
CONAPPICE 2006 - Selected Papers Presented at the 2nd National Congress on Fuel Cells (CONAPPICE 2006), Madrid, Spain, 18-20 October 2006., 2007. **169**(1): p. 9-16.

59. Sha, X., et al., *Study on La and Y co-doped ceria-based electrolyte materials.* Journal of Alloys and Compounds, 2007. **428**(1-2): p. 59-64.

60. Rupp, J.L.M. and L.J. Gauckler, *Microstructures and electrical conductivity of nanocrystalline ceria-based thin films.* Solid State Ionics
Solid State Ionics 15: Proceedings of the 15th International Conference on Solid State Ionics, Part II, 2006. **177**(26-32): p. 2513-2518.

61. Xu, X., et al., *LSM-SDC electrodes fabricated with an ion-impregnating process for SOFCs with doped ceria electrolytes.* Solid State Ionics
Solid State Ionics 15: Proceedings of the 15th International Conference on Solid State Ionics, Part I, 2006. **177**(19-25): p. 2113-2117.

62. Gil, V., J. Tartaj, and C. Moure, *Chemical and thermomechanical compatibility between Ni-GDC anode and electrolytes based on ceria.* Ceramics International. **In Press, Corrected Proof**.

63. Huang, T.-J. and M.-C. Huang, *Effect of Ni content on hydrogen production via steam reforming of methane over Ni/GDC catalysts.* Chemical Engineering Journal. **In Press, Accepted Manuscript**.

64. Huang, T.-J. and M.-C. Huang, *Electrochemical promotion of bulk lattice-oxygen extraction for syngas generation over Ni-GDC anodes in direct-methane SOFCs.* Chemical Engineering Journal, 2008. **135**(3): p. 216-223.

65. Ye, X.-F., et al., *Preparation and performance of a Cu-CeO2-ScSZ composite anode for SOFCs running on ethanol fuel.* Journal of Power Sources, 2007. **164**(1): p. 203-209.

66. Ye, X.-F., et al., *Use of a catalyst layer for anode-supported SOFCs running on ethanol fuel.* Journal of Power Sources, 2008. **177**(2): p. 419-425.

67. Fuerte, A., R.X. Valenzuela, and L. Daza, *Preparation and characterisation of SOFC anodic materials based on Ce-Cu.* Journal of Power Sources
CONAPPICE 2006 - Selected Papers Presented at the 2nd National Congress on Fuel Cells (CONAPPICE 2006), Madrid, Spain, 18-20 October 2006., 2007. **169**(1): p. 47-52.

68. Tavares, A.C., et al., *Novel copper-based anodes for solid oxide fuel cells with samaria-doped ceria electrolyte.* Journal of Power Sources, 2008. **183**(1): p. 20-25.

69. Kishimoto, H., et al., *Feasibility of liquid hydrocarbon fuels for SOFC with Ni-ScSZ anode.* Journal of Power Sources
ACS San Francisco 2006, Fuel and Cell Symposium. American Chemical Society National Meeting. San Francisco, CA Sept 10-14 2006, 2007. **172**(1): p. 67-71.

70. Macek, J., B. Novosel, and M. Marinsek, *Ni-YSZ SOFC anodes--Minimization of carbon deposition.* Journal of the European Ceramic Society
Refereed Reports IX Conference & Exhibition of the European Ceramic Society, IX Conference & Exhibition of the European Ceramic Society, 2007. **27**(2-3): p. 487-491.

71. Yamaji, K., et al., *Feasibility of Ni-based cermet anode for direct HC SOFCs: Fueling ethane at a low S/C condition to Ni-ScSZ anode-supported cell.* Journal of Power Sources, 2006. **159**(2): p. 885-890.

72. Tanaka, Y. and T. Kato, *Reforming of methane, ethylene, and desulfurized kerosene over Ni-8YSZ catalyst.* Applied Catalysis A: General, 2008. **348**(2): p. 229-235.

73. Lü, Z., et al., *Study on new copper-containing SOFC anode materials.* Journal of Alloys and Compounds, 2002. **334**(1-2): p. 299-303.

74. Li, X., et al., *La and Sc co-doped SrTiO3 as novel anode materials for solid oxide fuel cells.* Electrochemistry Communications. **In Press, Accepted Manuscript**.

75. Ruiz-Morales, J.C., et al., *On the simultaneous use of La0.75Sr0.25Cr0.5Mn0.5O3-[delta] as both anode and cathode material with improved microstructure in solid oxide fuel cells.* Electrochimica Acta, 2006. **52**(1): p. 278-284.

76. Leone, P., et al., *Experimental investigations of the microscopic features and polarization limiting factors of planar SOFCs with LSM and LSCF cathodes.* Journal of Power Sources, 2008. **177**(1): p. 111-122.

77. Princivalle, A. and E. Djurado, *Nanostructured LSM/YSZ composite cathodes for IT-SOFC: A comprehensive microstructural study by electrostatic spray deposition.* Solid State Ionics. **In Press, Corrected Proof**.

78. Piao, J., et al., *A study of process parameters of LSM and LSM-YSZ composite cathode films prepared by screen-printing.* Journal of Power Sources, 2008. **175**(1): p. 288-295.

79. Jin, C., et al., *Electrochemical characteristics of an La0.6Sr0.4Co0.2Fe0.8O3-La0.8Sr0.2MnO3 multi-layer composite cathode for intermediate-temperature solid oxide fuel cells.* Journal of Power Sources, 2008. **183**(2): p. 506-511.

80. Shah, M. and S.A. Barnett, *Solid oxide fuel cell cathodes by infiltration of La0.6Sr0.4Co0.2Fe0.8O3 - [delta] into Gd-Doped Ceria.* Solid State Ionics. **In Press, Corrected Proof**.

81. Tan, X., et al., *Enhancement of oxygen permeation through La0.6Sr0.4Co0.2Fe0.8O3-[delta] hollow fibre membranes by surface modifications.* Journal of Membrane Science, 2008. **324**(1-2): p. 128-135.

82. Zhen, Y.D., J. Li, and S.P. Jiang, *Oxygen reduction on strontium-doped LaMnO3 cathodes in the absence and presence of an iron-chromium alloy interconnect.* Journal of Power Sources
Special issue including selected papers from the International Power Sources Symposium 2005 together with regular papers, 2006. **162**(2): p. 1043-1052.

83. Monterrubio-Badillo, C., et al., *Preparation of LaMnO3 perovskite thin films by suspension plasma spraying for SOFC cathodes.* Surface and Coatings Technology, 2006. **200**(12-13): p. 3743-3756.

84. Kuscer, D., et al., *Interactions between a thick film LaMnO3 cathode and YSZ SOFC electrolyte during high temperature ageing.* Solid State Ionics, 1995. **78**(1-2): p. 79-85.

85. Holme, T.P., C. Lee, and F.B. Prinz, *Atomic layer deposition of LSM cathodes for solid oxide fuel cells.* Solid State Ionics
Solid State Ionics 16: Proceedings of the 16th International Conference on Solid State Ionics (SSI-16), Part II, 2008. **179**(27-32): p. 1540-1544.

86. Lee, B.-K., et al., *Monitoring of the LSM/YSZ interface in SOFCs using limited-contact geometry in impedance spectroscopy.* Solid State Ionics

Solid State Ionics 16: Proceedings of the 16th International Conference on Solid State Ionics (SSI-16), Part I, 2008. **179**(21-26): p. 955-959.

87. Nielsen, J. and T. Jacobsen, *SOFC cathode/YSZ -- Non-stationary TPB effects.* Solid State Ionics
Solid State Ionics 16: Proceedings of the 16th International Conference on Solid State Ionics (SSI-16), Part II, 2008. **179**(27-32): p. 1314-1319.

88. Yu, H.-C. and K.-Z. Fung, *Electrode properties of La1-xSrxCuO2.5-[delta] as new cathode materials for intermediate-temperature SOFCs.* Journal of Power Sources, 2004. **133**(2): p. 162-168.

89. Zhu, C., et al., *Preparation and performance of Pr0.7Sr0.3Co1 - yCuyO3 - [delta] as cathode material of IT-SOFCs.* Solid State Ionics
Solid State Ionics 16: Proceedings of the 16th International Conference on Solid State Ionics (SSI-16), Part II, 2008. **179**(27-32): p. 1470-1473.

90. Jin, C. and J. Liu, *Preparation of Ba1.2Sr0.8CoO4+[delta] K2NiF4-type structure oxide and cathodic behavioral of Ba1.2Sr0.8CoO4+[delta]-GDC composite cathode for intermediate temperature solid oxide fuel cells.* Journal of Alloys and Compounds. **In Press, Corrected Proof**.

91. Shaigan, N., D.G. Ivey, and W. Chen, *Co/LaCrO3 composite coatings for AISI 430 stainless steel solid oxide fuel cell interconnects.* Journal of Power Sources, 2008. **185**(1): p. 331-337.

92. Smeacetto, F., et al., *Characterization and performance of glass-ceramic sealant to join metallic interconnects to YSZ and anode-supported-electrolyte in planar SOFCs.* Journal of the European Ceramic Society, 2008. **28**(13): p. 2521-2527.

93. Huang, C.M., S.S. Shy, and C.H. Lee, *On flow uniformity in various interconnects and its influence to cell performance of planar SOFC.* Journal of Power Sources, 2008. **183**(1): p. 205-213.

94. Fergus, J.W., *Metallic interconnects for solid oxide fuel cells.* Materials Science and Engineering A, 2005. **397**(1-2): p. 271-283.

95. Zhu, W.Z. and S.C. Deevi, *Development of interconnect materials for solid oxide fuel cells.* Materials Science and Engineering A, 2003. **348**(1-2): p. 227-243.

96. Montero, X., et al., *MnCo1.9Fe0.1O4 spinel protection layer on commercial ferritic steels for interconnect applications in solid oxide fuel cells.* Journal of Power Sources, 2008. **184**(1): p. 172-179.

97. Piccardo, P., et al., *ASR evaluation of different kinds of coatings on a ferritic stainless steel as SOFC interconnects.* Surface and Coatings Technology
ICMCTF 2007, 34th International Conference and Metallurgical Coatings and Thin Films (ICMCTF 2007), 2007. **202**(4-7): p. 1221-1225.

98. Liu, Y., *Performance evaluation of several commercial alloys in a reducing environment.* Journal of Power Sources, 2008. **179**(1): p. 286-291.

99. Smeacetto, F., et al., *Glass-ceramic seal to join Crofer 22 APU alloy to YSZ ceramic in planar SOFCs.* Journal of the European Ceramic Society, 2008. **28**(1): p. 61-68.

100. Yang, Z., et al., *Investigation of iron-chromium-niobium-titanium ferritic stainless steel for solid oxide fuel cell interconnect applications.* Journal of Power Sources, 2008. **183**(2): p. 660-667.

101. Will, J., et al., *Fabrication of thin electrolytes for second-generation solid oxide fuel cells.* Solid State Ionics, 2000. **131**(1-2): p. 79-96.

102. Setoguchi, T., et al., *Application of the stabilized zirconia thin film prepared by spray pyrolysis method to SOFC.* Solid State Ionics, 1990. **40-41**(Part 1): p. 502-505.

103. Powell, J. and S. Blackburn, *The unification of paste rheologies for the co-extrusion of solid oxide fuel cells.* Journal of the European Ceramic Society. **In Press, Corrected Proof**.

104. Dikwal, C.M., W. Bujalski, and K. Kendall, *Characterization of the electrochemical performance of micro-tubular SOFC in partial reduction and oxidation conditions.* Journal of Power Sources
Fuel cells in a changing world selected papers from the tenth Grove fuel cells symposium, 2008. **181**(2): p. 267-273.

105. Jung, H.Y., et al., *Fabrication and performance evaluation of 3-cell SOFC stack based on planar 10 cm × 10 cm anode-supported cells.* Journal of Power Sources
Special issue including selected papers from the 3rd International Conference on Materials for Advanced Technologies (ICMAT 2005, Singapore, Malaysia) and the Summer School on Synthesis of Nanostructured Materials for Polymer Batteries (Augustów, Poland) together with regular papers, 2006. **159**(1): p. 478-483.

106. Han, M., et al., *Fabrication, microstructure and properties of a YSZ electrolyte for SOFCs.* Journal of Power Sources
IBA - HBC 2006 - Selected papers from the INTERNATIONAL BATTERY ASSOCIATION & HAWAII BATTERY CONFERENCE 2006 Waikoloa, Hawaii, USA 9-12 January 2006, 2007. **165**(2): p. 757-763.

107. Huang, B., et al., *Performance of La0.75Sr0.25Cr0.5Mn0.5O3-[delta] perovskite-structure anode material at lanthanum gallate electrolyte for IT-SOFC running on ethanol fuel.* Journal of Power Sources, 2007. **167**(1): p. 39-46.

108. Yamaguchi, T., et al., *Fabrication and characterization of high performance cathode supported small-scale SOFC for intermediate temperature operation.* Electrochemistry Communications, 2008. **10**(9): p. 1381-1383.

109. Yamaguchi, T., et al., *Evaluation of Extruded Cathode Honeycomb Monolith-Supported SOFC under Rapid Start-up Operation.* Electrochimica Acta. **In Press, Accepted Manuscript**.

110. Haart, L.G.J.d.V., I. C.; Janke, A.; Ringel, H.; Tietz, F., *New developments in stack technology for anode substrate based SOFC.* Solid oxide fuel cells . 7 : proceedings of the international symposium held in Tsukuba, 2001.

111. Haart, L.G.J.d.B., H. P.; Diekmann, U.; Kabs, H.; Stolten, D.; Stöver, D.; Vinke, I. C., *Status of the development of the anode supported planar SOFC system.* Fuel Cell Seminar, Palm Spring, CA, 1998.

112. Föger, K., *SOFC Micro-CHP of Ceramic Fuel Cells Ltd.- Products for Today, Ceramic Fuel Cells Limited.* 8th European Solid Oxide Fuel Cell Conference, Lucerne, 2008. **1**.

113. Kendall, K., *Micro-tubular cells: a novel SOFC design.* Middlesex University, 1993.

114. Kendall, K., International Forum on Fine Ceramics Japan Fine Ceramics Center, Nagoya Japan, 1992: p. 143 - 148.

115. Timothy LaBreche, J.B., and Aaron Crumm, *Commercializing Solid Oxide Fuel Cells Into Portable Markets, Adaptive Materials Incorporated.* 8th European Solid Oxide Fuel Cell Conference, Lucerne, 2008.

116. Volker Nerlich, D.A.S., *Galileo 1000 N from Hexis – Cogeneration with SOFC for Residential Application.* 8th European Solid Oxide Fuel Cell Conference, Lucerne, 2008.

117. N. Christiansena, J.B.H., H. Holm-Larsena, M.J. Jørgensena, L. Theil Kuhnb, P. V. Hendriksenb, A. Hagenb and S. Linderothb, *Solid Oxide Fuel Cell Research and Development at Topsoe Fuel Cell A/S and Risø/DTU.* 8th European Solid Oxide Fuel Cell Conference, Lucerne, 2008.

118. Gianmichele Orsello (1), A.C., J. Hoffmann (2) (1) TurboCare SpA, Torino / Italy (2) Siemens Power Generation, Pittsburgh, PA / USA, *Latest info about operation of the Siemens SOFC Generators CHP100 and SFC5 in a factory.* 8th European Solid Oxide Fuel Cell Conference, Lucerne, 2008.

119. Borglum, B., *Development of Solid Oxide Fuel Cells*
at Versa Power Systems. 8th European Solid Oxide Fuel Cell Conference, Lucerne, 2008.

120. Subhasish Mukerjee, K.H., Sean Kelly, Rick Kerr, Steven Shaffer, *Delphi's Solid Oxide Fuel Cell Technology Development*
for Transportation and Stationary Applications. 8th European Solid Oxide Fuel Cell Conference, Lucerne, 2008.

121. Gerry D. Agnew, S.H.P.a.R.P.T., *Large Scale Hybrid SOFC Power Generators from Rolls-Royce Fuel Cell Systems.* 8th European Solid Oxide Fuel Cell Conference, Lucerne, 2008.

122. Mallon, C., *NICKEL CERMET ANODE OPTIMISATION FOR MICRO-TUBULAR SOLID OXIDE FUEL CELL OPERATION ON ALKANES.* University of Birmingham, Thesis, 2006.

123. Suzuki, T., et al., *Fabrication of needle-type micro SOFCs for micro power devices.* Electrochemistry Communications, 2008. **10**(10): p. 1563-1566.

124. Du, Y., N.M. Sammes, and G.A. Tompsett, *Optimisation parameters for the extrusion of thin YSZ tubes for SOFC electrolytes.* Journal of the European Ceramic Society, 2000. **20**(7): p. 959-965.

125. Cai, P.Z., D. J. Green, *Constrained Densification of Alumina/Zirconia Hybrid Laminates, II: Viscoelastic Stress Computation.* Journal of the American Ceramic Society, 1997: p. 1940-1948.

126. Eiselel, P.E., *CHARACTERIZATION OF MATERIAL BEHAVIOR DURING THE MANUFACTURING PROCESS OF A CO-EXTRUDED SOLID OXIDE FUEL CELL.* Geogia Institute of Technology, 2003.

127. Laurencin, J., et al., *A numerical tool to estimate SOFC mechanical degradation: Case of the planar cell configuration.* Journal of the European Ceramic Society, 2008. **28**(9): p. 1857-1869.

128. Zhang, T., et al., *Stress field and failure probability analysis for the single cell of planar solid oxide fuel cells.* Journal of Power Sources
Selected papers from the International Workshop on Degradation Issues in Fuel Cells, 2008. **182**(2): p. 540-545.

129. C. S. Montross, H.Y., M. Dokiya, *Thermal Stresses in Planar Solid Oxide Fuel Cells due to Thermal Expansion Differences.* British Ceramic transactions, 2002. **101**: p. 85-93.

130. Lin, C.-K., et al., *Thermal stress analysis of a planar SOFC stack.* Journal of Power Sources, 2007. **164**(1): p. 238-251.

131. Yakabe, H., et al., *Evaluation of the residual stress for anode-supported SOFCs.* Journal of Power Sources, 2004. **135**(1-2): p. 9-16.

132. Chen, M., et al., *Preparation and electrochemical properties of Ni-SDC thin films for IT-SOFC anode.* Journal of Membrane Science, 2009. **334**(1-2): p. 138-147.

133. Zheng, Y., et al., *La and Ca co-doped ceria-based electrolyte materials for IT-SOFCs.* Materials Research Bulletin. **In Press, Accepted Manuscript**.

134. Cui, D. and M. Cheng, *Thermal stress modeling of anode supported micro-tubular SOFC.* Journal of Power Sources. **In Press, Accepted Manuscript**.

135. Moure, A., J. Tartaj, and C. Moure, *Synthesis, sintering and electrical properties of yttria-calcia-doped ceria.* Journal of the European Ceramic Society. **In Press, Corrected Proof**.

136. Simwonis, D., F. Tietz, and D. Stöver, *Nickel coarsening in annealed Ni/8YSZ anode substrates for solid oxide fuel cells.* Solid State Ionics, 2000. **132**(3-4): p. 241-251.

137. Mermelstein, J., M. Millan, and N.P. Brandon, *The impact of carbon formation on Ni-YSZ anodes from biomass gasification model tars operating in dry conditions.* Chemical Engineering Science, 2009. **64**(3): p. 492-500.

138. Offer, G.J. and N.P. Brandon, *The effect of current and temperature on the degradation of nickel cermet electrodes by carbon monoxide in solid oxide fuel cells.* Chemical Engineering Science, 2009. **64**(10): p. 2291-2300.

139. Lima da Silva, A., C.d.F. Malfatti, and I.L. Müller, *Thermodynamic analysis of ethanol steam reforming using Gibbs energy minimization method: A detailed study of the conditions of carbon deposition.* International Journal of Hydrogen Energy. **In Press, Corrected Proof**.

140. Cheng, Z., S. Zha, and M. Liu, *Influence of cell voltage and current on sulfur poisoning behavior of solid oxide fuel cells.* Journal of Power Sources, 2007. **172**(2): p. 688-693.

141. Galea, N.M., J.M.H. Lo, and T. Ziegler, *A DFT study on the removal of adsorbed sulfur from a nickel(111) surface: Reducing anode poisoning.* Journal of Catalysis. **In Press, Corrected Proof**.

142. Haga, K., et al., *Poisoning of SOFC anodes by various fuel impurities.* Solid State Ionics Solid State Ionics 16: Proceedings of the 16th International Conference on Solid State Ionics (SSI-16), Part II, 2008. **179**(27-32): p. 1427-1431.

143. Lohsoontorn, P., D.J.L. Brett, and N.P. Brandon, *Thermodynamic predictions of the impact of fuel composition on the propensity of sulphur to interact with Ni and ceria-based anodes for solid oxide fuel cells.* Journal of Power Sources, 2008. **175**(1): p. 60-67.

144. Tucker, M.C., et al., *A fundamental study of chromium deposition on solid oxide fuel cell cathode materials.* Journal of Power Sources, 2006. **160**(1): p. 130-138.

145. Komatsu, T., et al., *Chemical compatibility and electrochemical property of intermediate-temperature SOFC cathodes under Cr poisoning condition.* Journal of Power Sources, 2008. **176**(1): p. 132-137.

146. Fergus, J.W., *Effect of cathode and electrolyte transport properties on chromium poisoning in solid oxide fuel cells.* International Journal of Hydrogen Energy TMS06: Symposium on Materials in Clean Power Systems, 2007. **32**(16): p. 3664-3671.

147. Zhen, Y.D., et al., *La(Ni,Fe)O3 as a cathode material with high tolerance to chromium poisoning for solid oxide fuel cells.* Journal of Power Sources, 2007. **170**(1): p. 61-66.

148. Fujita, K., et al., *Relationship between electrochemical properties of SOFC cathode and composition of oxide layer formed on metallic interconnects.* Journal of Power Sources Selected papers presented at the Eighth Grove Fuel Cell Symposium, 2004. **131**(1-2): p. 270-277.

149. Larrain, D., J. Van herle, and D. Favrat, *Simulation of SOFC stack and repeat elements including interconnect degradation and anode reoxidation risk.* Journal of Power Sources, 2006. **161**(1): p. 392-403.

150. Iwata, T., *Characterization of Ni-YSZ Anode Degradation for Substrate-Type Solid Oxide Fuel Cells.* Journal of electrochemical Society, 1996. **143**(1521).

151. Birss, S.P.a.V., *Chromium Poisoning of LSM-YSZ SOFC Cathodes I. Detailed Study of the Distribution of Chromium Species at a Porous, Single-Phase Cathode.* Journal of electrochemical Society, 2004. **151**(11).

152. Konysheva, E., *Chromium Poisoning of Perovskite Cathodes by the ODS Alloy Cr5Fe1Y2O3 and the High Chromium Ferritic Steel Crofer22APU.* Journal of electrochemical Society, 2006. **153**(4).

153. A. Hagen, R.B., P. Hendriksen, and Y. Liu, *Effect of operational conditions on long term stability of SOFCs.* Proceedings. IX SOFC conference Lucerne, 2005. **1**: p. 503-513.

154. Kim, J.-H., et al., *Degradation of cathode current-collecting materials for anode-supported flat-tube solid oxide fuel cell.* Journal of Power Sources, 2009. **188**(2): p. 447-452.

155. Coors, W.G., J.R. O'Brien, and J.T. White, *Conductivity degradation of NiO-containing 8YSZ and 10YSZ electrolyte during reduction.* Solid State Ionics, 2009. **180**(2-3): p. 246-251.

156. C. M. Dikwal, W.B., K. Kendall, *Thermal cycling of microtubular SOFC.* 8th European Solid Oxide Fuel Cell Conference, Lucerne, 2008. **1**.

157. Bujalski, W., et al., *Cycling studies of solid oxide fuel cells.* Journal of Power Sources Selected papers presented at the Ninth Grove Fuel Cell Symposium, 2006. **157**(2): p. 745-749.

158. Bujalski, W., C.M. Dikwal, and K. Kendall, *Cycling of three solid oxide fuel cell types.* Journal of Power Sources

Scientific Advances in Fuel Cell Systems, Turin, Italy, 13-14 September 2006, 2007. **171**(1): p. 96-100.

159. Pusz, J., et al., *Fracture strength of micro-tubular solid oxide fuel cell anode in redox cycling experiments.* Journal of Power Sources

Selected Papers presented at the FUEL PROCESSING FOR HYDROGEN PRODUCTION SYMPOSIUM at the 230th American Chemical SocietyNational Meeting Washington, DC, USA, 28 August - 1 September 2005, 2007. **163**(2): p. 900-906.

160. M. Prica, T.A.a.K.K.I.U.S., S.C. Singhal, H. Tagawa and W. Lehnert, Proceedings of the Fifth International Symposium on Solid Oxide Fuel Cells (Sofc-V), 1997. **97(40)**: p. 619–625.

161. Prica, K.K.a.M., 1st European SOFC Forum Luzern, 1994. **1**: p. 163–170.

162. Sales, K.K.a.G., Second International Conference on 'Ceramics in Energy Applications' Institute of Energy, London, 1994: p. 55–63.

163. Malzbender, J. and R.W. Steinbrech, *Advanced measurement techniques to characterize thermo-mechanical aspects of solid oxide fuel cells.* Journal of Power Sources, 2007. **173**(1): p. 60-67.

164. Cable, T.L. and S.W. Sofie, *A symmetrical, planar SOFC design for NASA's high specific power density requirements.* Journal of Power Sources
Hybrid Electric Vehicles, 2007. **174**(1): p. 221-227.

165. Chou, Y.-S., et al., *Material degradation during isothermal ageing and thermal cycling of hybrid mica seals under solid oxide fuel cell exposure conditions.* Journal of Power Sources, 2006. **157**(1): p. 260-270.

166. Van herle, J., et al., *Ageing of anode-supported solid oxide fuel cell stacks including thermal cycling, and expansion behaviour of MgO-NiO anodes.* Journal of Power Sources

Selected papers from the International Workshop on Degradation Issues in Fuel Cells, 2008. **182**(2): p. 389-399.

167. Waldbillig, D., A. Wood, and D.G. Ivey, *Electrochemical and microstructural characterization of the redox tolerance of solid oxide fuel cell anodes.* Journal of Power Sources
Selected papers presented at the Fuel Cells Science and Technology Meeting, 2005. **145**(2): p. 206-215.

168. Laosiripojana, N. and S. Assabumrungrat, *The effect of specific surface area on the activity of nano-scale ceria catalysts for methanol decomposition with and without steam at SOFC operating temperatures.* Chemical Engineering Science, 2006. **61**(8): p. 2540-2549.

169. Marina, O.A., et al., *A solid oxide fuel cell with a gadolinia-doped ceria anode: preparation and performance.* Solid State Ionics, 1999. **123**(1-4): p. 199-208.

170. Waldbillig, D., A. Wood, and D.G. Ivey, *Thermal analysis of the cyclic reduction and oxidation behaviour of SOFC anodes.* Solid State Ionics, 2005. **176**(9-10): p. 847-859.

171. KONG, J., et al., *Electrochemical and microstructural characterization of cyclic redox behaviour of SOFC anodes.* Rare Metals, 2006. **25**(6, Supplement 1): p. 300-304.

172. Dhir, A., *Improved Microtubular Solid Oxide Fuel Cells*, in *Chemical Engineering*. 2008, University of Birmingham.

173. Christian Mallon, K.K., *Nickel cermet anode optimization for Micro-tubular SOFC on alkanes.* University of Birmingham,, June, 2006.

174. John preece, K.K., *Oxygenated hydrocarbon fuels for SOFCs.* University of Birmingham,, Dec 2005.

175. Kendall, K., et al., *Effects of dilution on methane entering an SOFC anode.* Journal of Power Sources, 2002. **106**(1-2): p. 323-327.

176. Kendall, K., N.Q. Minh, and S.C. Singhal, *Cell and Stack Designs*
High Temperature and Solid Oxide Fuel Cells, S.C. Singhal and K. Kendal, Editors. 2003, Elsevier Science: Amsterdam. p. 197-228.

177. Kendall, K., *Progress in solid oxide fuel cell materials.* International Materials Reviews, 2005: p. 257-264.

178. Kendall, K., M. Slinn, and J. Preece, *Formulating liquid ethers for microtubular SOFCs.* Journal of Power Sources

Selected papers presented at the Ninth Grove Fuel Cell Symposium, 2006. **157**(2): p. 750-753.
179. Lockett, M., M.J.H. Simmons, and K. Kendall, *CFD to predict temperature profile for scale up of micro-tubular SOFC stacks.* Journal of Power Sources
Selected papers presented at the Eighth Grove Fuel Cell Symposium, 2004. **131**(1-2): p. 243-246.

180. Mallon, C. and K. Kendall, *Sensitivity of nickel cermet anodes to reduction conditions.* Journal of Power Sources
Selected papers presented at the Fuel Cells Science and Technology Meeting, 2005. **145**(2): p. 154-160.

181. Saunders, G.J. and K. Kendall, *Reactions of hydrocarbons in small tubular SOFCs.* Journal of Power Sources, 2002. **106**(1-2): p. 258-263.

182. Saunders, G., *Reactions of Hydrocarbons in Zirconia Fuel Cells.* University of Birmingham,, 2004.

183. Foger, S.P.S.B.K., *Materials for solid oxide fuel cells,.* Materials Forum, 1997. **21**: p. 187-244.

184. Nelson, G.J., *Solid Oxide Fuel Cells Constriction resistance effects*, in *Master of Science in Mechanical Engineering*. 2006, Georgia Institute of Technology. p. 110.

185. Mogensen, M. and S. Skaarup, *Kinetic and geometric aspects of solid oxide fuel cell electrodes.* Solid State Ionics
Proceedings of the 10th International Conference on Solid State Ionics, 1996. **86-88**(Part 2): p. 1151-1160.

186. LeMasters, J., *THERMAL STRESS ANALYSIS OF LCA-BASED SOLID OXIDE FUEL CELLS*, in *Mechanical Engineering*. 2004, Georgia Institute of Technology: Atlanta.

187. Chou, Y.-S. and J.W. Stevenson, *Long-term thermal cycling of Phlogopite mica-based compressive seals for solid oxide fuel cells.* Journal of Power Sources, 2005. **140**(2): p. 340-345.

188. Pihlatie, M., T. Ramos, and A. Kaiser, *Testing and Improving the Redox Stability of Ni-based Solid Oxide Fuel Cells.* Journal of Power Sources. **In Press, Accepted Manuscript**.

189. Sarantaridis, D., R.A. Rudkin, and A. Atkinson, *Oxidation failure modes of anode-supported solid oxide fuel cells.* Journal of Power Sources, 2008. **180**(2): p. 704-710.

190. Laurencin, J., et al., *Solid Oxide Fuel Cells damage mechanisms due to Ni-YSZ re-oxidation: Case of the Anode Supported Cell.* Journal of Power Sources, 2009. **192**(2): p. 344-352.

191. Delette, G., et al., *Measurement of the fracture energy at the interface between porous cathode layer and electrolyte in planar solid oxide fuel cells.* Scripta Materialia, 2008. **59**(1): p. 31-34.

192. Pihlatie, M., A. Kaiser, and M. Mogensen, *Mechanical properties of NiO/Ni-YSZ composites depending on temperature, porosity and redox cycling.* Journal of the European Ceramic Society. **In Press, Corrected Proof**.

193. Fujita, K., et al., *Evaluation of the redox stability of segmented-in-series solid oxide fuel cell stacks.* Journal of Power Sources. **In Press, Accepted Manuscript**.

194. Blennow, P., et al., *Electrochemical characterization and redox behavior of Nb-doped SrTiO3.* Solid State Ionics. **In Press, Corrected Proof**.

195. Hjalmarsson, P., M. Søgaard, and M. Mogensen, *Electrochemical performance and degradation of (La0.6Sr0.4)0.99CoO3 - [delta] as porous SOFC-cathode.* Solid State Ionics
Solid State Ionics 16: Proceedings of the 16th International Conference on Solid State Ionics (SSI-16), Part II, 2008. **179**(27-32): p. 1422-1426.

196. Malzbender, J., W. Fischer, and R.W. Steinbrech, *Studies of residual stresses in planar solid oxide fuel cells.* Journal of Power Sources
Selected papers from the International Workshop on Degradation Issues in Fuel Cells, 2008. **182**(2): p. 594-598.

197. D. Sarantaridis, A.A., *Mechanical Modelling of Redox Cycling Damage in*

Solid Oxide Fuel Cells. The 7th European Fuel Cell Forum, 2006. **3**(2007): p. 246-258.

198. Church, B.C., *Fabrication and Characterization of Solid Oxide Fuel Cell Interconnect Alloys.* Georgia Institute of Technology
Atlanta, Georgia, 2004.

199. Fischer, W., et al., *Residual stresses in planar solid oxide fuel cells.* Journal of Power Sources, 2005. **150**: p. 73-77.

200. J. Laurencin, G.D., F. Lefebvre-Joud, M. Dupeux, *Oxidation stress of solid oxide fuel cells.* Journal of electrochemical Society, 2008. **28**(2008): p. 1857 - 1869.

201. J.W.Hutchinson, Z.S., *Advanced Applications Mechanics*. Vol. 3. 1992, Boston: John Wiley. 63-191.

202. Callister, W.D., *Materials Science and Engineering: An Introduction*. 6th ed. 2003, Utah: John Wiley.

203. Atkinson, A. and A. Selçuk, *Mechanical behaviour of ceramic oxygen ion-conducting membranes.* Solid State Ionics, 2000. **134**(1-2): p. 59-66.

204. Atkinson, A. and A. Selçuk, *Residual stress and fracture of laminated ceramic membranes.* Acta Materialia, 1999. **47**(3): p. 867-874.

205. Zhou, Z., et al., *A new thermal-shock-resistance model for ceramics: Establishment and validation.* Materials Science and Engineering: A, 2005. **405**(1-2): p. 272-276.

206. Sajid Ahmad, C.D., Kevin Kendall, *Thermal Shock Behaviour of Tubular SOFC*, in *Department of Chemical Engineering*. 2007, University of Birmingham: Birmingham, UK. p. 13 - 21.

207. Bessette, D.N., *Status of the Acumentrics SOFC Program*, D.N. Bessette, Editor. 2004, SECA Annual Workshop: Boston, MA.

Nomenclature and Abbreviations

Abbreviation	Full Description
AFC	Alkaline Fuel Cell
CHP	Combined Heat and Power
CO	Carbon monoxide
CO_2	Carbon Dioxide
DMFC	Direct Methanol fuel Cell
H_2	Hydrogen
LSM	Lanthum Strontium Manginate (cathode)
MCFC	Molton Carbonate Fuel Cell
NiO	Nickel Oxide
Ni/YSZ	Nickel/Yttria Stabilised Zirconia Cermet
OCV	Open Circuit Voltage
PAFC	Phosphoric acid Fuel Cell
PEM	PEMFC Proton exchange membrane fuel cell

SOFC	Solid Oxide Fuel Cell
YSZ	Yttria Stabilised Zirconia
CTE	Coefficient of Thermal Expansion
TPB	Triple Phase Boundary
MEA	Membrane-Electrode-Assembly
PEN	Positive-Electrolyte-Negative
MTBF	Mean Time Between Failures
FEA	Finite Element Analysis
SOFC	Solid Oxide Fuel Cell
Redox	Reduction and Oxidation
LSCF	Lanthanum Strontium Cobalt Ferrite
LVDT	Linear Variable Differential Transducer
GDC	Gadolinium doped Ceria
BOP	Balance of plants
DC	Direct Current
EU	European Union
MW	Mega Watts
SECA	Solid State Energy Conversion Alliance
GC	Gas Chromatograph
IP-SOFC	Integrated Planar-SOFC

RRFCS	Rolls Royce Fuel Cells Systems
CFCL	Ceramic Fuel Cells LTD

Publications

1. Journal of Power Sources

Characterization of the electrochemical performance of micro-tubular SOFC in partial reduction and oxidation conditions, Dikwal, C.M., Bujalski, W. Kendall, K.

2. Journal of Power Sources

The effect of temperature gradients on the thermal cycling and isothermal ageing of micro-tubular SOFC, Dikwal, C. M., Bujalski, W. Kendall, K.

3. Eleventh International Symposium on Solid Oxide Fuel Cells, SOFC (SOFC-XI, Vienna Oct 2009.,

Cycling studies of micro-tubular solid oxide fuel cells, Dikwal, C. M and Kendall, K

4. Journal of Power Sources

Cycling of three solid oxide fuel cell types, Bujalski Waldemar
Dikwal Chinnan M., Kendall, Kevin

5. Kendall, K., Dikwal, C. M. and Bujalski, W. Comparative Analysis of Thermal and Redox Cycling for Microtubular SOFCs. Poster. 2007. ECS Transactions, Pennington, NJ. 10th International Symposium on Solid Oxide Fuel Cells, June 3-8, 2007, Nara, Japan.

6. Thermal cycling of microtubular SOFC, 8th European Solid Oxide Fuel Cell Conference, Lucerne, Dikwal C. M., Bujalski W., Kendall K.